

# We are IntechOpen, the world's leading publisher of Open Access books Built by scientists, for scientists

6,300

Open access books available

171,000

International authors and editors

190M

Downloads

Our authors are among the

154

Countries delivered to

TOP 1%

most cited scientists

12.2%

Contributors from top 500 universities



WEB OF SCIENCE™

Selection of our books indexed in the Book Citation Index  
in Web of Science™ Core Collection (BKCI)

Interested in publishing with us?  
Contact [book.department@intechopen.com](mailto:book.department@intechopen.com)

Numbers displayed above are based on latest data collected.  
For more information visit [www.intechopen.com](http://www.intechopen.com)



---

# Improved Performance of a Photovoltaic Panel by MPPT Algorithms

---

Djamel Eddine Tourqui, Achour Betka,  
Atallah Smaili and Tayeb Allaoui

Additional information is available at the end of the chapter

<http://dx.doi.org/10.5772/intechopen.79709>

---

## Abstract

This work is devoted to the presentation and realization of a digital control card (maximum power point tracking) which serves to improve the performance of a photovoltaic generator (GPV). This makes it possible to increase the profitability of the latter, on the one hand, and the stability of electrical networks, on the other hand. The command card has been developed using simple circuits, and tested on a system that includes a photovoltaic panel powering a resistive load under changing weather conditions. The aim of this paper is to implement three well-known MPPT algorithms (Hill-Climbing, Pertube & Observe and Incremental Conductance), using a PIC microcontroller type 16F877A.

**Keywords:** photovoltaic panel, MPPT, PIC 16F877A, P&O, Hill-climbing, incremental conductance

---

## 1. Introduction

Solar energy is among the most widely used sources of renewable energy on a global scale with an installed global capacity of up to 100 GW [1]. This source is considered one of the most promising and best alternative energy source because of its natural availability and cleanliness [2, 3].

It is known that photovoltaic panels have a non-linear characteristic  $I = f(V)$  with a single point where the power generated is maximum (PPM). It is known that PV panels have a non-linear characteristic  $I = f(V)$  with a single point where the power generated is maximum (MPP). This maximum power strongly depends on the intensity of solar radiation and the temperature, which changes during the day.

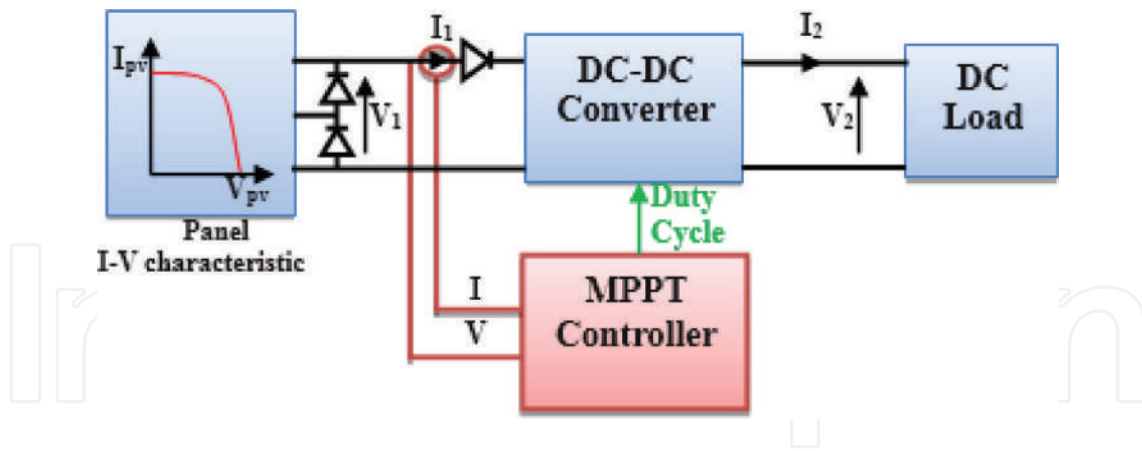


Figure 1. Elementary components of a PV power system.

However, the most difficulties associated with the use of a photovoltaic panel is the perfect non-coupling between the GPV photovoltaic generator and the load [4]. In direct connection mode, a technological barrier that exists in this type of coupling is the problem of transferring the maximum power of the GPV to the load, which often suffers from a bad adaptation. The resulting point of exploitation is then sometimes very far from the real MPP. In other words, it becomes difficult under these conditions to extract the maximum output power of PV panel in all weather conditions [5]. In order to extract at all times the maximum power available at the GPV terminals and transfer it to the load, an MPPT strategy is necessary in order to pursue the maximum power point of the PV panel [6]. There have been many research methods in the literature ranging from the simplest method like Disrupt & Observer (P & O) and IncCond to more sophisticated and complex [7–9].

Static converters, adapted to solar photovoltaic energy, are often called “solar converters” [10]. This adaptation can be achieved by inserting a series chopper controlled by a tracking mechanism “maximum power point tracking” (MPPT). Figure 1 represents an elementary photovoltaic conversion elementary chain associated with an MPPT control.

## 2. Modeling of a photovoltaic generator

Figure 2 shows the equivalent electrical circuit (single-diode model) of a photovoltaic generator, which is used to calculate the power supplied by this generator under all irradiation and temperature conditions [11].

The relationship between the cell terminal current  $I$  and voltage  $V$  is given by [12, 13]:

$$I = I_{ph} - I_D \left[ \exp \left( \frac{V + R_s \times I}{\frac{m \times K_B \times T_{amb}}{q}} \right) - 1 \right] - \frac{V + R_s \times I}{R_{sh}} \quad (1)$$

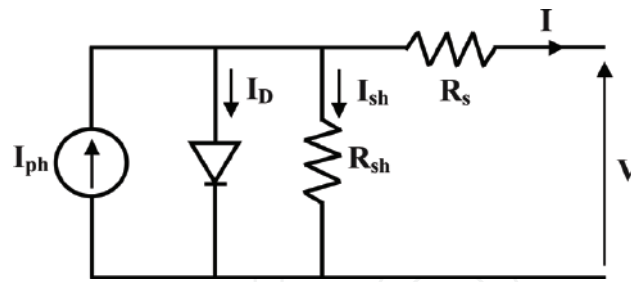


Figure 2. Equivalent circuit of the PV generator.

With:

**I**: output current, **I<sub>D</sub>**: reverse saturation diode current, **I<sub>ph</sub>** photovoltaic current, **KB**: Boltzmann constant ( $1.3854 \times 10^{-23} \text{ JK}^{-1}$ ), **m**: ideality factor, **q**: Charge of an electron ( $1.6021 \times 10^{-19} \text{ C}$ ), **R<sub>s</sub>**: the series resistance ( $\Omega$ ) and **R<sub>sh</sub>**: the shunt resistance ( $\Omega$ ).

As mentioned previously, the characteristic  $I = f(V)$  (Figure 1) of a solar cell strongly depends on the illumination (**E**) and the ambient temperature (**T<sub>amb</sub>**) [14]. The empirical model developed by Garcia and Balenzatgui gives the mathematical relation of the temperature of the photovoltaic module as follows [11, 15]:

$$T_m = T_{amb} + \frac{(\text{NOCT} - 20)E}{800} \quad (2)$$

In order to calculate the solar generator power (**P**), we used the model developed by Skoplaki and Palyvos [14] as follows:

$$P = E \times A \times \eta_{Tref} \left( 1 - B_{ref} (T_m - 25) \right) \quad (3)$$

### 3. Overview of MPPT algorithms used

In the literature, there are various examples of MPPT technologies that serve to improve [8, 16, 17]. The Hill-Climbing, IncCond and Perturbe & Observe techniques are the most widely used because of their simplicity and ease of implementation. The operating principle of these three techniques is briefly summarized below:

#### 3.1. Perturb and observe (P&O)

The principle of the P&O type MPPT commands consists in disturbing the panel voltage ( $V_{PV}$ ) of a small amplitude around its initial value and analyzing the behavior of the instantaneous power variation  $P_{PV}$  of the photovoltaic panel before and after the disturbance [16, 18, 19]. If the change in  $dP_{PV}$  power increases, this implies that  $V_{PV}$  should be set in the same direction as in the previous cycle. If the power of  $dP_{PV}$  decreases, it means that the system is far from the optimal point, so the disturbance size must be reduced in order to bring the operating point around to

the point of maximum power [20]. In summary, if following a voltage disturbance, the PV power increases, the disturbance direction is maintained. If not, it is reversed to resume convergence to the new MPP. The implementation steps of the P & O technique are illustrated in **Figure 3**.

**3.2. Hill-climbing method**

The hill-climbing method [16, 21] consists in moving the operating point along the characteristic  $I = f(V)$  in the direction in which the instantaneous power  $PPV$  increases. For this, the disturbance is applied for the duty cycle  $D$  of the converter. The search stops theoretically until the operating power oscillates at the MPP [22, 23]. The flow diagram of this method is illustrated in **Figure 4**.

**3.3. Incremental conductance method**

To find the MPP, this other technique is based on the knowledge of the GPV conductance variation and the consequences on the position of the operating point with respect to a PPM [24, 25]. Thus, the conductance of the photovoltaic module is defined by the ratio between the current and the voltage of the GPV as indicated below:

The conductance  $G$  of the PV circuit is:

$$G = I_{pv} / V_{pv} \tag{4}$$

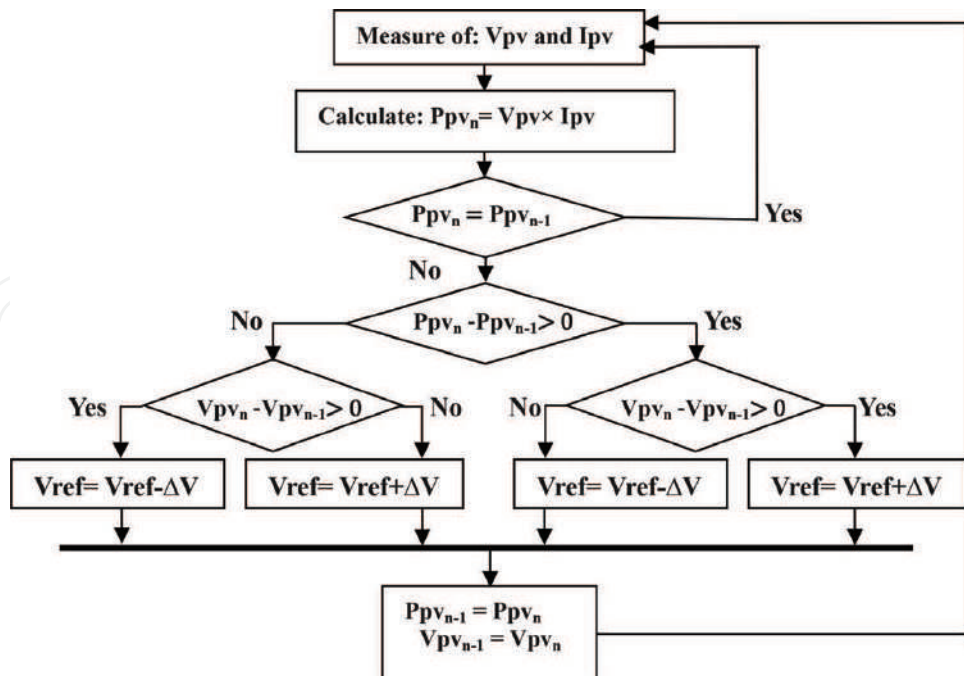


**Figure 3.** Algorithm of an MPPT command based on the P&O method.

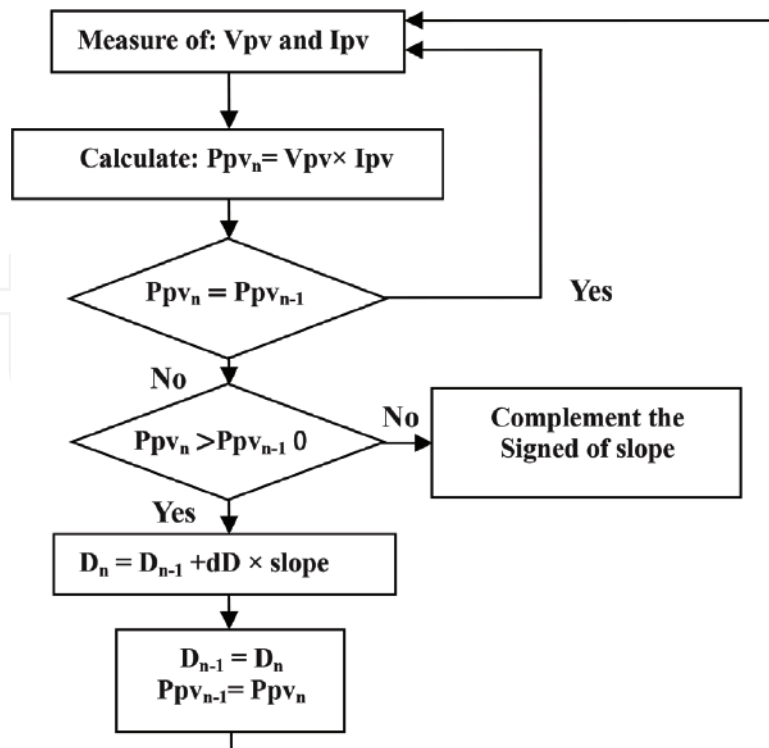


Figure 4. Algorithm of an MPPT command based on the hill-climbing method.

Moreover, an elementary variation (increment) conductance can be defined by:

$$dG = dI_{pv} / dV_{pv} \quad (5)$$

Figure 5 shows the position of the operating point on the power characteristic of the PV generator.

The equation of PV panel power is:

$$P_{pv} = V_{pv} \times I_{pv} \quad (6)$$

$$\left\{ \begin{array}{l} \frac{dP_{pv}}{dV_{pv}} = \frac{d(V_{pv} \times dI_{pv})}{dV_{pv}} \\ \frac{dP_{pv}}{dV_{pv}} = I_{pv} + V_{pv} \frac{dI_{pv}}{dV_{pv}} \\ \frac{1}{dV_{pv}} \times \frac{dP_{pv}}{dV_{pv}} = \frac{I_{pv}}{V_{pv}} + \frac{dI_{pv}}{dV_{pv}} \end{array} \right. \quad (7)$$

where:

$$P_{pv} = P_{pv_n} - P_{pv_{n-1}}, \quad dV_{pv} = V_{pv_n} - V_{pv_{n-1}} \quad \text{and} \quad dI_{pv} = I_{pv_n} - I_{pv_{n-1}} \quad (8)$$

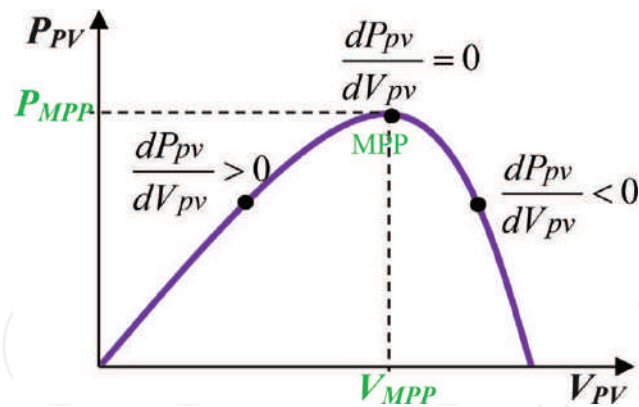


Figure 5. PV power characteristic for different operating points.

On the other hand, the evolution of the power of the module ( $P_{PV}$ ) with respect to the voltage ( $V_{PV}$ ) gives the position of the operating point relative to the PPM. When the power derivative is zero, it means that it is on the PPM, if it is positive the operating point is to the left of the maximum, when it is negative, it is to the right of the MPP [23]. Figure 5 allows to write the following conditions:

$$dP_{pv}/dV_{pv} = 0 \quad \text{At the MPP.} \quad (9)$$

$$dP_{pv}/dV_{pv} > 0 \quad (10)$$

$$dP_{pv}/dV_{pv} < 0 \quad (11)$$

#### 4. Design and realization of the digital MPPT algorithm

At this stage of the research, we will explain the design steps and the realization of the electronic card based on the MPPT algorithms integrated in a microcontroller ( $\mu C$ ) PIC. This digital MPPT control based  $\mu C$  has several advantages over analog MPPT control [26, 27]. Our control board contains three important blocks: power block, power supply, and control block.

##### 4.1. Dimensioning of the power block

The control block consists of two essential parts: the measuring circuit is used to read the voltage and current of our photovoltaic panel at the input of the control unit. The second part, which is actually the brain of this block is formed by a microcontroller PIC 16F877A, to program the various proposed MPPT algorithms, and sends the control signal (the duty cycle) of the chopper to the power block, after isolation and amplification.

- **Tensions measurement:** So that the microcontroller can read the voltage of the photovoltaic panel, we must perform the operation of transforming a voltage of 0–22 V into a voltage of 0–5 V.

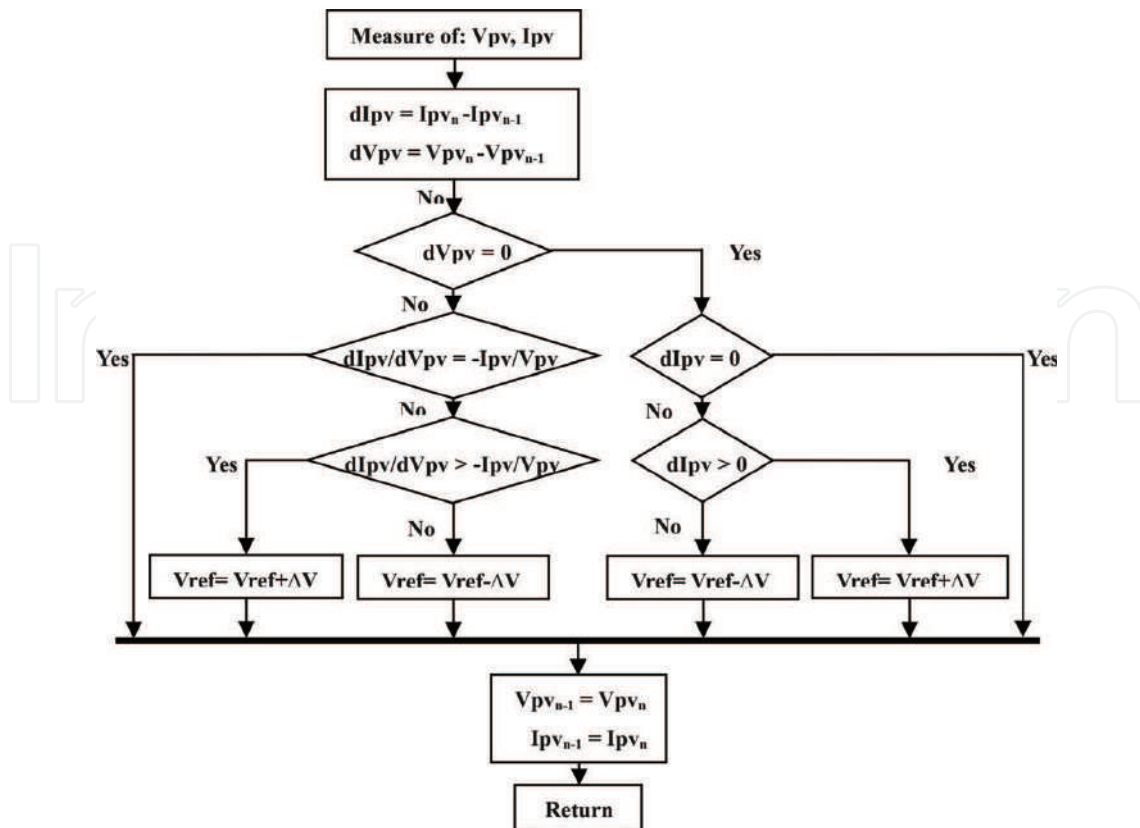


Figure 6. MPPT control algorithm based on IncCond [10].

It is therefore with a simple voltage divider bridge that we perform this operation as show in **Figure 10**. The voltage input to PIC ( $\Delta V_{PIC}$ ) will be connected to pin AN1 of port A configured as input:

#### Calculation of the resistances:

We choose  $V_{PV} = 22(\text{Volts})$  (photovoltaic panel open circuit voltage) and  $V_{PIC} = 5(\text{Volt})$  as the maximum input value to the microcontroller:

$$V_{PIC} = \left( \frac{R_2}{R_1 + R_2} \right) \cdot V_{PV} \Rightarrow \frac{V_{PIC}}{V_{PV}} = \left( \frac{R_2}{R_1 + R_2} \right) \quad (12)$$

Digital application:  $\frac{5}{22} = \left( \frac{R_2}{R_1 + R_2} \right)$ .

For:  $R_2 = 1 \text{ (K}\Omega) \iff R_1 = 3.4 \text{ (K}\Omega)$ .

- **Current measurement**

For the measurement of the current derived from the PV module, an inverter amplifier based on an operational amplifier TL082 was chosen. This configuration allowed us to read the value of the current of the panel, with the mass chosen on the side of the load.

The following formulas determine the parameters of this circuit:

$$V_S = \left( -\frac{R_4}{R_3} \right) \cdot V_E \quad \text{With } (V_E = R_{sh} \cdot I_{PV} ) \quad (13)$$

So output voltage:

$$V_S = (R_{sh} \cdot I_{PV}) \cdot \left( \frac{R_4}{R_3} \right) \quad (14)$$

With:

$R_{sh} = 0,1(\Omega)$ ,  $V_S$ : output voltage,  $V_E$ : Tension d'entrée input voltage.

#### 4.2. The power block

A Buck converter, or chopper, is a switching power supply that converts a DC voltage into another DC voltage of lower value. Using this converter, the DC input voltage, which is for example generated by the photovoltaic generator (GPV) as shown in **Figure 7**, can be lowered. This serial converter can be used as a source-load adapter, when the direct-coupled operating point is to the left of the MPP. For points to the right of the MPP point, the boost converter is more efficient [28].

It consists of a DC-DC buck converter based on IGBT BUP 314, and ensuring the transfer of all of the power extracted from the solar panel to a resistive load.

If switch **S1** is turned on, diode **D** is reverse biased and a circuit current occurs, but does not pass through this diode (**Figure 8**).

The current  $i_L$  does not increase immediately, but increases with a rate imposed by inductance **L** [28]:

$$\frac{di_L}{dt} = \frac{V_{PV} - V_{ch}}{L} \quad (15)$$

Meantime, the inductor stores the energy in a magnetic form. If switch **S1** is deactivated after  $t = t_1$ , the load is separated from the source (system supplied). The current is however maintained

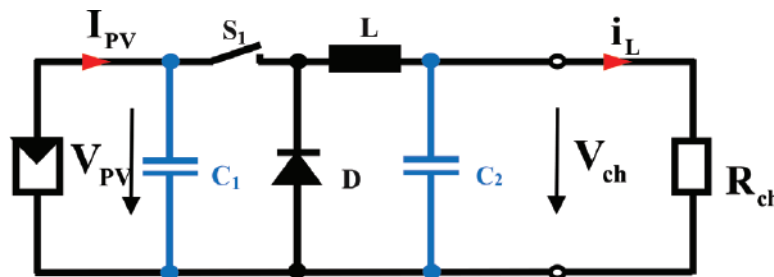


**Figure 7.** Diagram of the electrical circuit of a Buck converter.

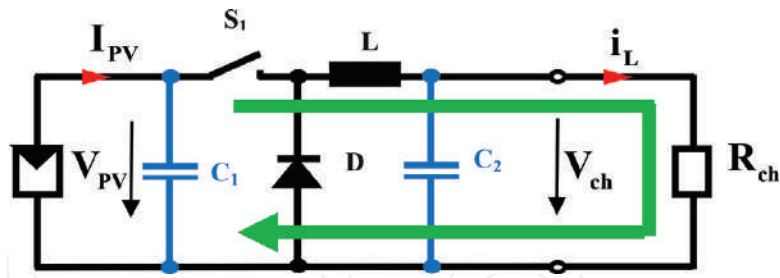


Figure 8. Convertisseur buck Durant l'état on.

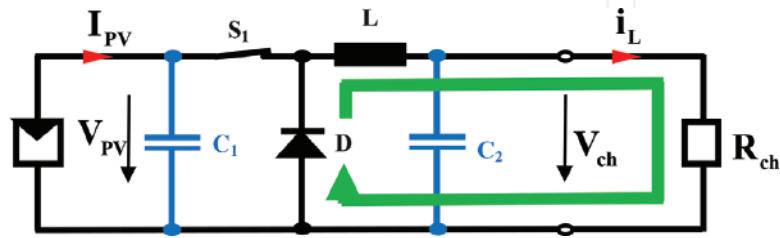


Figure 9. Convertisseur buck Durant l'état off.



Figure 10. PV module employed in the experiment.

by the energy stored in the inductor  $L$  and flows by means of the freewheeling diode (Figure 9). By neglecting the voltage drop across the diode, the current falls, however, because of the following equation:

$$\frac{di_L}{dt} = \frac{-V_{ch}}{L} \quad (16)$$

Capacitor  $C1$  is used to support the supply voltage ( $V_{pv}$ ). In principle, the switch  $S1$  is activated and deactivated with a switching frequency  $f$ .

The 80 Watt PV panel used in this study is shown in Figure 10.

We operate our serial converter in continuous conduction mode (CCM) and the parameters of this circuit are  $C1 = 2200 \mu F$ ,  $C2 = 200 \mu F$  and  $L = 600 \mu H$ . This value of 'L' has been chosen so that the converter operates in TLC according to the following equation [29, 30]:

$$L > \frac{V_{pv}}{4 \times dI_L \times f} \tag{17}$$

### 4.3. The energy block

The operation of our control circuit requires a power supply at three voltage levels. For this, we realized four power supplies based on a voltage regulator:

- The LM 7805 voltage regulator to supply the microcontroller with a fixed voltage equal to 5 V.
- The two LM 7815 and LM 7915 voltage regulators to provide power required current sensor (−15 V and +15 V), based on an operational amplifier the TL082.
- A second LM 7815 regulator to power the 4 N25 optocoupler with +15 V voltage. The latter will serve as a driver for the power switch, to ensure the galvanic isolation between the power block and the control block.

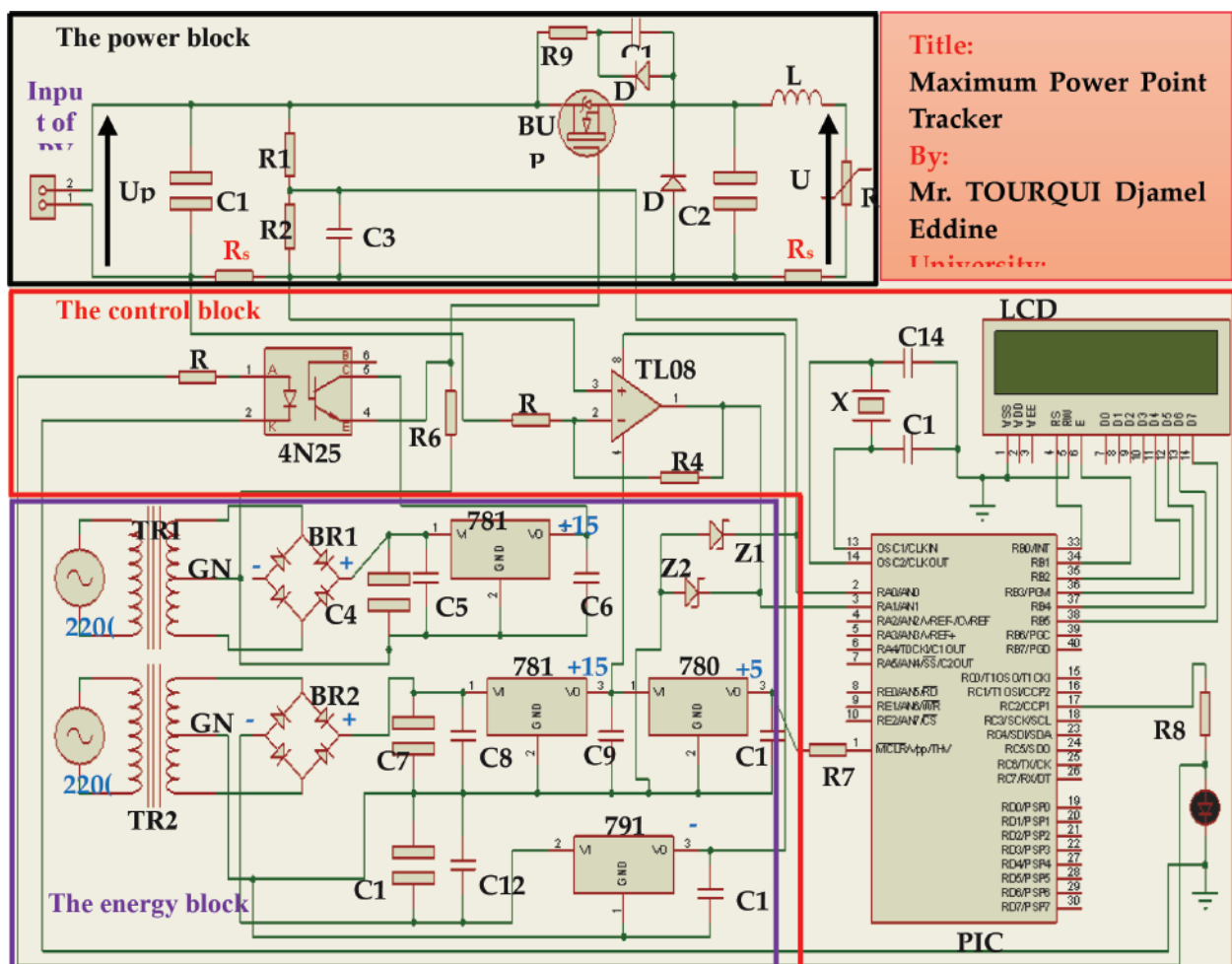
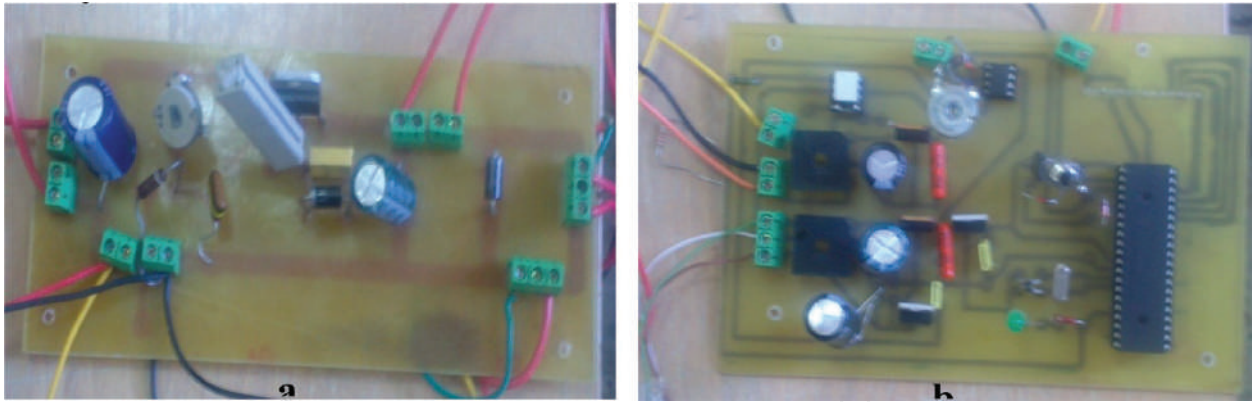


Figure 11. Electrical diagram of the prototype realized.



**Figure 12.** Practical realization of the electronic cards.

The diagram of **Figure 11**, representing the prototype to be produced, was made under the Proteus PCB design software designed by 'Labcenter Electronics', which makes it possible to draw electronic diagrams, to simulate them and to produce the corresponding printed circuit.

**Figure 12a** and **b** represents the prototype, which has been realized practically for the digital MPPT control.

## 5. Results obtained from the MPPT control

In this part, we present the experimental results of the three numerical MPPT algorithms: Perturbed & Observed, Hill-Climbing, and Incremental Conductance, tested on a resistive load ( $R_m = 3.1 \text{ } (\Omega)$ ), which is lower than the load of the maximum power point (MPP) within three (03) clear days. These experiments have been done under the following operating conditions: (1) direct coupling of the load with the photovoltaic panel without MPPT control, (2) using digital MPPT control (DMPPT), (3) by manual MPPT until finding a position to the MPP (manual variation of the load value).

As a result of characteristic  $I = f(V)$ , we have found that the power generated ( $P$ ) by the solar panel is related to the intensity of the radiation  $E$  and the temperature  $T_{amb}$ . We will take the measurements of:  $E$ ,  $T_{amb}$ ,  $P$  and efficiency of control  $\eta$  for each of the three MPPT algorithms studied (Perturb and Observe, Hill-climbing and Incremental Conductance). **Tables 1–3** illustrate the results obtained from the different experiments studied.

The histograms of **Figures 13–15** for these three methods show the difference between the power in the case of direct coupling and the power recovered when applying digital MPPT control that it is compared by the maximum power point search method manually.

**Figure 16** illustrates current and voltage ( $U_{pv}$ ,  $I_{pv}$ ) of the photovoltaic generator, current and voltage of the resistive load ( $U_{ch}$ ,  $I_{ch}$ ) for direct coupling and MPPT cases based on the P & O technique.

Time (hh:mm)	P for direct coupling (watt)	P for DMPPT (watt)	P in MPP (watt)	$\eta$ (%)	E (watt/m <sup>2</sup> )	Tamb (°C)
10:10	18	43	43	100	672	35.6
11:20	25	54	54	100	809	39.3
15:45	12	40	41	97.5	546	39.5
16:11	9	35	35	100	466	35.5
16:30	6	31	32	96.8	404	34.5

**Table 1.** Experimental values identified by the P&O control

Time (hh:mm)	P for direct coupling (watt)	P for DMPPT (watt)	P in MPP (watt)	$\eta$ (%)	E (watt/m <sup>2</sup> )	Tamb (°C)
09:58	14	39	42	92.8	547	41.5
10:55	18	48	49	97.9	697	44.3
11:27	22	52	52	100	749	46.5
12:10	22	52	53	98.1	774	45.5
13:50	20	47	47	100	686	45.5

**Table 2.** Experimental values identified by hill-climbing control

Time (hh:mm)	P for direct coupling (watt)	P for DMPPT (watt)	P in MPP (watt)	$\eta$ (%)	E (watt/m <sup>2</sup> )	Tamb (°C)
13:05	27	54	54	100	774	39.3
13:55	22	53	53	100	835	41
14:25	21.5	54	54	100	772	42
14:46	18	50	50	100	715	45.5
15:12	15	45	45.5	98.9	645	45.5

**Table 3.** Experimental values identified by IncCond control

The duty cycle of the converter in the case of the P & O algorithm is illustrated in **Figure 17**.

The results of current and voltage of PV panel and the load obtained by Hill-climbing algorithm as shown in **Figure 18**. **Figure 19** explains the duty cycle that controlled the DC-DC converter.

Finally, the same experiment is performed using IncCond control and the results shown in **Figure 20**. **Figure 21** shows the duty cycle generated by the IncCond algorithm.

- **Interpretation and discussion of the results**

The results obtained previously in the power tables and histograms clearly show the efficiency of the electronic control card filled for different control algorithms used. The energy extracted from the solar panel using the digital MPPT technique is very large compared to the direct

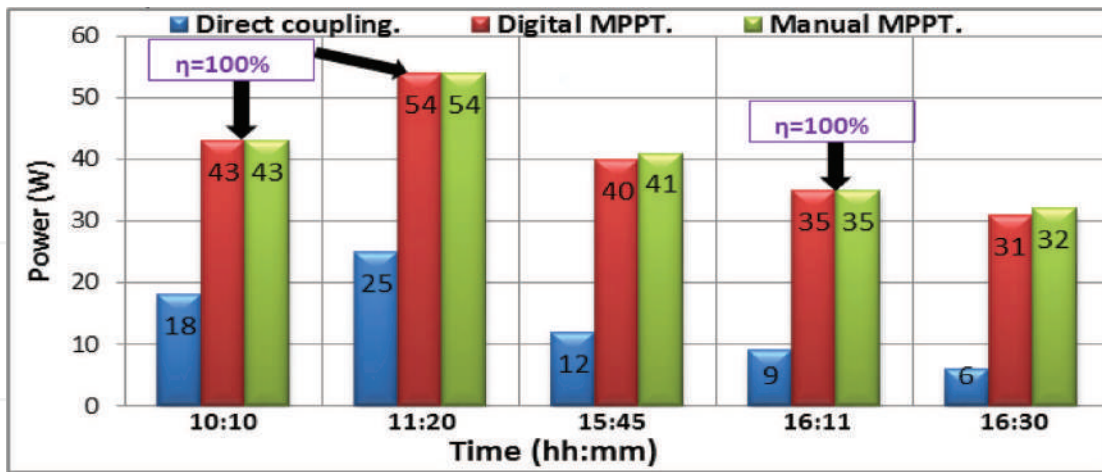


Figure 13. Histogram of powers to P&O algorithm.

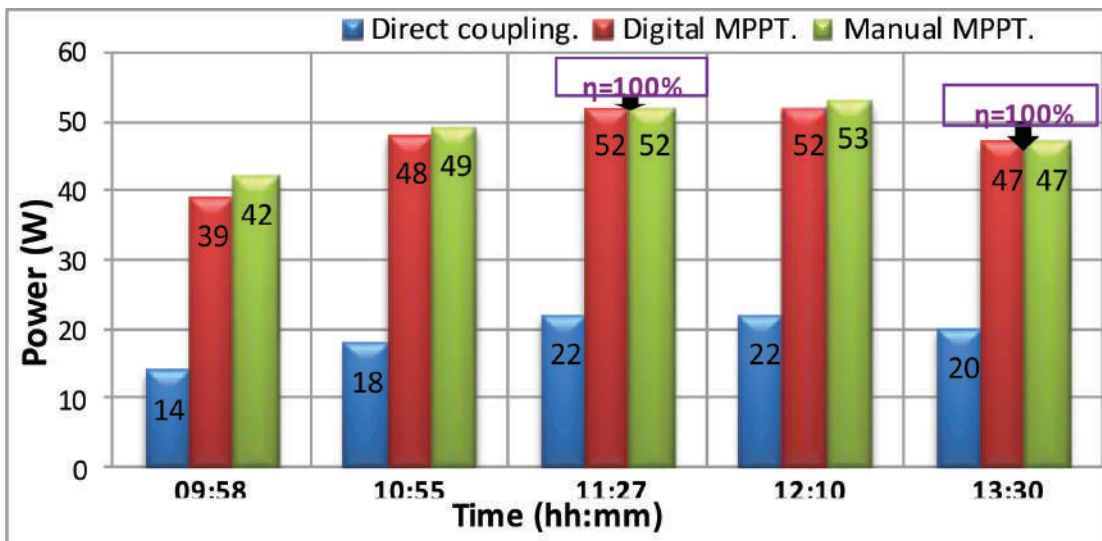


Figure 14. Histogram of powers to hill-climbing algorithm.

charge connection method with the panel. Therefore, in the case of a direct connection between the generator and the load is unlikely to place the PV system at its maximum power point PPM. However, the digital MPPT technique can automatically find the operating voltage of the PV panel that corresponds to the PPM. However, comparing the results obtained by the three algorithms shows the Incremental Conductance technique is the most accurate and closest to the MPP compared to the other two methods.

In addition, the results clearly show the effectiveness of the tracking system ( $\eta$ ) which in many cases reaches 100%. This efficiency represents the ratio between the maximum power obtained manually and the other using the MPPT command as indicated in the following equation:

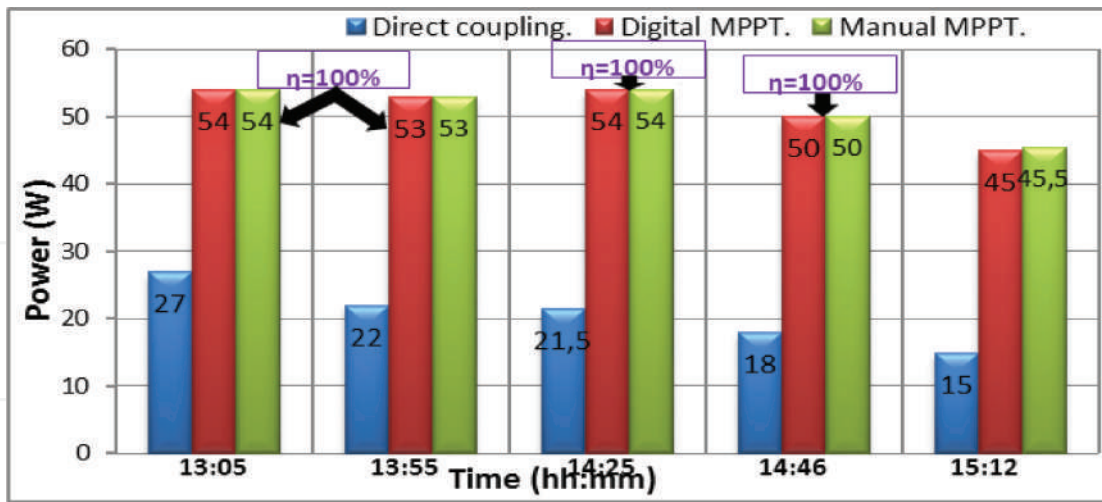


Figure 15. Histogram of powers to incremental conductance algorithm.

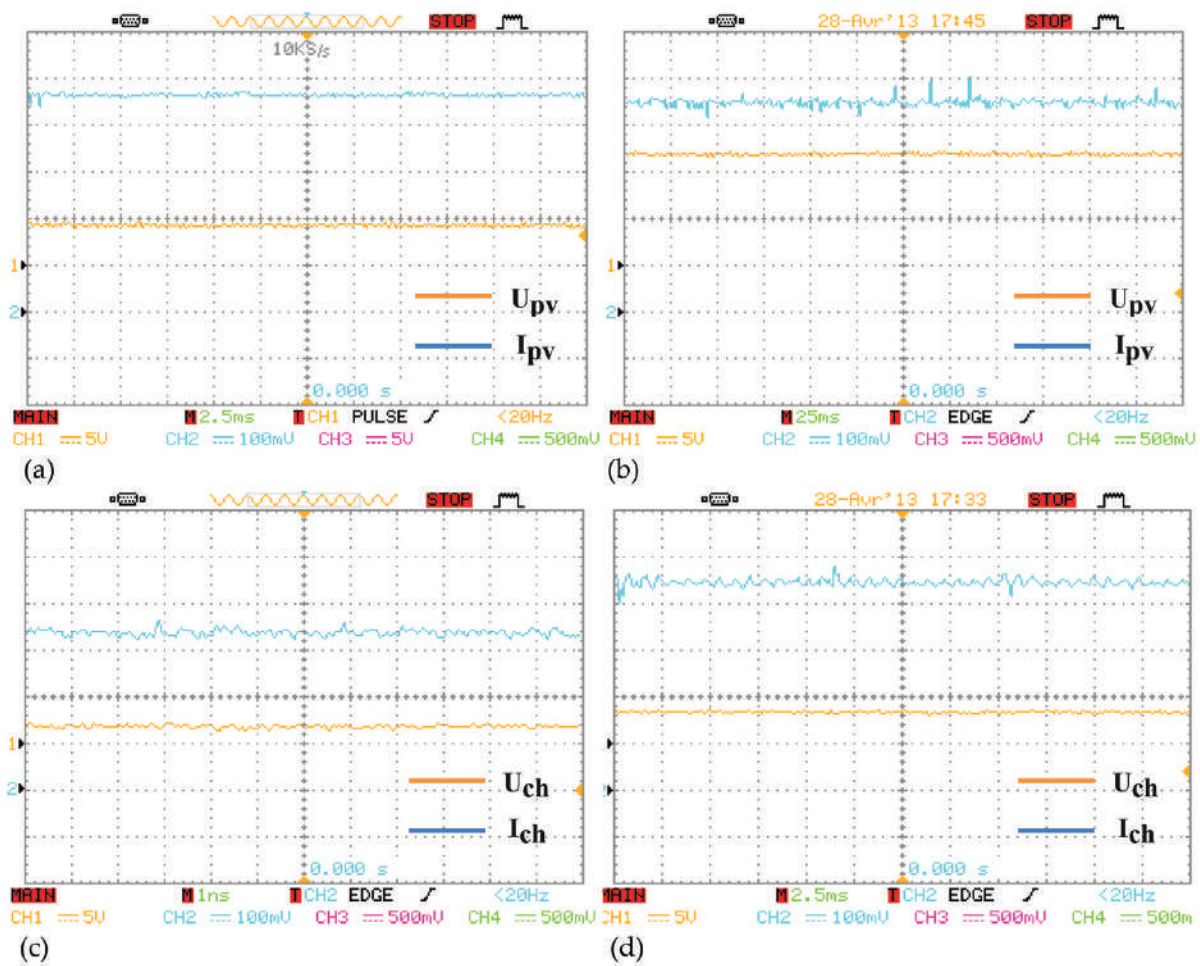


Figure 16. Current and voltage of the photovoltaic generator and the load. (a) ( $U_{pv}$ ,  $I_{pv}$ ) using direct coupling, (b) ( $U_{pv}$ ,  $I_{pv}$ ) using digital MPPT control, (c) ( $U_{ch}$ ,  $I_{ch}$ ) using direct coupling, (d) ( $U_{ch}$ ,  $I_{ch}$ ) using digital MPPT control.

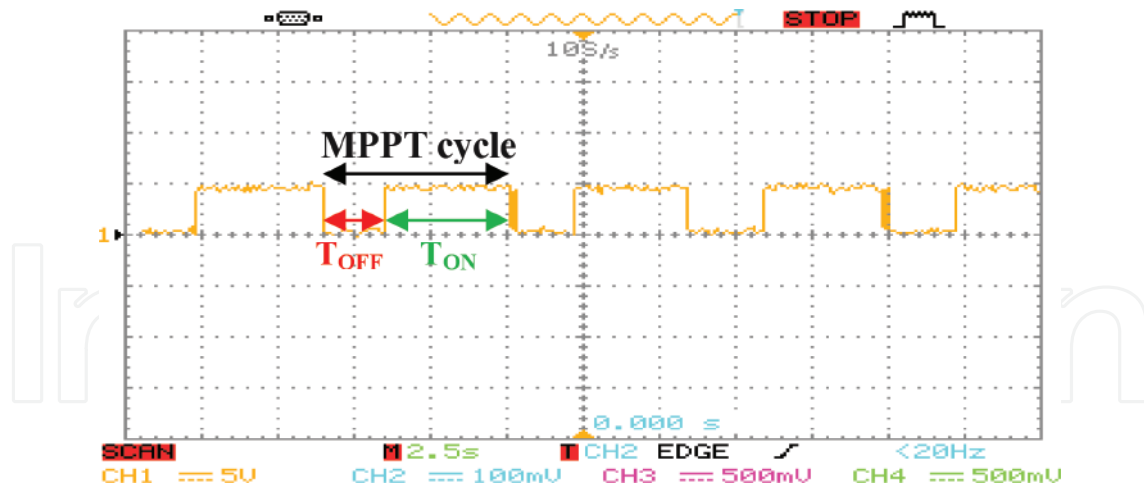


Figure 17. The duty cycle of the P&O algorithm.

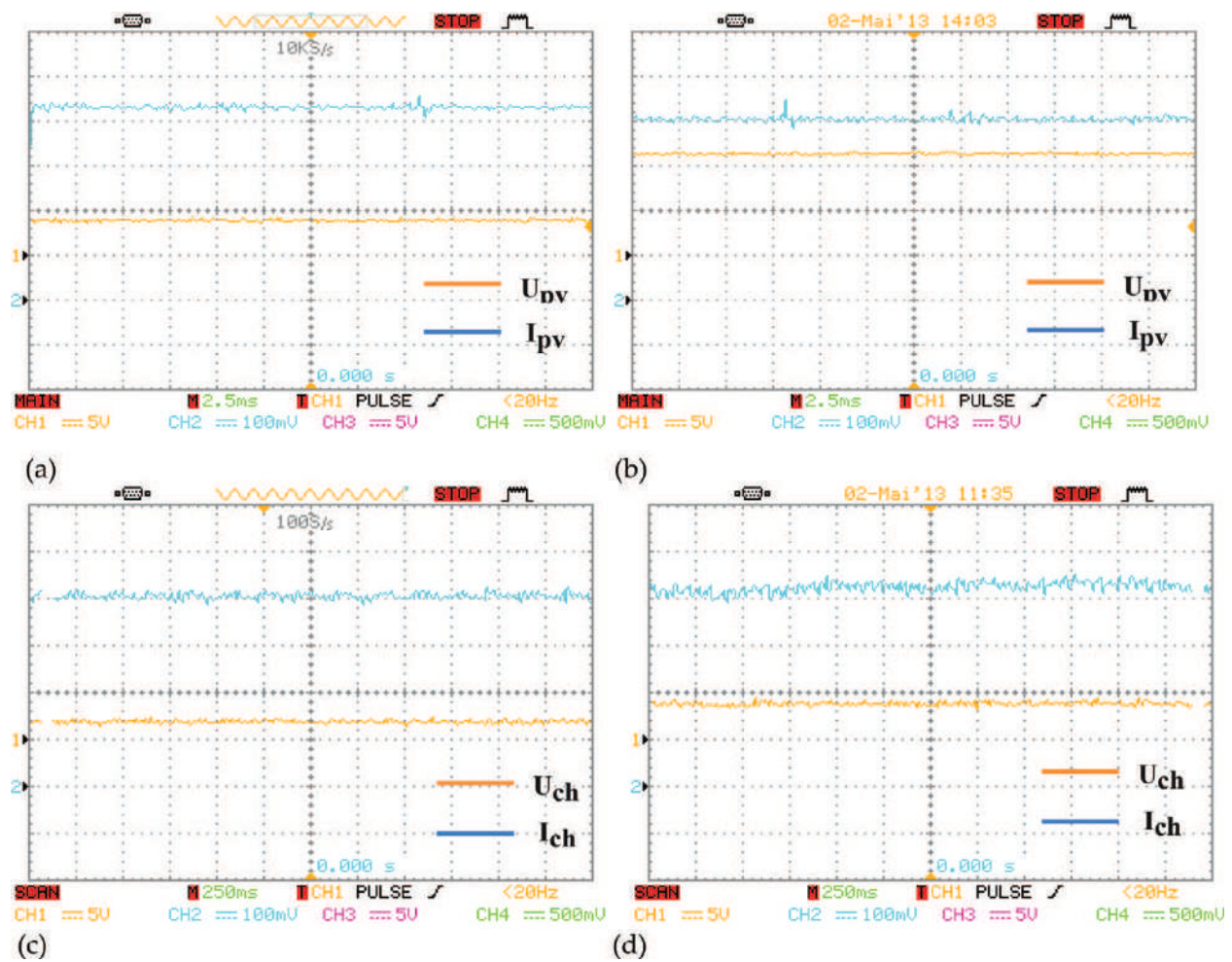


Figure 18. Current and voltage of the photovoltaic generator and the load. (a) ( $U_{pv}$ ,  $I_{pv}$ ) using direct coupling, (b) ( $U_{pv}$ ,  $I_{pv}$ ) using digital MPPT control, (c) ( $U_{ch}$ ,  $I_{ch}$ ) using direct coupling, (d) ( $U_{ch}$ ,  $I_{ch}$ ) using digital MPPT control.

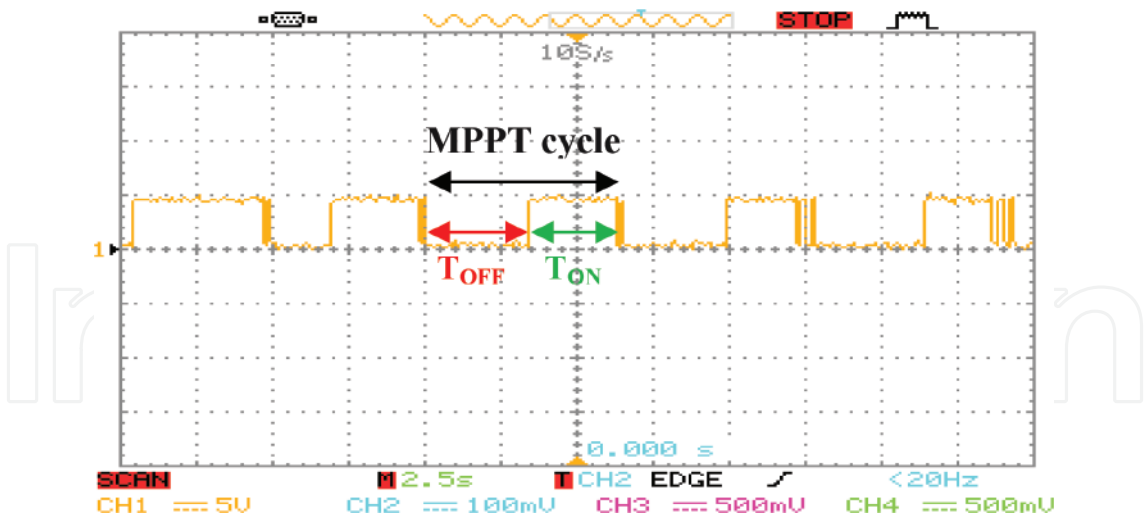


Figure 19. The duty cycle of the hill-climbing algorithm.

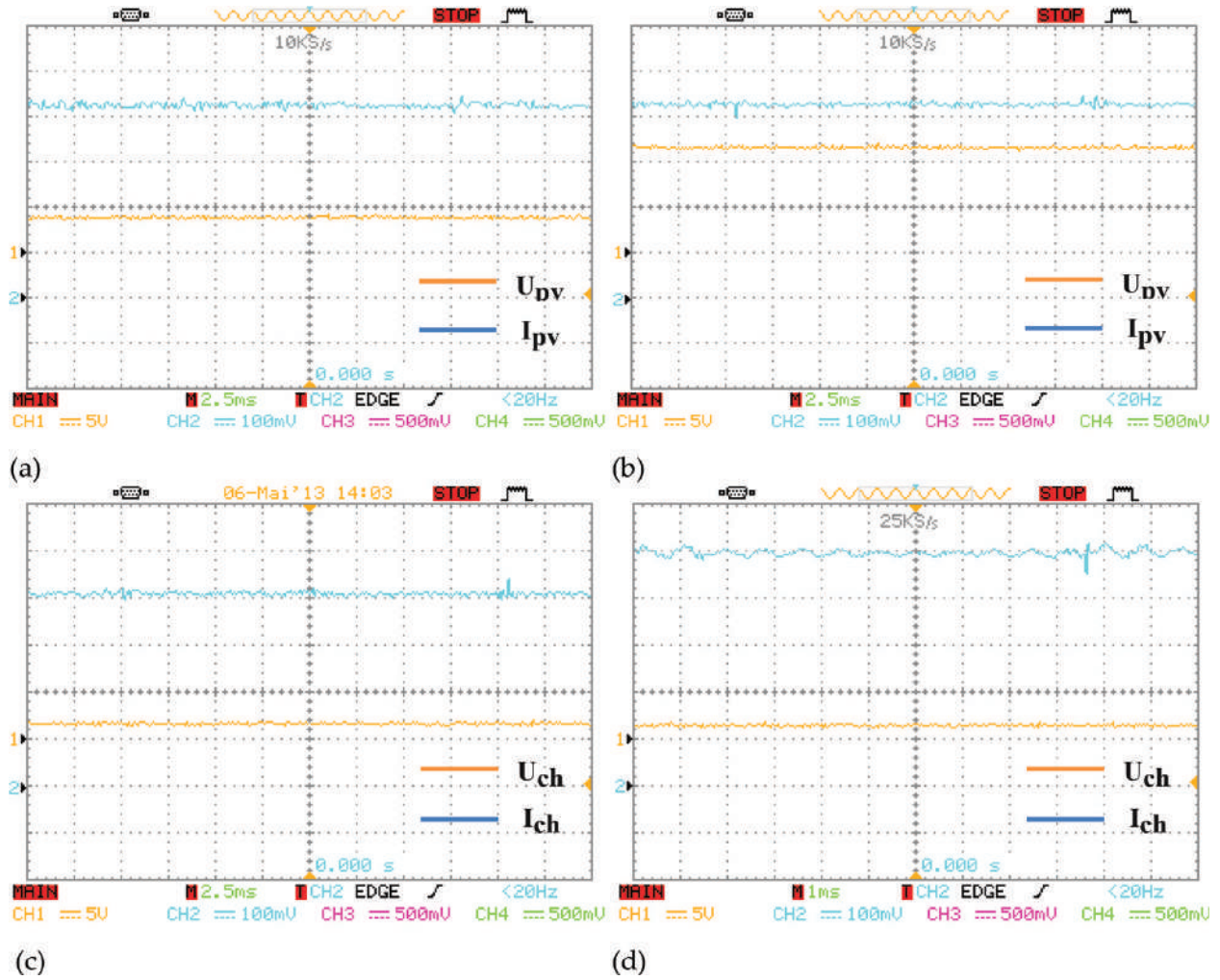


Figure 20. Current and voltage of the photovoltaic generator and the load. (a) ( $U_{pv}$ ,  $I_{pv}$ ) using direct coupling, (b) ( $U_{pv}$ ,  $I_{pv}$ ) using digital MPPT control, (c): ( $U_{ch}$ ,  $I_{ch}$ ) using direct coupling, (d) ( $U_{ch}$ ,  $I_{ch}$ ) using digital MPPT control.

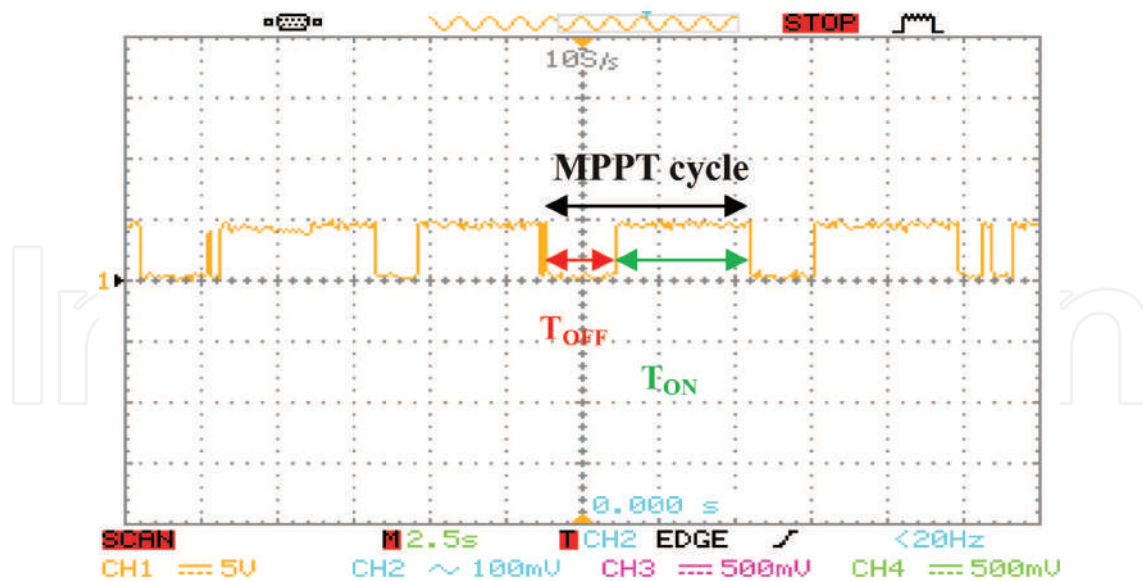


Figure 21. The duty cycle of the incremental conductance algorithm.

$$\eta(\%) = \frac{P_{DMPPT}}{P_{MPP}} \times 100 \quad (18)$$

where  $P_{DMPPT}$  represent the power reached by using the proposed of DMPPT controller and  $P_{MPP}$  is the expected maximum power output in the MPP.

Figures 16, 18 and 20 show that the chopper operates as a voltage step-down, with a voltage of the photovoltaic module stabilizes at  $V_{pv} = 14.5$  (V). For the current of the load, it is found that the current is in continuous conduction, with a ripple of 2 kHz.

Finally, because of the integration of the PWM control signal into PIC, the duty cycle signal frequency generated by the MPPT command (Figures 18, 20 and 21) is of the order of 2 kHz. If the desired maximum power point voltage ( $V_{MPP}$ ) is higher than the measured panel voltage ( $V_{pv}$ ), the duty cycle must be incremented; it must be decreased according to the control technique used. This ratio is adjusted in real time, with the meteorological variations ( $E$  and  $T_{amb}$ ), and this to position itself on the optimum point.

## 6. Conclusion and future action

The paper presented a simplified design and implementation of impedance matching stage using a DC-DC buck converter supplying a resistive load controlled by one low cost microcontroller. This circuit allows the acquisition and processing of measured current and voltage signals and generates the appropriate control signals for controlling the switching of the power unit designed primarily around the buck converter. Three popular MPPT algorithms for extracting the maximum power of the photovoltaic panel namely P&O, Hill-Climbing and IncCond have been considered.

MPPT control has led to improved speed of response, a better MPP search accuracy and good control in the presence of perturbations such as sudden variations of the illumination and the temperature.

This work enables us to increase the cost-effectiveness of solar systems as well as reduce the cost which were imported from abroad and the worldwide costly in terms of our scientific laboratory or sector level using this energy in sustainable development agriculture deployed locally as photovoltaic pumping, irrigation and domestic use.

In the future, experiment of these prototypes on other PV installations (like the PV pumping which is available in our laboratory) will be presented in future works.

## Author details

Djamel Eddine Tourqui<sup>1\*</sup>, Achour Betka<sup>2</sup>, Atallah Smaili<sup>3</sup> and Tayeb Allaoui<sup>3</sup>

\*Address all correspondence to: tourqui.djamel@gmail.com

1 Morsli Abdellah University Center of Tipaza, Algeria

2 Mohamed Khider University, Biskra, Algeria

3 Ibn Khaldoun University, Tiaret, Algeria

## References

- [1] Mellit A, Massi PA. Performance prediction of 20kWp grid-connected photovoltaic plant at Trieste (Italy) using artificial neural network. *Energy Conversion and Management*. 2010;**51**:2431-2441
- [2] Parida B, Iniyamb S, Goicc R. A review of solar photovoltaic technologies. *Renewable and Sustainable Energy Reviews*. 2011;**15**:1625-1636
- [3] Mellit A, Kalogirou SA, Hontoria L, Shaari S. Artificial intelligence techniques for sizing photovoltaic systems: A review. *Renewable and Sustainable Energy Reviews*. 2009;**13**:406-419
- [4] Shraif MF. Optimisation et Mesure de Chaîne de Conversion d'Énergie Photovoltaïque en Énergie Électrique [Phd]. Toulouse, France: Paul Sabatier University; 2002
- [5] Orabi M, Hilmy F, Shawky A, Jaber AAQ, Hasaneen E, Gomaa E. On-chip integrated power management MPPT controller utilizing cell-level architecture for PV solar system. *Solar Energy*. 2015;**117**:10-28
- [6] Sivakumar P, Abdullah AK, Yogeshraj K, Arutchelvi M. Analysis and enhancement of PV efficiency with incremental conductance MPPT technique under non-linear loading conditions. *Renewable Energy*. 2015;**81**:543-550

- [7] Anaya-Lara O, Jenkins N, Ekanayake J, Cartwright P, Hughes M. Wind Energy Generation, Modelling and Control. John Wiley & Sons; 2009. ISBN: 978-0-470 71433-1
- [8] ESRAM T, Chapman PL. Comparison of photovoltaic array maximum power point tracking techniques. IEEE Transactions on Energy Conversion. 2007;**22**:439-449
- [9] De Brito MAG, Galotto L, Sampaio LP, de Azevedo EMG. Evaluation of the main MPPT techniques for photovoltaic applications. IEEE Transactions on Industrial Electronics. 2013;**60**:1156-1167
- [10] Learreta AB. Réalisation de commandes MPPT numériques. Report. Tarragona, Spain: Rovira i Virgili University; 2006
- [11] Sharaf Eldin SA, Abd-Elhady MS, Kandil HA. Feasibility of solar tracking systems for PV panels in hot and cold regions. Renewable Energy. 2016;**85**:228-233
- [12] Ingegnoli A, Iannopolo A. A maximum power point tracking algorithm for stand-alone photovoltaic systems controlled by low computational power devices. In: 15th IEEE 2010 Mediterranean Electro-Technical Conference; 26–28 April 2010. Valletta, Malta: IEEE. pp. 1522-1527
- [13] Villalva MG, Gazoli JR, Ernesto RF. Comprehensive approach to modeling and simulation of photovoltaic arrays. IEEE Transactions on Power Electronics. 2009;**24**:1198-1208
- [14] Nema P, Nema RK, Rangnekar S. A current and future state of art development of hybrid energy system using wind and PV-solar. Renewable and Sustainable Energy Reviews. 2009;**13**:2096-2103
- [15] Garcia A, Balenzategui JL. Estimation of photovoltaic module yearly temperature and performance based on nominal operation cell temperature. Renewable Energy. 2004;**29**: 1997-2010
- [16] Cabal C. Optimisation énergétique de l'étage d'adaptation électronique dédié à la conversion photovoltaïque [Phd]. Toulouse, France: Paul Sabatier III University; 2008
- [17] Hohm DP, Ropp ME. Comparative study of maximum power point tracking algorithms using an experimental programmable maximum power point tracking test bed. In: IEEE 2000 Photovoltaic Specialists Conference; 15-22 September 2000; Anchorage, Alaska, USA: IEEE. pp. 1699-1702
- [18] Femia N, Petrone G, Spagnuolo G, Vitelli M. Optimization of perturb and observe maximum power point tracking method. IEEE Transactions on Power Electronics. 2005;**20**:963-973
- [19] Sera D, Kerekes T, Teodorescu R, Blaabjerg F. Improved MPPT algorithms for rapidly changing environmental conditions. In: Power Electronics and Motion Control Conference 2006; 30 August-1 September 2006; Portoroz, SLOVENIA: IEEE. 2006. pp. 1614-1619
- [20] Onat N. Recent developments in maximum power point tracking technologies for photovoltaic systems. International Journal of Photoenergy. 2010;**2010**:11. Article ID 245316. DOI: 10.1155/2010/245316

- [21] Xiao W, Dunford WG. Evaluating maximum power point tracking performance by using artificial lights. In: IEEE 2004 Industrial Electronics Society; 2–6 November 2004. Busan, Korea: IEEE; 2004. pp. 2883-2887
- [22] Shimizu TH, Kimura OG. A novel high performance utility interactive photovoltaic inverter system. IEEE Transactions on Industrial Electronics. 2003;18:704-711
- [23] Nur AK, Chee WT. A comprehensive review of maximum power point tracking algorithms for photovoltaic system. Renewable and Sustainable Energy Reviews. 2014;37:585-598
- [24] Lee JH, Bae H, Cho BH. Advanced incremental conductance MPPT algorithm with a variable step size. In: Power Electronics and Motion Control Conference; 30 August-1 September 2006, 2006. Portoroz, SLOVENIA: IEEE. pp. 603-607
- [25] Kim TY, Ahn HG, Park SK, Lee YK. A novel maximum power point tracking control for photovoltaic power system under rapidly changing solar radiation. In: IEEE 2001 International Symposium on Industrial Electronics; 12–16 June 2001. Busan, Korea: IEEE; 2001. pp. 1011-1014
- [26] Oi A. Design and simulation of photovoltaic water pumping system [MSc]. California, USA: California Polytechnic State University; 2005
- [27] Pongratananukul N. Analysis and simulation tools for solar array power systems [Phd]. Florida, USA: Central Florida Orlando University; 2005
- [28] Luque A, Hegedus S. Handbook of Photovoltaic Science and Engineering. USA: John Wiley & Sons Ltd; 2003
- [29] Group 01gr509. Power Supply for the AAU Cubesat. Report. AALBORG University; 2001
- [30] Erickson RW. Fundamentals of Power Electronics. New York, NY: Chapman & Hall; 1997

# We are IntechOpen, the world's leading publisher of Open Access books Built by scientists, for scientists

6,300

Open access books available

171,000

International authors and editors

190M

Downloads

Our authors are among the

154

Countries delivered to

TOP 1%

most cited scientists

12.2%

Contributors from top 500 universities



WEB OF SCIENCE™

Selection of our books indexed in the Book Citation Index  
in Web of Science™ Core Collection (BKCI)

Interested in publishing with us?  
Contact [book.department@intechopen.com](mailto:book.department@intechopen.com)

Numbers displayed above are based on latest data collected.  
For more information visit [www.intechopen.com](http://www.intechopen.com)



---

# A Quick Maximum Power Point Tracking Method Using an Embedded Learning Algorithm for Photovoltaics on Roads

---

Koichiro Yamauchi

Additional information is available at the end of the chapter

<http://dx.doi.org/10.5772/intechopen.79711>

---

## Abstract

This chapter presents a new approach to realize quick maximum power point tracking (MPPT) for photovoltaics (PVs) bedded on roads. The MPPT device for the road photovoltaics needs to support quick response to the shadow flickers caused by moving objects. Our proposed MPPT device is a microconverter connected to a short PV string. For real-world usage, several sets of PV string connected to the proposed microconverter will be connected in parallel. Each converter uses an embedded learning algorithm inspired by the insect brain to learn the MPPs of a single PV string. Therefore, the MPPT device tracks MPP via the perturbation and observation method in normal circumstances and the learning machine learns the relationships between the acquired MPP and the temperature and magnitude of the Sun irradiation. Consequently, if the magnitude of the Sun beam incident on the PV panel changes quickly, the learning machine yields the predicted MPP to control a chopper circuit. The simulation results suggested that the proposed MPPT method can realize quick MPPT.

**Keywords:** photovoltaics bedded on road, embedded learning algorithm, incremental learning, insect brain, modal regression on a fixed memory budget, maximum power point tracking (MPPT), shadow flicker, partial shading, micro converter

---

## 1. Introduction

In recent years, renewal energy technologies have attracted considerable attention as they prevent degradation of the environment to a large extent. Photovoltaics (PVs) are one such technology. However, the drawbacks of photovoltaic systems are that they are unstable while generating electricity and that they require a wide area to catch a large amount of sunlight.

---

One solution is to place photovoltaics on roads. As the total area covered by roadways in the world is extremely high, it is worth using it as PV sites. Still, objects moving on the road cause shadows. In particular, the shadow flickers on PV systems cause power conditioners connected to the PVs to behave in an unstable manner. Such unstable behavior forms the origin of degradation and greatly reduces the amount of electricity generated.

As shown in Section 2, PVs demonstrate highly nonlinear characteristics and its maximum power point cannot be analytically derived. Therefore, maximum power point tracking (MPPT) devices track MPP using various heuristics. As mentioned in previous survey papers [1, 2], the most preliminary technique for realizing MPPT is the perturbation and observation (P&O) method. P&O is a type of hill-climbing algorithm. The P&O method provides a perturbation to the current and the voltage and checks whether the output power increases. If the power has increased, the P&O method employs the same voltage change in the next step and vice versa. Although the P&O method is easy to implement within small embedded systems, there is no guarantee that the perturbed voltage is suitable for obtaining MPP. The incremental conductance (IncCond) [3] and the ripple correlation (RCC) methods [4] overcome this problem by estimating the gradient of the power curve. These two methods can be realized in analog circuits and can demonstrate quick convergence behaviors. Fuzzy logic control methods are also usually used for controlling the change in duty ratio for the chopper circuit. Fuzzy logic controllers can work appropriately even if its inputs are ambiguous, and they show a quick convergence behavior to the MPP. For example, a previous paper [5] demonstrated the use of fuzzy logic that yielded a change in the duty ratio from the difference between the current photovoltaic output voltage and the predicted MPP. Neural network-based MPPT methods are also proposed (e.g., [6]). The model predicts MPP and its corresponding maximum current using a pretrained neural network. The model cannot adjust its neural network for changing environments. In our previous study, a hybrid system involving the P&O method and an embedded learning machine was constructed [7]. The learning machine studies the MPP acquired by the P&O method when solar irradiation is stable. When solar irradiation changes quickly, the learning machine predicts MPP. However, these methods do not support MPPT under an inhomogeneous isolation condition, where the voltage-power curve has several local peaks.

Recently, a particle swarm optimization (PSO)-based MPPT method was proposed [8]. This method can estimate all local power peak points and select the best one. However, the resultant solutions are highly depending on the initial particles.

On the contrary, a previous study [9] demonstrated that a swing technique can acquire the voltage-power curve by scanning within a certain short interval. It shorts the series-connected PV string and an inductor simultaneously observe the voltage and power until the output voltage reaches zero. Therefore, the device can detect MPP during the scan. However, it needs special hardware to realize the swing.

To overcome this problem, we use a quick converter connected to a PV string. The main challenge here is finding the MPP from the complex power-voltage curve.

In our previous study [7], we proposed a model that uses an incremental learning method based on general regression neural network. The method is used to obtain the magnitude of solar irradiation  $s_t$ , temperature  $T_t$ , and MPP derived by the P&O method. Although the system

quickly detects MPPs of a single solar panel, which has a single cluster, it cannot detect the MPP of solar panels with several clusters or solar panels connected in series.

In this chapter, we propose an MPPT converter that detects MPPs of solar panels with several clusters using a modal regression method on a fixed memory budget. To realize quick MPPT, the proposed method uses a learning machine on a fixed memory budget. The learning machine on a fixed budget is a small learning machine that can continue online learning on a fixed storage space. Therefore, it is suitable to be embedded to a small microcomputer. The learning on a budget should be executed on a system with a small amount of storage space with low computational power.

To this end, it is worth referencing the mechanisms of an insect's brain. Although the precise mechanism of an insect's small brain that is a source of their intelligence is not known, it is true that their sensory system is much smaller than that of humans. Therefore, the dimensions of their sensory inputs are small. As mentioned in Section 3.2, the storage space for recording the kernels is proportional to the number of input dimensions. From this insight, we should be able to reduce the input dimensions to reduce the storage space for the learning machine.

The rest of the chapter is organized as follows. Section 2 describes the photovoltaic properties, and Section 3 introduces an MPPT algorithm accelerated by a learning machine using a modal regression on a budget. Section 4 shows computer simulation results of the new MPPT algorithm, and Section 5 concludes this chapter.

## 2. Properties of photovoltaics

Photovoltaics are a type of current sources, whose current flow is determined by the strength of solar irradiation. A normal solar panel comprises several photovoltaic cells. These cells are usually connected in series, and the series-connected cells are then connected in parallel. Such solar panels show highly nonlinear characteristics and is usually modeled by using the following equation [10, 11]. Let us denote the output voltage and current from the photovoltaic as  $V_{pv}$  and  $I_{pv}$ , respectively. According to the equivalent circuit shown in **Figure 1**,  $I_{pv}$  is represented by (1).

$$I_{pv} = N_p I_{sc} \left( \frac{I_r}{100} \right) - N_p I_o \left[ \exp \left( \frac{qV_{pv}}{nkTN_s} \right) - 1 \right], \quad (1)$$

where  $V_{pv}$ , the terminal voltage of the photovoltaic [V];  $I_{pv}$ , output current from the photovoltaic [A];  $I_p$ , photocurrent [A];  $I_o$ , saturation current [A];  $I_{sc}$ , short-circuit current [A];  $I_r$ , irradiation [%];  $n$ , ideality factor;  $q$ , charge of electron [C];  $k$ , Boltzmann's constant;  $T$ , junction temperature [°C];  $N_p$ , number of cells in parallel;  $N_s$ , number of cells in series.

In Eq. (1),  $I_r$  is given by the ratio of actual strength of solar irradiation to the irradiation of standard test condition [11]. Therefore,  $I_r = 100G/G_{ref}$ , where  $G$  and  $G_{ref}$  are solar irradiation ( $w/m^2$ ) and that of under the standard test condition:  $G_{ref} = 1000(w/m^2)$ , respectively. The range of  $I_r$  is  $I_r \in [0, 100]$ . An example of the output voltage and current relationship is shown in **Figure 2**. We can see that the solar panel is a type of current sources, but the current is

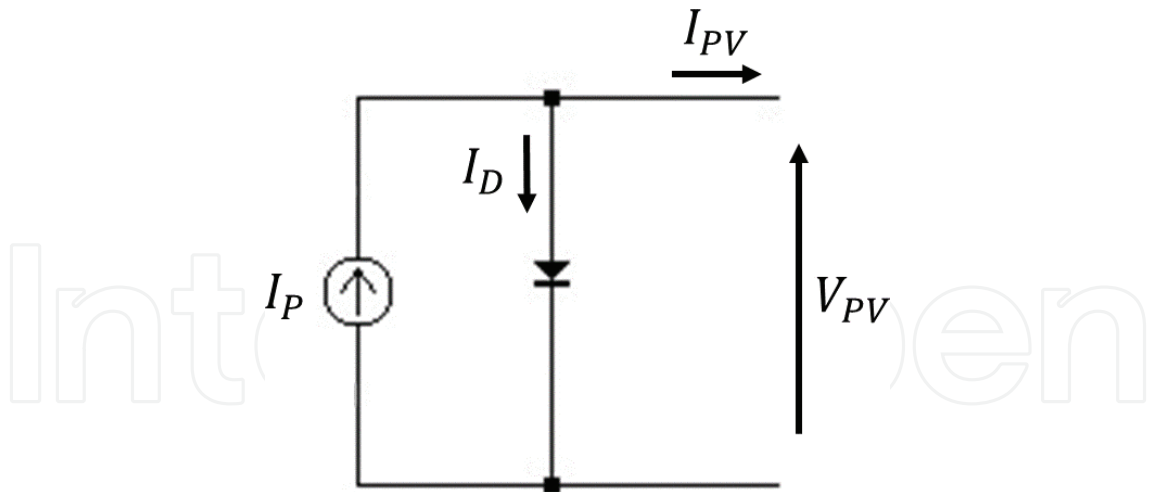


Figure 1. Equivalent circuit of a photovoltaic.

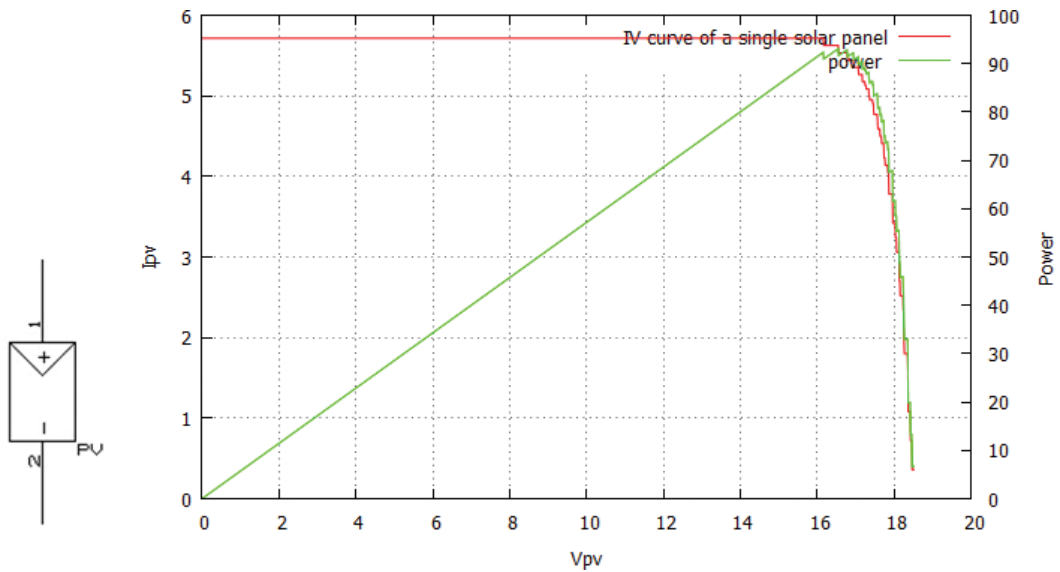
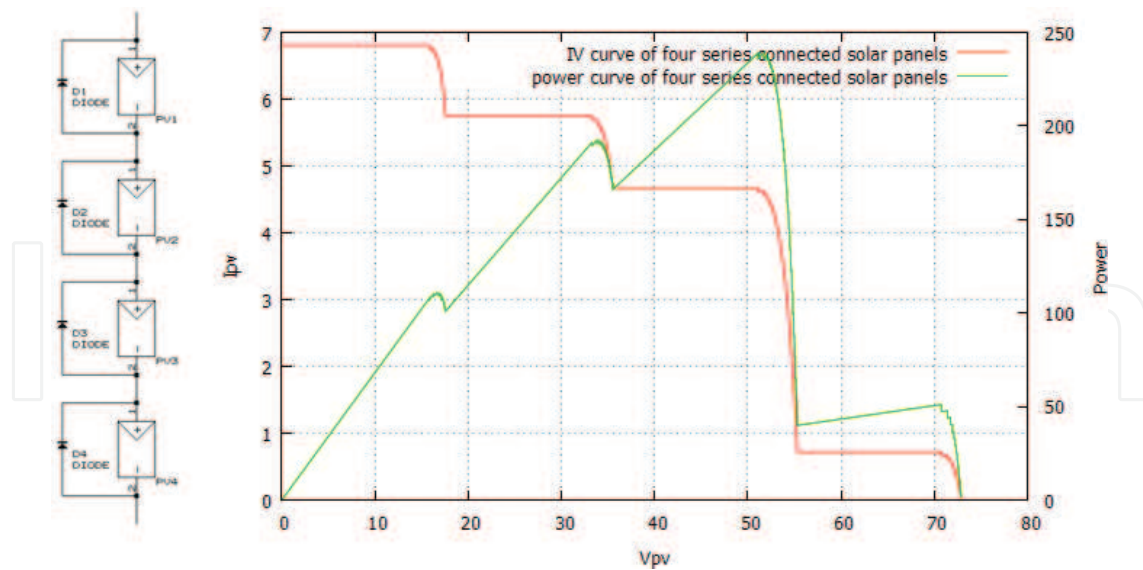


Figure 2. Single solar panel property. ( $I_r = 80\%$ ,  $N_p = 4$ ,  $N_s = 12$ ,  $I_{sc} = 1.8[A]$ ,  $T = 298.15$ ,  $q = 1.6 \times 10^{-19}$ ).

reduced when the voltage is higher than a certain value. The solar panel does not pass current if the panel is covered by a shadow. If series-connected solar panels have a partial shadow, the output current from the solar panels are down to zero even if a part of solar panels do not have a shadow. To prevent such a situation, a bypass diode is connected to each solar panel in parallel. Using this circuit, the solar panels can generate a certain amount of electricity even if they are partially shadowed. Such series-connected solar panels, however, show highly nonlinear characteristics (see **Figure 3**).

To extract maximum power, the voltage of the photovoltaic should be maximized. However, if the voltage is too high, the current decreases. Therefore, there is an optimal voltage value that maximizes the power. Such voltage is called the MPP and the power conditioner or converter connected to the PV tracks the MPP.



**Figure 3.** An example of series-connected solar panel property. The irradiancies for the four panels are 10, 80, 65, and 95%.

Another noticeable property is that the current flow of photovoltaics stops when it has a shadow. Thus, if a photovoltaic is connected to the other photovoltaics in series and it has a shadow, no power is outputted from the series-connected solar panels.

This problem is solved by connecting a bypass diode in parallel with each photovoltaic. Using this architecture, we can get some amount of power even if a part of the solar panels are under a shadow. However, in such a case, the voltage-power curve of the photovoltaics shows a nonlinear form. As the voltage-power curve has several peaks, the power conditioner cannot obtain the correct MPP only using a hill-climbing technique. The most reliable method to solve this problem is for the power conditioner/DC converter to acquire the current voltage-power curve and detect the global maximum point.

### 3. MPPT algorithm accelerated by learning machines

One way to realize a quick MPPT without involving any special device is to use a photovoltaic model to predict the MPP. Moreover, the apparent property of photovoltaic varies due to the accumulated dust on the solar panel surfaces. This means that the photovoltaic model is not stable, but is valid depending on the solar panel's situation. To adjust to such changes in the property, an on-site learning machine should learn the MPP acquired by the P&O method to construct the PV model and apply prediction using the learning machine. In our previous work [7], we demonstrated that an incremental learning method on a budget on a microcomputer can manage the learning and prediction of MPPs. The learned results were applied only when solar irradiation changes drastically and the learning machine know the appropriate MPP that fits the current situation.

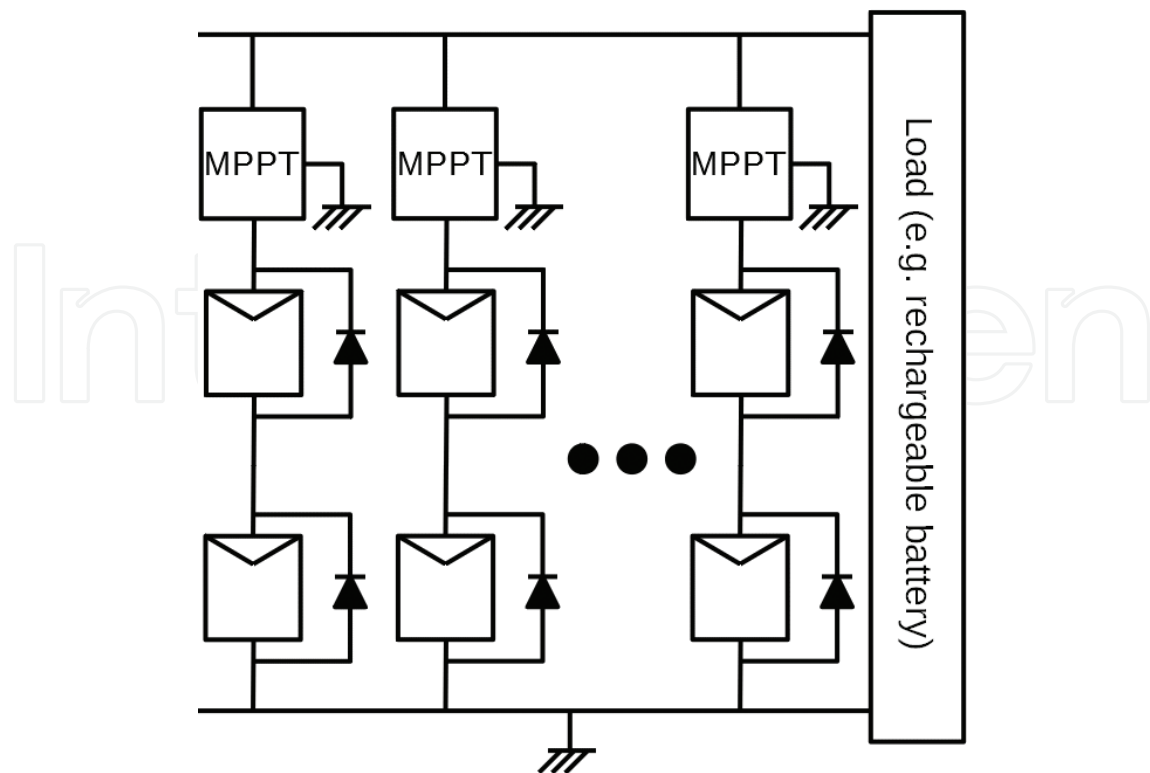


**Figure 4.** The photovoltaic circuit design bedded on road. Several solar panel strings with the MPPT converter are connected in parallel.

The previous system, however, cannot support the MPPT for series-connected PVs with bypass diodes, as shown in **Figure 4**. This is because even if the strength of solar irradiation is a certain stable value, there are several different solutions depending on the variety of the shadow patterns on the solar panels. To overcome this difficulty, we propose a new MPPT method in this chapter that is based on modal regression on a budget, which is a modal regression with a fixed number of kernels. Modal regression has the ability to approximate multivalued functions. Modal regression on a budget continues the learning with a fixed number of kernels so that it is suitable to be embedded in a small microcomputer. Therefore, it is able to record several different MPPs corresponding to the strength of solar irradiation. The proposed MPPT has a modified P&O method that enables tracking of MPPs from the voltage-power curve having several peaks using modal regression on a budget.

During the service, the proposed MPPT tracks the peaks by changing the initial search points. If an MPP is observed, the kernel density estimator (KDE) in the modal regression records the peak by adding a new kernel that records the current peak (see **Figure 5**). However, the microcomputer has limited storage space. Thus, if the number of kernels in the KDE equals the budget, one of the existing kernels will be replaced by the new kernel.

### 3.1. A perturbation and observation (P&O) method with changing initial point

Even if the system uses modal regression, it cannot be used before learning. Thus, it needs to obtain the MPPs first. To find several peaks, a modified P&O method is presented. The modified

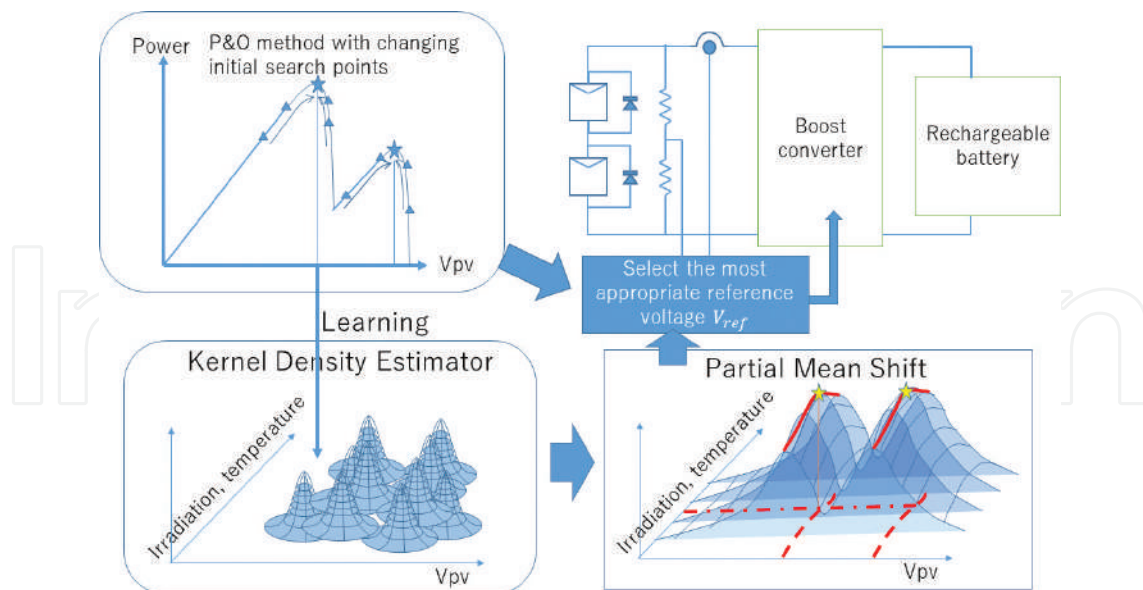


**Figure 5.** Outline of the MPPT accelerated by the modal regression on a budget.

one searches the peak points roughly at first. For example, if the solar panel comprises  $m$  number of clusters, the number of peaks would be up to  $m$ . Therefore, the new P&O estimates following  $C (> m)$  initial points. This operation concludes when irradiation is greatly changed.

$$v_n^i = n \frac{V_{pv}^{max}}{C}, \text{ where } n = 1, \dots, C, \quad (2)$$

where  $V_{pv}^{max}$  denotes the open circuit voltage of the photovoltaic. To obtain this value, the circuit should be opened for a while when the irradiation changes. The system finds the  $v_{n^*}^i$  that leads to maximum MPP.

$$n^* = \text{argmax}_n \{P_{pv}(v_n^i)\}, \quad (3)$$

where  $P_{pv}(v_n^i)$  denotes the power from the solar panel for the voltage  $v_n^i$ . In this method,  $m$  number of clusters are needed to be preset.

### 3.2. Modal regression on a budget for reasoning from too less sensory inputs

In general, if the device has too few sensors, the system cannot properly detect the current status. The partial shadow problem is one such problem. Therefore, if the device has illuminance sensors for each solar cell, it can accurately detect the status and can form complete relationships between the large number of sensory inputs and MPP. However, such strategy is impractical for real applications. Moreover, we should reduce the number of dimensions to construct an insect's brain like compact learning machine. From a theoretical viewpoint, the system having too few sensory inputs should yield several possible solutions. Therefore, the system has to check the suitability of all possible solutions and choose the best solution. One way to solve this problem is to employ a quick search

algorithm such as the PSO algorithm. However, PSO searches possible solutions for arbitrary initial setting of particles and wasted some time for the search. An alternative way to speed up the procedure is by implementing a learning machine to quickly obtain some good solution candidates. However, to realize such tasks, the learning machine has to have an ability to approximate multivalued functions. Such ability cannot be served by normal regression methods.

Modal regression approximates a multivalued function to search the local peaks of a given sample distribution. Modal regression comprises the KDE with a partial mean shift (PMS) method. We have already presented a minimum modal regression, which minimizes the number of kernels for the modal regression [12].

The model, however, does not support learning on a fixed budget. In this chapter, we propose an improved version of our previous work, which enables learning on a fixed budget.

### 3.2.1. Original modal regression method

Modal regression comprises KDE followed by the PMS. KDE is a variation of the Parzen window [13]. Let  $\mathfrak{X}$  be the set of learning samples and  $\mathfrak{X} = \{\mathbf{x}_p \in \mathfrak{X}^N | p = 1, 2, \dots, N\}$ . The estimator approximates the probability density function using a number of kernels, namely the support set  $S_i$ . The kernels used are Gaussian kernels and

$$p(\mathbf{x}) \propto \sum_{i \in S_i} K\left(\frac{\|\mathbf{x} - \mathbf{x}_i\|}{h_x}\right) \quad (4)$$

where

$$K\left(\frac{\|\mathbf{x} - \mathbf{x}_i\|}{h_x}\right) \equiv \exp\left(-\frac{\|\mathbf{x} - \mathbf{x}_i\|^2}{h_x^2}\right) \quad (5)$$

Normally, the same number of kernels as that of the dataset is required. However, if the storage capacity of a target device is small, the number of kernels must be restricted. There are several ways to realize density estimation using a limited number of kernels. Traditionally, self-organizing feature maps or learning vector quantization methods approximate the distribution using a fixed number of templates.

As mentioned in a previous study [14], the KDE used in modal regression should approximate the number of peak points of the distribution, rather than the distribution itself. Let  $\hat{p}(\mathbf{x})$  be

$$\hat{p}(\mathbf{x}) \equiv \sum_{i \in S_i} K\left(\frac{\|\mathbf{x} - \mathbf{x}_i\|}{h_x}\right) \quad (6)$$

then  $\hat{p}(\mathbf{x})$  should satisfy the following condition.

$$\begin{cases} \nabla_x \hat{p}(x)|_{x=x^*} = \nabla_x p(x)|_{x=x^*} = 0 \\ \nabla_x^2 \hat{p}(x)|_{x=x^*} < 0, \nabla_x^2 p(x)|_{x=x^*} < 0 \end{cases} \quad (7)$$

where  $x^*$  denotes a local peak point of the distribution.

Modal regression searches the peaks of the distribution model represented by the KDE. The PMS method realizes quick convergence to the nearest peak from the initial point. Let us denote the initial point as  $x_0$ , representing the starting point for searching the peaks. Thus, modal regression repeats the modification of the current  $y$  as follows:

$$y_{new} \leftarrow \frac{\sum_i y_{old} K\left(\frac{|y_{old}-y_i|}{h_y}\right) K\left(\frac{\|x-x_i\|}{h_x}\right)}{\sum_j K\left(\frac{|y_{old}-y_j|}{h_y}\right) K\left(\frac{\|x-x_j\|}{h_x}\right)} \quad (8)$$

### 3.2.2. Modal regression on a fixed budget

To embed the modal regression, we have to pay attention to how to reduce the number of kernels for the KDE. Especially, we have to fix the upper bound for the number of kernels. In this case, the aim of the KDE is to approximate the peaks in the distribution rather than approximating the distribution. From this viewpoint, we should prune redundant kernels that do not contribute to approximating the peaks.

In our previous work [12], we demonstrated that the kernel, which is linearly dependent on the other kernels, can be removed without changing existing peaks. To this end, before pruning, the pruned kernel should be projected to the space spanned by the other remaining kernels. However, preparing the gram matrix wastes huge memory space.

Moreover, in this practical application, we should pay attention to the concept drift phenomena, wherein the labels change over time. This is caused by environmental changes such as the accumulation of dust on the solar panels and the changes in properties of the solar panel materials. The learning methods should support these issues.

To overcome these difficulties, we propose a simplified version of the modal regression method on a fixed number of kernels.

To discuss the learning rule of the KDE, let us rewrite the kernel output value as the dot product of the two vectors of  $k(x_i, \cdot)$  and  $k(x, \cdot)$  as follows.

$$\langle k(x_i, \cdot), k(x, \cdot) \rangle \equiv K\left(\frac{\|x-x_i\|}{h_x}\right), \quad (9)$$

where  $\langle \cdot, \cdot \rangle$  denotes the dot product operator. This expression is based on the kernel method. Fortunately, the Gaussian kernel is a type of reproducing kernel in which we can rewrite the learning rule using the dot product of vectors. Using this representation, we can rewrite the

learning rule in algebraic expressions, which can be very easily understood. Now, let us denote a vector  $\widehat{P}_t$  as the learning result after the  $t$ -th sample presentation. Then, we obtain

$$\widehat{P}_{t-1} \equiv \sum_{i \in S_{t-1}} W_i k(\mathbf{x}_i, \cdot), \quad (10)$$

where  $S_{t-1}$  denotes the support set after the  $t - 1$ -th presentation of a given sample. The KDE output to an input vector  $\mathbf{x}$  is calculated by

$$\widehat{P}_{t-1}(\mathbf{x}) = \langle \widehat{P}_{t-1}, k(\mathbf{x}, \cdot) \rangle. \quad (11)$$

Eq. (10) enables us to represent the learning rule as

$$\widehat{P}_t = \widehat{P}_{t-1} + y_t k(\mathbf{x}_t, \cdot), \quad S_t = S_{t-1} \cup \{t\} \quad (12)$$

However, the proposed method restricts the number of kernels to a certain number as  $|S_t| \leq B$ . To overcome this problem, the proposed method replaces one of the kernels with a new kernel whose centroid is the new input vector, or moves the nearest kernel centroid to close to the current new input vector. Therefore, if the nearest kernel

$$n_t = \underset{j}{\operatorname{argmin}} \left\{ \|\mathbf{x}_t - \mathbf{x}_j\|^2 \right\}, \quad (13)$$

satisfies the following condition

$$\|\mathbf{x}_t - \mathbf{x}_{n_t}\|^2 < \theta_{\text{activity}}, \quad (14)$$

its kernel center is modified to be the mean vector of the original kernel center and the new sample as follows. The extension coefficient  $W_{n_t}$  is increased by  $\Delta$ .

$$\mathbf{x}_{n_t} = \frac{\left(\frac{W_{n_t}}{\Delta}\right) \mathbf{x}_{n_t} + \mathbf{x}_t}{\left(\frac{W_{n_t}}{\Delta}\right) + 1}, \quad W_{n_t} = W_{n_t} + \Delta \quad (15)$$

The extension coefficient includes information on how many samples did the kernel learn. The extension coefficient is also reflected to a weighted PMS method in Eq. (20). However, if the kernel center does not satisfy the Eq. (14), one of the kernels should be replaced with the new tentative kernel. Therefore, if the new sample  $\mathbf{x}_t$  is too far from the nearest kernel center, one of the kernels should be replaced with it to adjust to the new sample. In such a case, the least recently or frequently used (LRFU) kernel is to be replaced with the new one. The LRFU evaluation method proposed in [15] is an improved version of the LRU page-replacement algorithm for virtual memory systems on operating systems. Using this evaluation method, the most ineffective kernel, which seems to be unused for a long time interval, is replaced with the new kernel. To realize this evaluation, a variable that represents the value of each kernel is introduced. Let  $C_i$  be the value of the  $i$ -th kernel. When the  $i$ -th kernel centroid is the closest to current sample  $\mathbf{x}_t$ ,  $C_i$  is enlarged, but is decreased, otherwise. Therefore, for each round, the following equation is executed.

$$C_i = \begin{cases} C_i + 1, & i = n_t \\ \eta C_i, & i \neq n_t \end{cases} \quad (16)$$

where  $\eta = 1 - \epsilon$ ,  $\epsilon \ll 1$ . Then, the  $j^* = \operatorname{argmin}_i C_i$  kernel is to be replaced with the new kernel. Therefore,

$$x_{j^*} = x_t, \quad w_{j^*} = \Delta, \quad C_{j^*} = 1, \quad y_{j^*} = y_t \quad (17)$$

$h_x$  determines the width of each kernel. The performance of the system is also sensitive to this value, so we have to set this value carefully. In a previous study [16], the optimal value of  $h_x$  for a standard distribution was derived as

$$h_x = \left( \frac{4}{d+2} \right)^{\frac{1}{d+4}} n^{-\frac{1}{d+4}}, \quad (18)$$

where  $d = \dim(x_t)$  is the dimension of the input vector and  $n$  is the number of samples. In this study, the number of samples is unknown. However, the number of kernels are bounded to the budget  $B$  so that  $n = B$ . Equation (18), however, cannot be used for practical applications. Therefore, we should consider a scaling factor for (18). To this end, in this study, we rewrite (18) as follows.

$$h_x = v_0 \cdot \left( \frac{4}{d+2} \right)^{\frac{1}{d+4}} n^{-\frac{1}{d+4}}, \quad (19)$$

where  $v_0$  denotes the scaling factor and was set to 0.3 in this simulation described in Section 4. Actually, in the simulation described in Section 4, each input dimension was normalized before the execution of the modal regression. Concretely, each element of  $x_t$  of modal regressor was multiplied by a gain  $g_i$  to make the range of the  $i$ th element of  $x_t$  be  $|g_i x_{ti}| \leq 1$ . The output from the modal regressor (20) was divided by the corresponding gain  $y = y/g_o$ . For simplicity, however, following text omit the description of these gains.

The regression output is also delivered by the PMS method described in (8). In this model, the PMS method should account for the extension parameter  $W_i$ . To this end, this method also uses the weighted PMS method as is done in our previous work [12]. Note that (20) includes the extension parameter  $W_i$  in both the numerator and the denominator.

$$y_{new} \leftarrow \frac{\sum_i y_{old} W_i K\left(\frac{|y_{old} - y_i|}{h_y}\right) K\left(\frac{\|x - x_i\|}{h_x}\right)}{\sum_j W_j K\left(\frac{|y_{old} - y_j|}{h_y}\right) K\left(\frac{\|x - x_j\|}{h_x}\right)} \quad (20)$$

The weighted PMS should be repeated by substituting derived  $y_{new}$  to  $y_{old}$  until it converges to a certain value. In the computer simulation described in Section 4, the weighted PMS was repeated 10 times for every initial point. This process is executed for all initial values of  $y_{old}$  to obtain all local peaks. The simplest way to set the initial points is choosing uniform random initial values for  $y_{old}$ . However, the random initial values usually make some unexpected

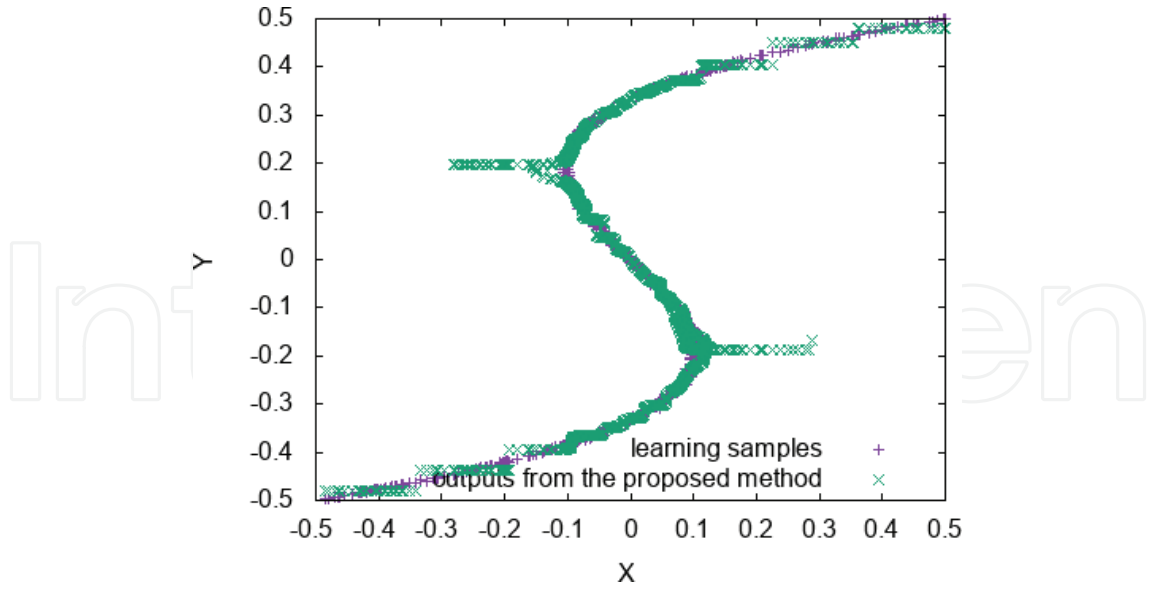


**Figure 6.** The response for the third-order data. The green curve is the response of the proposed model with 50 kernels.

converged values for  $y$ . To more appropriately set up the initial value  $y_0$ , the proposed method chooses the initial value as the corresponding element of each kernel center. Therefore, let us assume that a kernel center  $x_i$  is similar to the current input. Then, the initial value should be  $y_0 = x_{ij}$ , where  $j$  is the corresponding unknown dimension. The set of such kernel centers is

$$S_{active} \equiv \left\{ i \mid \exp \left( \sum_{j \neq \text{unknown}} \frac{-(x_{ij} - x_{tj})^2}{h_x^2} \right) > \theta_{init} \right\}, \tag{21}$$

where  $\theta_{init}$  denotes the threshold for choosing the kernel. The above equation does not contain the distance calculation for the unknown dimension. The initial values for  $y_0$  are

$$y_0 = x_{k \text{ unknown}} \text{ where } k \in S_{init}. \tag{22}$$

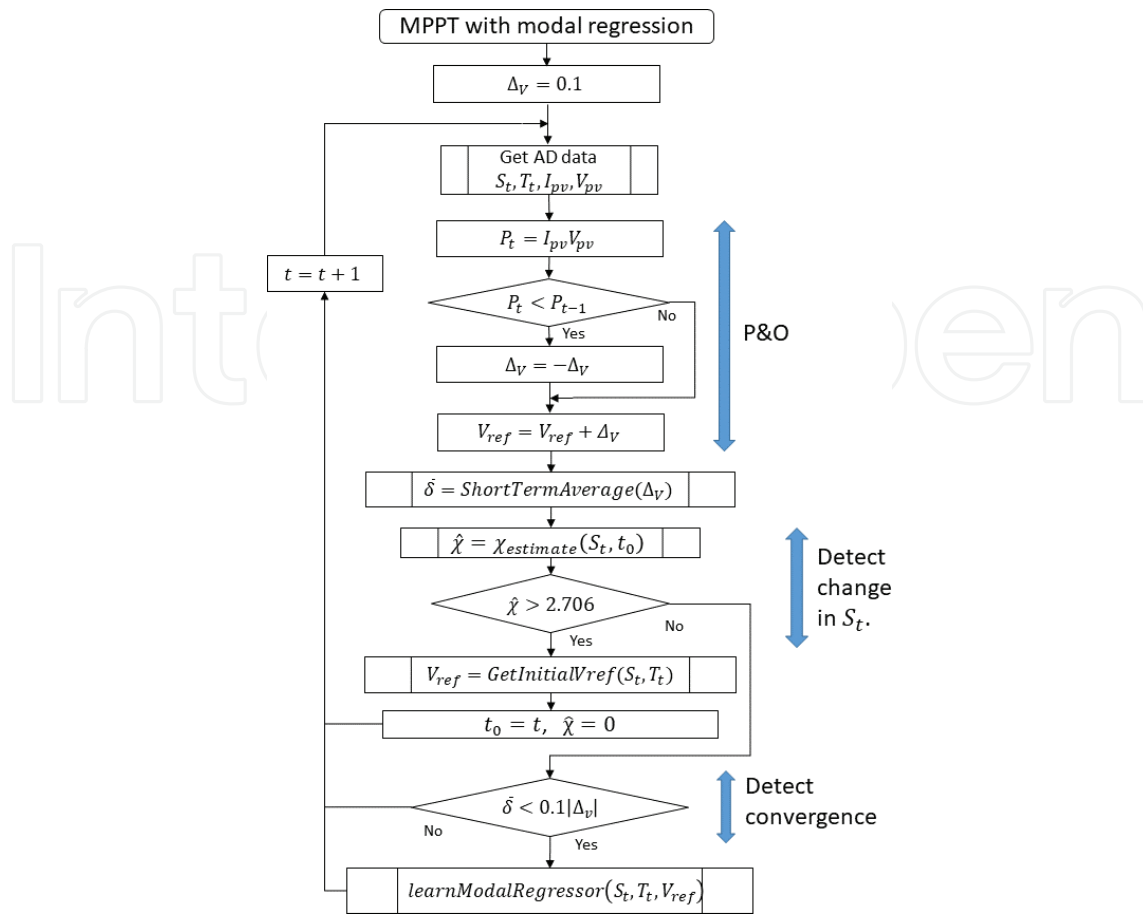
### 3.2.3. An example of the modal regression outputs

The modal regression approximates multivalued functions. As an example, **Figure 6** shows the regression output for 800 sets of third-order synthetic data with 50 kernels. We can observe that the proposed method partly approximates multivalued function.

### 3.3. Whole algorithm

**Algorithms 1–4** are presented below. Note that  $S_t$  in these algorithms shows the averaged solar irradiation for all clusters. Therefore, solar irradiation is assumed to be sensed by a single illuminance sensor; thus, the obtained value is the average of the values of both clusters.

The algorithm is roughly divided into two parts: one is the normal P&O part, and the other deals with searching for the reference voltage using the proposed modal regression. The second part is executed when the solar irradiation is changed abruptly.

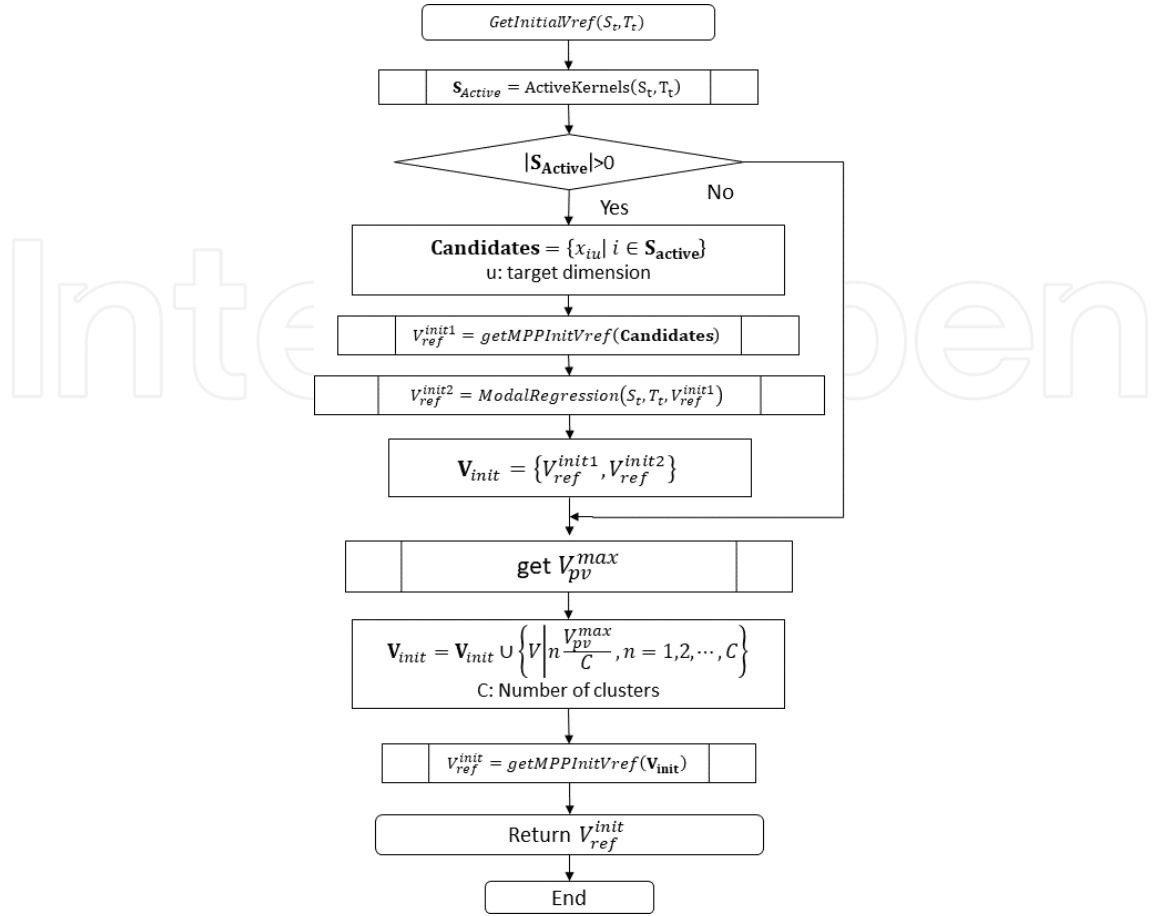


**Algorithm 1.** Algorithm of the MPPT with modal regression. Note that  $V_{ref}$  is referenced by the proportional-integral-derivative (PID) control thread at each time interval.  $GetInitialVref()$  is described in **Algorithm 2**.  $learnModalRegressor()$  is described in Eqs. (12)–(19).

To this end, the sensed solar irradiation is statistically analyzed by  $\chi_{estimate}(S_t, t_0)$ , that is chi-square test for  $S_t$  from the previously changed time  $t_0$  till now. If it includes an obvious change, **Algorithm 2** is called to search for an appropriate initial  $V_{ref}$ 's for searching the optimal value of  $V_{ref}$ . **Algorithm 2** is the algorithm for searching initial  $V_{ref}$ . This algorithm conducts a search using the proposed modal regressor followed by a search of the initial  $V_{ref}$  using the proposed modified P&O algorithm described by Eq. (2). The reason why it executes an additional search is that there is a possibility that the modal regressor yields incomplete solution candidates. Such a situation usually occurs when the modal regressor is in the early stage of learning.

### 3.4. Computational cost and required memory capacity

The computational cost for the MPPT with modal regression is mainly wasted by the modal regressor. Hence, let us consider the computational cost for the modal regression. Now, we assume that the number of kernels in the modal regressor is  $B$  and that the number of dimensions is  $N$ . Note that  $N=3$  because input vector is  $x_t = [S_t, T_t, V_{ref}]^T$ . To calculate the kernel outputs for current input  $x_t$ , it needs  $(N+1)B$  times multiplies and  $B$  times of division and  $B$  times of calculation of  $\exp()$ . If we assume that the calculation of  $\exp()$  is  $C_{exp}$ , the



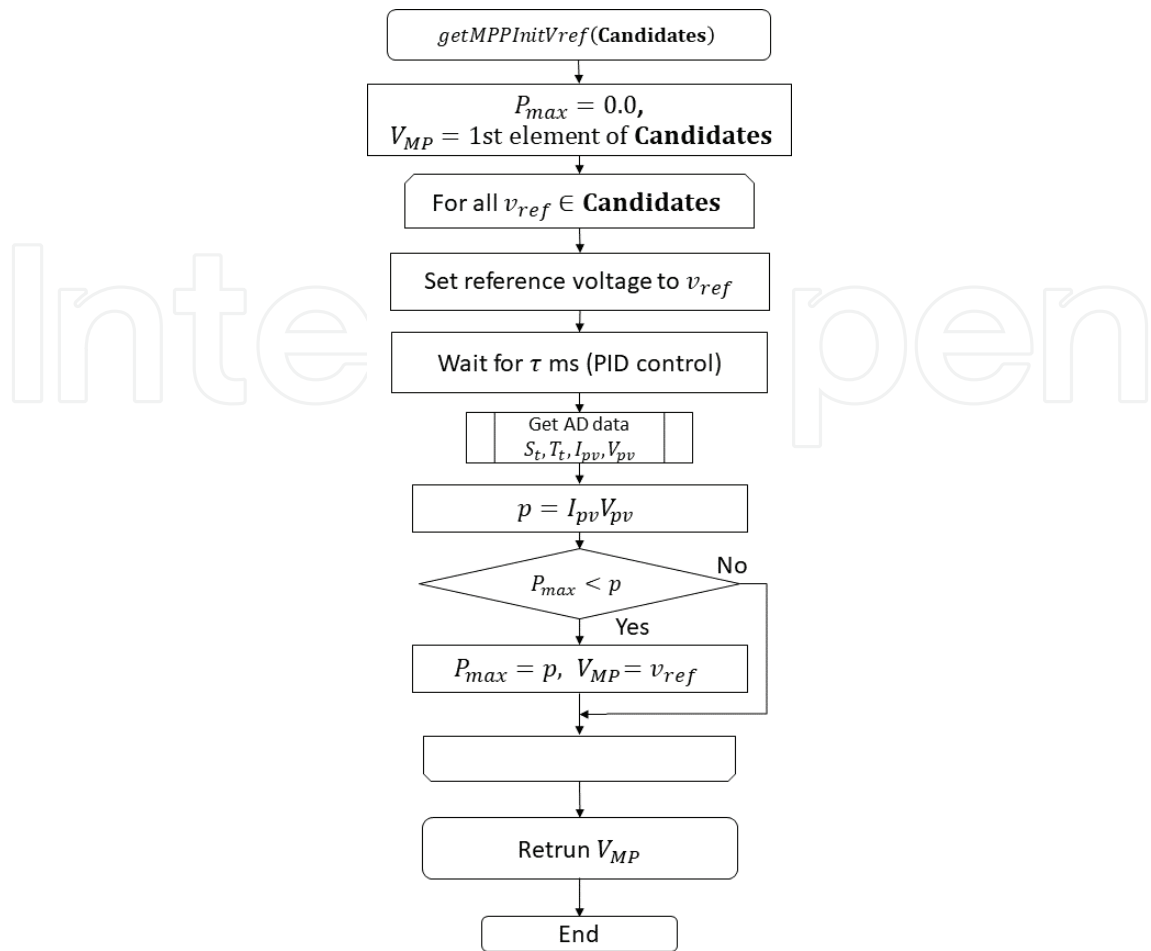
**Algorithm 2.** Pseudo code for getting initial reference voltage.  $ActiveKernels()$  is derived by (21).  $getMPPInitVref()$  is described in **Algorithm 3**.  $ModalRegression()$  is the five time repeats of the partial mean shift:(8).

computational cost is proportional to  $B(N+2+C_{exp})$ . Therefore, to derivate a kernel set  $S_{active}$  in (21), it needs  $O(B)$ . The partial mean shift (20) needs  $B(N+8+2C_{exp})+B(N+7+2C_{exp})+1=B(2N+15+4C_{exp})+1$ . Thus, if the partial mean shift is repeated for  $M$  times for each trial, the total computational power of modal regression is proportional to  $MB(2N+15+4C_{exp})+1$ .

The computational power required for the learning of the modal-regressor is the cost of executing (13), (14), and (16). Thus, it needs  $BN+N+(2N+1)$  multiplications. After all, the computational complexity of the modal regression is  $O(B)$ .

The required memory capacity also depends on the number of kernels. Each kernel records the center of kernel  $x_i$ , corresponding label  $y_i$ , the extension parameter  $W_i$  and the parameter  $C_i$  for the LRFU estimation. As each float variable requires 4 bytes, one kernel requires  $4(N+2)$  bytes. Thus, the total amount of memory storage for all kernels is  $4B(N+2)$  bytes.

The boost converter step ups the voltage of the solar panel string and charges the battery. The MPPT unit, which includes the proposed method, sends the predicted MPP:  $V_{ref}$  to the feedback controller. The P-type MOSFET is assumed to be used for making an open circuit in a short-time interval to get  $V_{pv}^{max}$  (see **Algorithm 2**). As shown in **Figure 4**, several sets of this circuit are connected in parallel to the same rechargeable battery.



Algorithm 3. Flowchart for *getMPPInitVref()*.

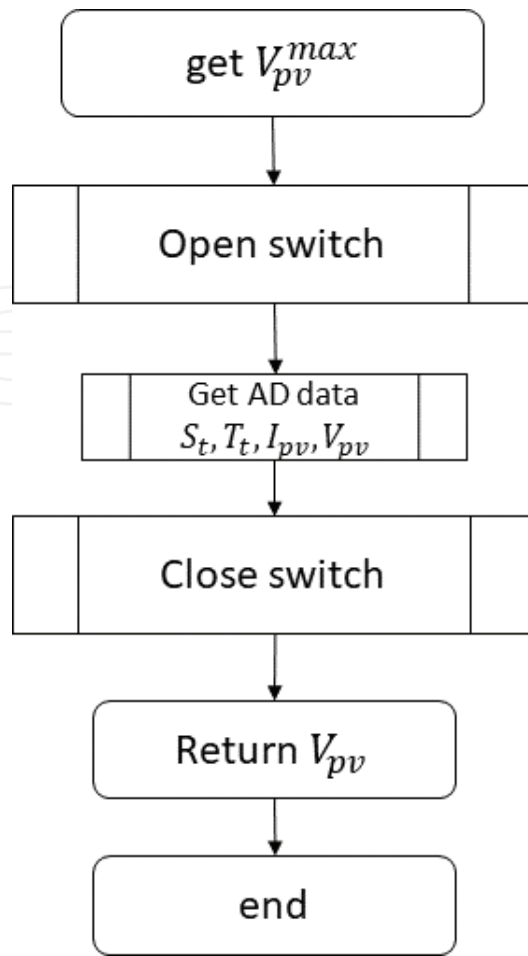
#### 4. Computer simulation

The performance of the proposed MPPT was evaluated via a simulation. Particularly, the convergence speed to MPP is a very important property that should be evaluated. The simulated circuit comprises a short string of solar panels connected to a boost converter (see Figure 7).

The MPPT unit sends the reference voltage  $V_{ref}$  for the feedback controller, and the boost chopper circuit adjusts the output voltage of the PV string to  $V_{ref}$ . In this simulation, we assume that the load is a rechargeable battery, whose voltage is kept to a certain constant voltage. Using this load, each boost converter is not affected by the change in the other converter’s output power.

For simplicity, the simulator of the boost converter simply updates  $V_{pv}$  to be  $V_{ref}$  and calculates the corresponding  $I_{pv}$  by using the photovoltaic model. Therefore, the detailed transient response of the boost converter was not realized in the simulator.

To realize the simulation, we constructed a simulator of photovoltaics and circuits as the Java application. The solar irradiation, temperature, and the properties of the solar panels are also represented in the thread of environment class (see Figure 8).



Algorithm 4. Flowchart for getting  $V_{pv}^{max}$ . Open and close switch denote enabling and disabling the FET in Figure 7.

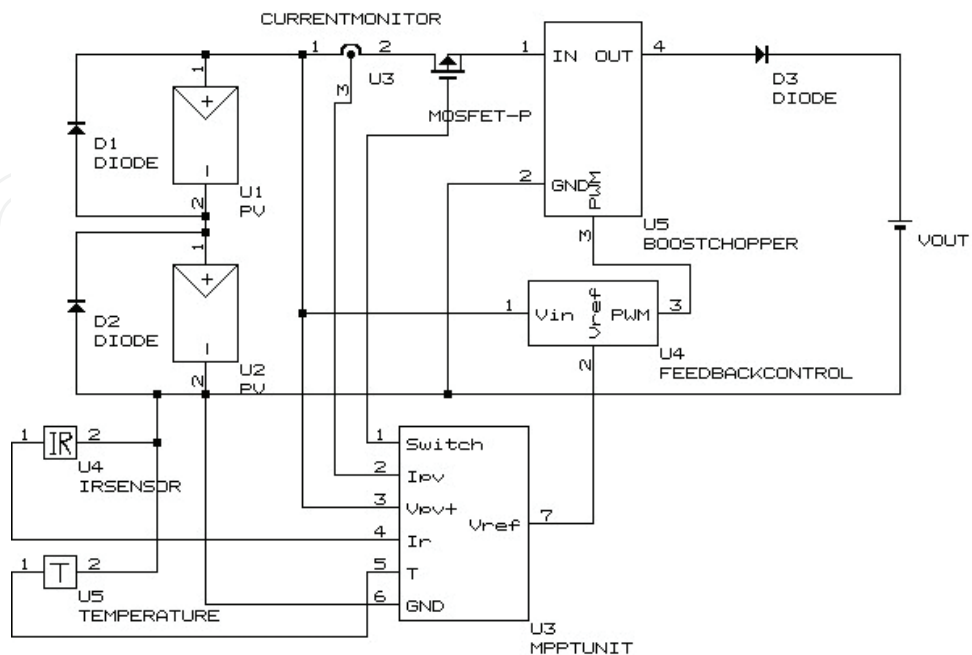


Figure 7. The circuit for the simulation.

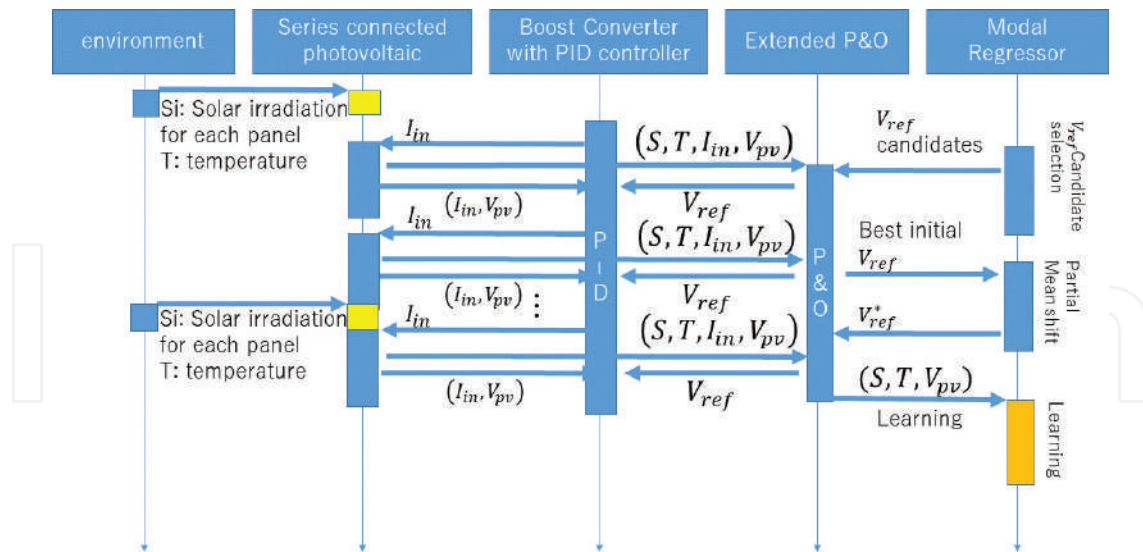


Figure 8. Sequence diagram of the simulator.

For simplicity, the strength of solar irradiation and temperatures varies for a certain scenario, but the effect of the specific heat of the solar panel material was not considered.

The solar panel is a homogeneous two cluster panel such that it has two peaks under partial shadow conditions. The MPPT with modal regression is also represented by the MPPT thread class. The chopper circuit with the feedback controller is assumed to control the output voltage from the solar panel to  $V_{ref}$ , which is assigned by the MPPT unit, within 1 ms. Note that  $V_{ref}$  is yielded by the modified P&O method or the modal regressor. Similar to the simulation method proposed in [10], the chopper circuit is simulated so as to change  $I_{pv}$ . As a result, the series-connected solar panel simulator yields a new  $V_{pv}$  due to the change in  $I_{pv}$ . The new  $V_{pv}$  is then sent to the boost converter simulator to calculate the next step.

We have compared the proposed method with the existing models under partial shadow conditions. For this comparison, the following three models were prepared: MPPT with the modal regression, the P&O method by changing initial points described in Section 3.1, and MPPT with PSO. There are various PSO-based MPPT methods [8, 17]. In this simulation, we prepared a model that is based on the model proposed in [17] because it has a similar

$\Delta_v$ : Change in voltage for P&O (Algorithm 1)	0.1
$\theta_{init}$ in Eq. (21)	0.9
$\eta$ in Eq. (16)	0.001
d in Eq. (19)	3
Time interval for changing $V_{ref}$ by P&O, modal regression and PSO ( $=\tau$ in Algorithm 3)	1 [ms]
Time interval for changing solar irradiation	250 [ms]
Scaling factor $v_0$ in (19)	0.3
Number clusters ( $= C$ in Algorithm 2). This value should be greater than the actual number of clusters.	3

Table 1. Parameters used in this simulation.

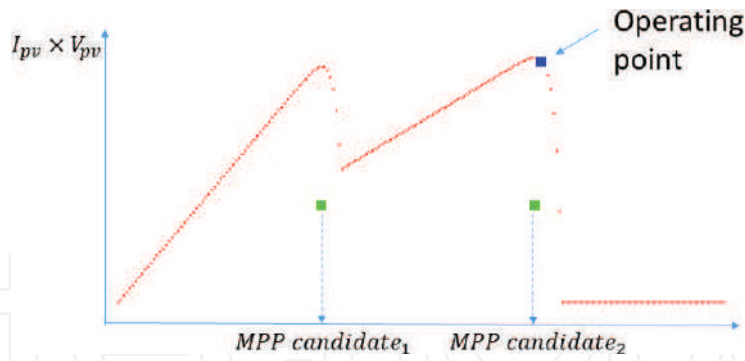


**Figure 9.** An example of snapshot of the maximum power tracking of the proposed method. The green points are the center points of the proposed modal regressor, namely the initial MPP candidates (see (21)).

architecture to ours. The PSO-based MPPT method used in this simulation executes the PSO optimization when solar irradiation changes is occurred. The condition for detecting solar irradiation changes was the same as the method described in Section 3.3. The detailed parameters used in this simulation are listed in **Table 1**.

We evaluated the electric power generation behavior of each model. If the generated power is higher than the others, the model finds MPP faster than the others.

**Figure 9** shows a snapshot of the behavior of our proposed MPPT. In this situation, the power-voltage curve of the solar panel has two peak points. The activated kernel centers of the modal-regression at this situation are shown as the two green points<sup>1</sup>. The proposed method set choose one of them as the start point for the MPPT. After that, the modal regression output was used for the

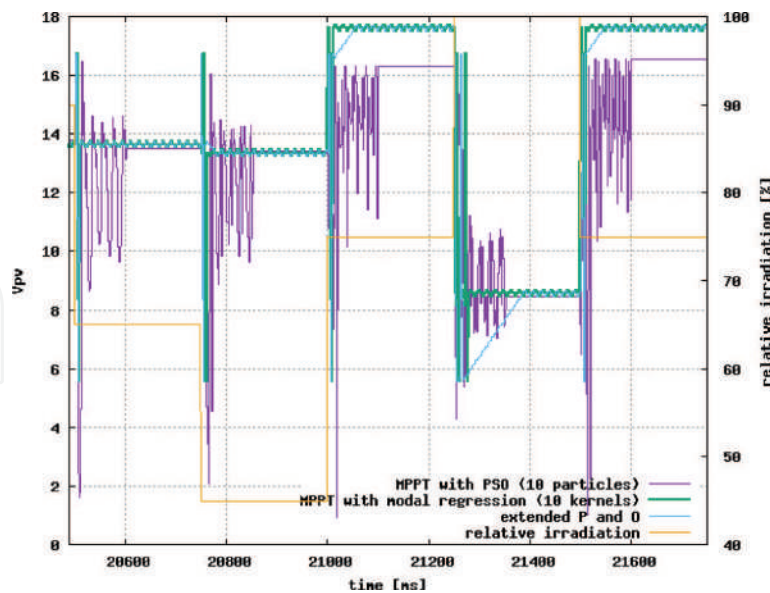


**Figure 10.** An example of  $V_{pv}$  VS time.

<sup>1</sup>The activated kernel centroids without the power element were pointed as the green points. However, the height of the green points have been set to a certain fixed value for easy seeing.

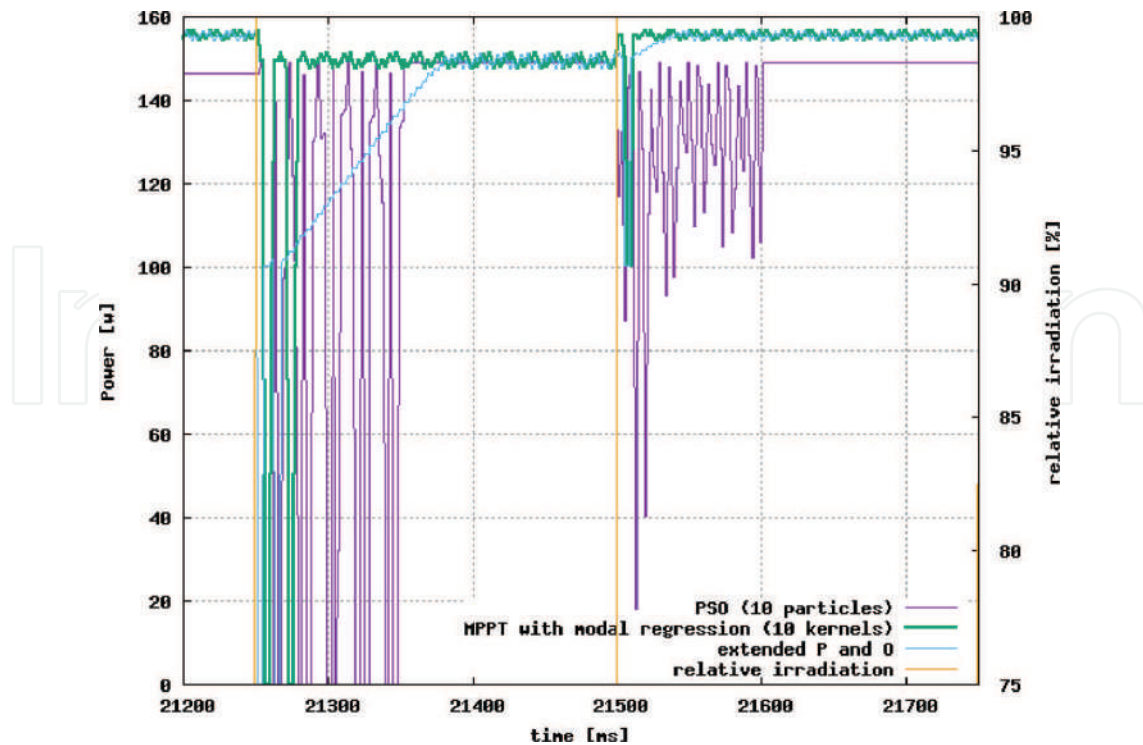


**Figure 11.** The magnified power curves. Note that the power curve has changed immediately after the change of irradiation.

initial point for starting the P&O procedure. As a result, the proposed method finds the MPP faster than the P&O method. The quick search ability is suitable for generating electricity under changing irradiation. In **Figure 10**, the green, blue, and purple curves show the  $V_{pv}$  of the proposed one, P&O-, and PSO-based MPPT methods, respectively. The  $V_{pv}$  of the PSO-based method changes drastically for approximately 100 ms immediately after the change in solar irradiation. Although the proposed and P&O methods also change  $V_{pv}$  immediately after the change in solar irradiation, the changing period is shorter than that of the PSO-based method. Moreover,  $V_{pv}$  of P&O-based method sometimes needs a time interval to converge to be a steady state. On the contrary, the proposed method makes  $V_{pv}$  reach the steady state faster than the others.

The magnified **Figure 11** shows that the power generation of our proposed method quickly aligned immediately after the change in solar irradiation, whereas the extended P&O method gradually converges to the power of the proposed method. The PSO-based MPPT shows the less power generation than the other methods. In the case of PSO, the results are greatly affected by the initial points of the particles. In this simulation, we have set the initial points by uniform random voltages in  $[0, V_{PV}^{max}]$ , where  $V_{PV}^{MAX}$  is the open-circuit voltage of the solar panel string. The initial points should be distributed uniformly in the interval. However, if the number of particles is small due to the restriction of the device, the initial point distribution usually becomes to be an unbalanced distribution. As a result, the quality of the solution is degraded. To check the performances under the various sizes of kernels or particles, the averaged generated power for the proposed method with 5 and 10 kernels, and the PSO-based MPPT methods with 5 and 10 particles were compared. Moreover, the generated electricity power from the proposed method and the extended P&O

Time interval for changing solar insolation	Method	Averaged electricity power
250 ms	MPPT with modal regression (5 kernels)	151.2 W
	MPPT with modal regression (10 kernels)	151.9 W
	Extended P&O	150.3 W
	MPPT with PSO (5 particles)	127.1 W
	MPPT with PSO (10 particles)	128.2 W
200 ms	MPPT with modal regression (10 kernels)	151.4 W
	Extended P&O	149.4 W

**Table 2.** Comparison of averaged electricity power generated during the first 200 [s]. The time interval for solar irradiation change were 250 and 200 [ms].

methods were compared with two different time intervals of changing solar irradiation. **Table 2** shows the results. We can see that the averaged generated power of the proposed method of 5 and 10 kernels are almost the same. On the other hand, the PSO-based methods reduced the power if the size of particles is reduced. The proposed method's generated power was also larger than the extended P&O method because the convergence speed is higher than that of the P&O method. The difference in the generated power is caused by their different convergence speed. Therefore, if there are fewer changes in solar irradiation, the difference decreases because the convergence process does not occur. As evidence, **Table 2** shows that if the time interval of changing solar irradiation is 250 ms, the differences between the two averaged generated power was 1.6 W, whereas the difference was 2 W when the time interval is 200 ms.

## 5. Conclusion

In this chapter, we proposed a new MPPT method accelerated by modal regression on a budget, which approximates multivalued functions. The modal regression on a budget is a simplified version of our previously proposed method, namely limited modal regression [12].

The proposed MPPT method comprises an irradiation sensor, temperature sensor, and modal regression on a budget. We assume that the irradiation sensor gets the averaged strength of irradiation of all solar panels. In the case for MPPT of PV strings, the device has to obtain the highest local peak point from the several peak points in the voltage-power curve. Therefore, the MPPT device with the incomplete sensory input has to approximate a multivalued function between the sensory inputs and the MPP.

Normally, modal regression estimates provide sample distribution and yield local peak points that are related to the specified input.

The modal regression on a budget can approximate such relationships between the sensory inputs and the MPP's. The proposed MPPT method is a combination of modal regression on a budget and a modified (extended) P&O method. The modified P&O method obtains the MPPs even if there are several local peak points. The obtained MPPs are recorded in the modal regressor.

The proposed method was evaluated by computer simulation under partial shadow conditions. The simulation results suggest that the MPPT with modal regressor obtain an MPP faster than other existing methods such as the MPPT with PSO. This property is suitable for electricity generation using the solar panels bedded on roads.

## Acknowledgements

This study is sponsored and supported by KYODO Corporation, Toyota-city, Aichi-ken.

## Author details

Koichiro Yamauchi

Address all correspondence to: [k\\_yamauchi@isc.chubu.ac.jp](mailto:k_yamauchi@isc.chubu.ac.jp)

Department of Computer Science, Chubu University, Kasugai-shi, Aichi, Japan

## References

- [1] Bendib B, Belmili H, Krim F. A survey of the most used mppt methods: Conventional and advanced algorithms applied for photovoltaic systems. *Renewable and Sustainable Energy Reviews*. 2015;**45**:637-648
- [2] ESRAM T, Chapman PL. Comparison of photovoltaic array maximum power point tracking techniques. *IEEE Transactions on Energy Conversion*. 2007;**22**(2):439-449
- [3] Boehringer AF. Self-adapting dc converter for solar spacecraft power supply. *IEEE Transactions on Aerospace and Electronic Systems*. 1968;**AES-4**(1):102-111
- [4] ESRAM T, Kimball JW, Krein PT, Chapman PL, Midya P. Dynamic maximum power point tracking of photovoltaic arrays using ripple correlation control. *IEEE Transactions on Power Electronics*. 2006;**21**(5):1282-1291
- [5] Veerachary M, Senjyu T, Uezato K. Neural-network-based maximum-power-point tracking of coupled-inductor interleaved-boost-converter-supplied pv system using fuzzy controller. *IEEE Transactions on Industrial Electronics*. 2003;**50**(4):749-758
- [6] Akkaya R, Kulaksiz AA, Aydogdu O. Dsp implementation of a pv system with ga-mlp-nn based mppt controller supplying bldc motor drive. *Energy Conversion and Management*. 2007;**48**:210-218
- [7] Yamauchi K. Incremental learning on a budget and its application to quick maximum power point tracking of photovoltaic systems. *Journal of Advanced Computational Intelligence and Intelligent Informatics*. 2014;**18**(4):682-696

- [8] Liu C-L, Luo Y-F, Huang J-W, Liu Y-H. A pso-based mppt algorithm for photovoltaic systems subject to inhomogeneous insolation. In: The 6th International Conference on Soft Computing and Intelligent Systems. 2012. pp. 721-726
- [9] Noguchi T, Togashi S, Nakamoto R. Short-current pulse-based maximum-power-point tracking method for multiple photovoltaic-and-converter module system. IEEE Transactions on Industrial Electronics. 2002;**49**(1):217-223
- [10] Tan YT, Kirschen DS, Jenkins N. A model of pv generation suitable for stability analysis. IEEE Transactions on Energy Conversion. 2004;**19**(4):748-755
- [11] Bellia H, Youcef R, Fatima M. A detailed modeling of photovoltaic module using matlab. NRIAG Journal of Astronomy and Geophysics. 2014;**3**:53-61
- [12] Koichiro Y, Vanamala Narashimha B. Minimum modal regression. In Maria De Marsico, Gabriella Sanniti di Baja, and Ana Fred, editors, ICPRAM2018 7th International Conference on Pattern Recognition Applications and Methods, pages 448-455, 2018
- [13] Parzen E. On estimation of a probability density function and mode. Annals of Mathematical Statistics. 1962;**33**(3):1065-1076
- [14] Sasaki H, Ono Y, Sugiyama M. Modal regression via direct log-density derivative estimation. In: Hirose A, Ozawa S, Doya K, Ikeda K, Lee M, Liu D, editors. Neural Information Processing –23rd International Conference, ICONIP 2016–, Volume Part II. Springer-Verlag; 2016
- [15] Lee D, Noh SH, Min SL, Choi J, Kim JH, Cho Y, Sang KC. Lrfu: A spectrum of policies that subsumes the least recently used and least frequently used policies. IEEE Transactions on Computers. 2001;**50**(12):1352-1361
- [16] Silverman BW. Density Estimation for Statistics and Data Analysis. CRC Press; 1986
- [17] Rajasekar N, Vysakh M, Thakur HV, Mohammed Azharuddin S, Muralidhar K, Paul D, Jacob B, Balasubramanian K, Sudhakar Babu T. Application of modified particle swarm optimization for maximum power point tracking under partial shading condition. Energy Procedia. 2014;**61**:2633-2639

# We are IntechOpen, the world's leading publisher of Open Access books Built by scientists, for scientists

6,300

Open access books available

171,000

International authors and editors

190M

Downloads

Our authors are among the

154

Countries delivered to

TOP 1%

most cited scientists

12.2%

Contributors from top 500 universities



WEB OF SCIENCE™

Selection of our books indexed in the Book Citation Index  
in Web of Science™ Core Collection (BKCI)

Interested in publishing with us?  
Contact [book.department@intechopen.com](mailto:book.department@intechopen.com)

Numbers displayed above are based on latest data collected.  
For more information visit [www.intechopen.com](http://www.intechopen.com)



---

# Optimal Designing Grid-Connected PV Systems

---

Ali Reaz Reisi and Ashkan Alidousti

Additional information is available at the end of the chapter

<http://dx.doi.org/10.5772/intechopen.79685>

---

## Abstract

Photovoltaic systems, direct conversion of solar energy to electrical energy, are produced in the form of DC power by photovoltaic arrays bathed in sunlight and converted into AC power through an inverter system, which is more convenient to use. There are two main paradigms for optimal designing of photovoltaic systems. First, the system can be designed such that the generated power and the loads, that is, the consumed power, match. A second way to design a photovoltaic system is to base the design on economics, as pinpointed in the following. Photovoltaic grid connected through shunt active filter by considering maximum power point tracking for these systems is known as the optimal design. This chapter is organized as follows: First, we discuss an overview of grid-connected photovoltaic systems. After that, we take a more detailed look on grid-connected photovoltaic system via active filter; in this section, we explain the modeling of photovoltaic panel and shunt active filter. In the next section, we learn different maximum power point tracking methods and also learn how to design DC link as a common bus of shunt active filter and photovoltaic system. Finally, MATLAB/Simulink simulations verify the performance of the proposed model performance.

**Keywords:** optimal designing, grid-connected, photovoltaic systems, shunt active filter, maximum power point tracking

---

## 1. Introduction

Global warming, environmental pollution, and possible scarcity of fossil fuel reserves are some of the main driving forces behind the urge for installing grid-connected photovoltaic (PV) systems. Moreover, utilities and customers can benefit from installing these systems. The main gain for customers is to take advantage of the incentives provided by the governments upon

installing PV systems. For utilities, the gains of installing PV systems are mainly operational benefits, especially if the PV system is installed at the customer side on rural feeders. For example, PV systems can be used to decrease the feeder losses, improve the voltage profile of the feeder, and reduce the lifetime operation and maintenance costs of transformer load tap changers. Moreover, if the peak output of the PV system matches the peak loading of the feeder, then the loading of some transformers present in the network can be reduced during peak load periods. The power-quality index of the grid could be improved if PV system was connected to grid via active filters; they are energy conditioners, which include DC/AC-controllable converters. These filters, based on their control schemes, can compensate both source voltage deficiencies and undesirable load-terminal current, which leads to have a source end purely sinusoidal current.

Current harmonic drawn by direct PV grid connected via DC/AV inverters and also nonlinear loads disturb the waveform of the voltage at the point of a common coupling (PCC) and lead to voltage harmonics. Therefore, it is necessary to develop techniques to reduce all the harmonics as it is recommended in the IEEE 519–1992 standard [1]. The first approach consists of the design of LC filters. However, passive filters are not well adapted as they do not take into account the time variation of the loads and the network. They can also lead to resonance phenomena. So, since several years, a more interesting technique is studied: the active filter based either on voltage source or on current source inverters, yielding the harmonic currents required by the load.

Recently, efforts [1, 2] have been made to combine the active filters with renewable energy production systems to benefit from advantages of both a renewable source of energy and a power conditioner to provide pollution-free and high-quality power to the consumers. It seems that it is necessary to use power conditioners, for example, active filters, to compensate the power-quality problems caused by renewable sources of energy in some cases. Since passive filter like LC filters lack the capability to fully compensate these problems in the presence of nonlinear loads, they are not preferred rather than active filters. This type of modular and renewable technology has many advantages like the capability to be expanded and being practically applied in almost everywhere. Furthermore, since one less converter is used in this scheme, there will be capital investment saving in comparison with a separated shunt active filter (SAF) and a PV system; since here by a common DC bus for both SAF and PV systems is used, the cost of the produced power will be reduced.

## 2. Models of PV and SAF

### 2.1. PV model

The equivalent circuit of a PV cell is presented in **Figure 1**. Photovoltaic cells of a solar panel have three kinds of external connections, namely series, parallel, and series-parallel. Eq. (1) presents voltage-current characteristic of a solar panel [1], and  $I_{pv}$  and  $I_o$  are calculated based on the following:

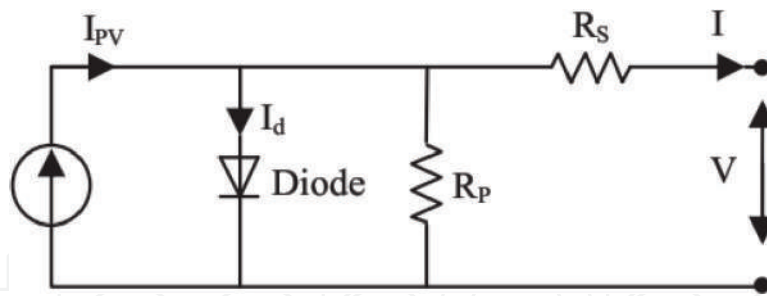


Figure 1. Equivalent circuit of a PV cell.

$$I = I_{PV} - I_0 \left[ \exp\left(\frac{V + R_s I}{aV_t}\right) - 1 \right] - \frac{V + R_s I}{R_p} \quad (1)$$

$$I_{PV} = (I_{PV,n} + K_I \Delta T) \frac{G}{G_n} \quad (2)$$

$$I_0 = \frac{I_{SC,n} + K_I \Delta T}{\exp(V_{OC,n} + K_V \Delta T) / aV_t - 1} \quad (3)$$

where  $I_{PV}$  and  $I_0$  are the photovoltaic current and saturated reverse current, respectively, while “ $a$ ” and “ $K$ ” are the ideal diode constant and Boltzmann constant, respectively. Also, we have  $V_t = N_s K T q^{-1}$  which is the thermal voltage,  $N_s$  is the number of series cells,  $q$  is the electron charge, and  $T$  is the temperature of p-n junction.  $R_s$  and  $R_p$  are series and parallel equivalent resistance of the solar panels, respectively.  $I_{PV}$  is varied with light intensity in a linear relation and also varies with temperature variations.  $I_0$  is dependent on temperature variations.

We have  $I_{PV,n}$ ,  $I_{SC,n}$ , and  $V_{OC,n}$  which are photovoltaic current, short-circuit current (SCC), and open-circuit voltage (OCV) in standard conditions ( $T_n = 25^\circ\text{C}$  and  $G_n = 1000 \text{ Wm}^{-2}$ ), respectively.  $K_I$  stands for the coefficient of short-circuit current to temperature,  $\Delta T = T - T_n$  presents the temperature deviation from standard temperature,  $G$  is the light intensity, and  $K_V$  shows the ratio coefficient of open-circuit voltage to temperature.

Three important points of I-V characteristic of solar panels are open-circuit voltage, short-circuit current, and voltage-current corresponding to the maximum power. The mentioned points are varied by changes in atmospheric conditions. Short-circuit current and open-circuit voltage can be calculated in different atmospheric conditions by using Eqs. (4) and (5) which are derived from PV model equations, as follows:

$$I_{SC} = (I_{SC,n} + K_I \Delta T) \frac{G}{G_n} \quad (4)$$

$$V_{OC} = V_{OC,n} + K_V \Delta T \quad (5)$$

## 2.2. SAF

SAF is used to eliminate load-terminal current harmonics and consequently having a pure sinusoidal source-end current. The Generalized Theory of Instantaneous Power (GTIP) theory,

as control algorithm, is used for generating reference signal in the activating algorithm of the shunt active filter [3].

$U(t)$  is assumed as the load voltage which consists of all voltage sequences ( $U(t) = U^+(t) + U^-(t) + U^0(t)$ ), in which  $U^+(t)$ ,  $U^-(t)$ , and  $U^0(t)$  are positive, negative, and zero sequences of  $U(t)$ , respectively. As a result, using the Optimal Solution theory (OS theory), the source-end current can be rewritten as

$$\left\{ \begin{array}{l} i_g(t) = i_g^+(t) + i_g^-(t) + i_g^0(t) \\ i_g^+(t) = \lambda \cdot U^+(t) \\ i_g^-(t) = \lambda \cdot U^-(t) \\ i_g^0(t) = \lambda \cdot U^0(t) \\ \lambda = \frac{\bar{P}(t)}{U(t) \cdot U(t)} \\ i_g(t) = \frac{\bar{P}_g(t)}{U(t) \cdot U(t)} U(t) \\ i_c(t) = i_{Load}(t) - \frac{\bar{P}_g(t)}{U(t) \cdot U(t)} U(t) \end{array} \right. \quad (6)$$

where  $i_g(t)$ ,  $i_c(t)$ ,  $i_{Load}(t)$ ,  $\lambda$ , and  $P_g(t)$  are the source current, the compensation current, the current that must be compensated, the instantaneous power factor, and the instantaneous power, in the same order. In Eq. (6),  $U(t)$  is the source of distortion due to the fact that it is non-sinusoidal.

Distorted current will be injected by the SAF compensation algorithm. For this reason, the compensation algorithm derived from the GTIP under the two asymmetric and distorted three-phase load-terminal voltages supplies unacceptable outcomes. To tackle these problems, a solution is adopted on the basis of A-GTIP theory.

In other words, a non-sinusoidal load current in addition to  $i^+(t)$  is composed of  $i^-(t)$  and  $i^0(t)$ . Negative and zero sequences must be supplied with SAF and positive sequence with source ( $i_g(t)$ ). But due to  $U(t)$  is non-sinusoidal and consist of positive, negative and zero sequences, based on equation (6), the calculate  $i_c(t)$  (SAF injected currents) cannot remove total negative and zero sequences of  $i_g(t)$ . This means compensation is not optimal.

- One suggestion to overcome voltage asymmetry is to replace  $U(t)$  by  $U^+(t)$  in Eq. (6). Hence, the new source-end currents and the SAF-injected currents are obtained as follows:
- The source-end currents remain purely sinusoidal, while  $U^+(t)$  does not include any harmonic components. Apart from that, the non-sinusoidal  $U^+(t)$  in the term  $U^+(t)$  acts as the source of distortion. Therefore, the SAF compensation algorithm will inject a distorted current. The SAF new-injected current will cause sinusoidal source-end currents in four-wire systems as follows:

$$i_g(t) = \frac{\overline{P_g}(t)}{U_1^+(t) \cdot U_1^+(t)} U_1^+(t)$$

$$i_c(t) = i_{Load}(t) - \frac{\overline{P_g}(t)}{U_1^+(t) \cdot U_1^+(t)} U_1^+(t) \tag{7}$$

In which  $U_1^+(t)$  is the fundamental component of  $U^+(t)$ . The SAF-controller block diagram is shown in **Figure 2**.

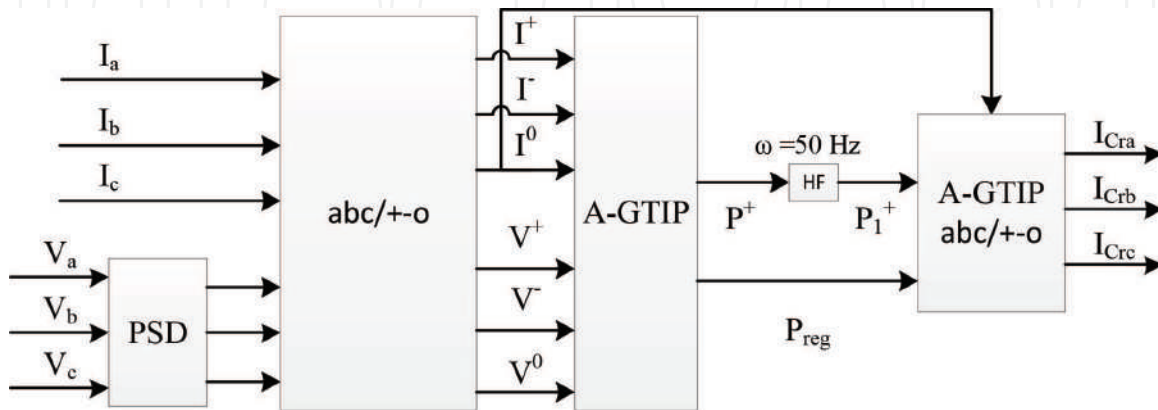


**Figure 2.** A SAF controller block diagram [1].

In this section, how the PV cells and SAF can be modeled has been explained; in the next section, how the grid-connected PV system and SAF can be related and the proposed block diagram will be presented.

### 3. SAF-PV system

**Figure 3** illustrates the operating principle and current wave form  $I_{Load}$  at the load. The PV system is modeled as two parallel current sources. The first one,  $I_{pv}$ , is proportional to the

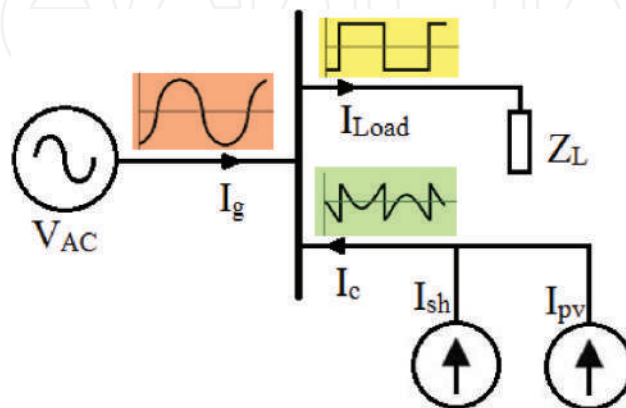


**Figure 3.** The operating principle of a SAF-PV system.

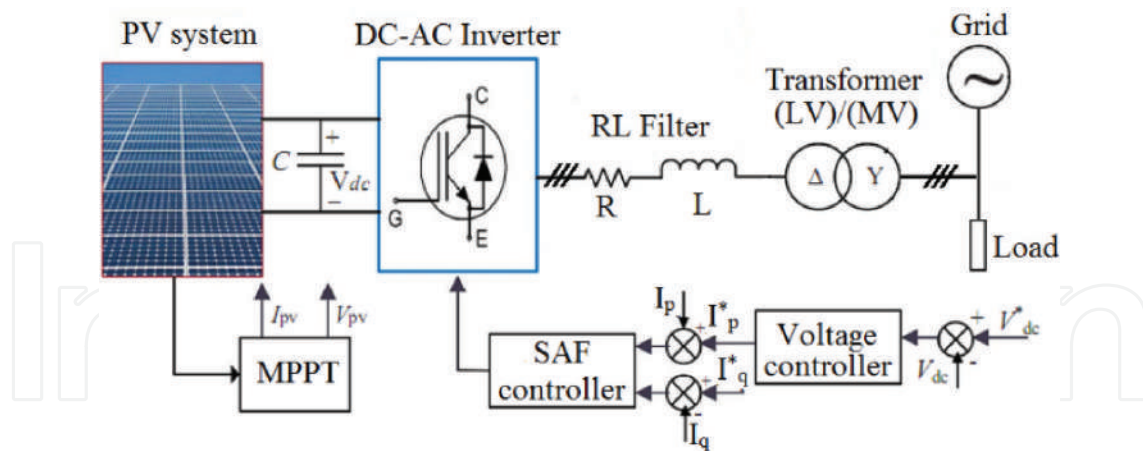


**Figure 4.** A schematic diagram of the single-stage SAF-PV system.

maximum power available from the PV cells, and its frequency and phase are equal to those of the voltage of the mains. The second current source supplies a wave form, which is equal to the total amount of the harmonics drawn by the load. The current supplied by the mains,  $I_g$ , is a purely sinusoidal wave, and the PV system reacts as an active filter to some of the active power and harmonic currents drawn by the load.

The schematic diagram of **Figure 4** shows the power stage of the grid-connected single-stage PV system. It includes the PV array, maximum power point tracking (MPPT) technique, which was used to extract the maximum available power from the PV array, and the DC-link capacitors that connect to the output terminal of the PV array. In addition, a three-phase VSI with its control is based on SAF, RL filter, which is connected to the low voltage AC grid, and a step-up transformer-connected distribution side of the grid.

The design of SAF incorporated with PV system can be decomposed into two issues: (1) maximum power point tracking (MPPT) of the PV system and (2) a control strategy of the voltage of the DC link ( $V_{DC}$ ) common between SAF and PV systems.

### 3.1. MPPT

The relatively higher cost required for generating this type of energy in comparison with the energy produced by conventional power generation systems or other renewable sources such as wind power is known as the main disadvantage of the PV systems. Therefore, the optimal operation of the PV systems is critical and achieved by maximizing the efficiency of power delivered to the output by tracking the maximum power point. The PV system is connected to the grid via DC-DC converters. MPPT in PV systems is achieved by applying a control signal to the converters and regulating the PV terminal voltage (or current).

MPPT not only enables an increase in the power delivered from the PV module to the load but also enhances the operating lifetime of the PV system [4]. The solar cell maximum output power at the appropriate operating point and a given cell efficiency depend on the radiation intensity, ambient temperature, and load impedance. It is essential to ensure the efficient operation of the solar cell array that there is a single operating point in which through

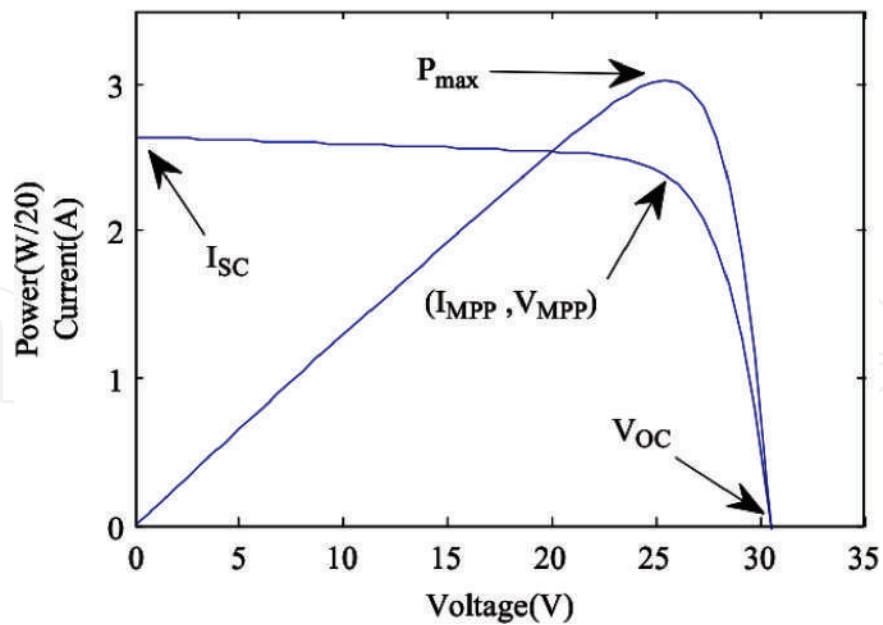


Figure 5. I-V and P-V characteristics of solar cell.

variations in radiation intensity and temperature, the maximum power point tracking is achieved (Figure 5). The problematic aspect of MPPT is that PV arrays automatically produce a maximum output power determined by PV output voltage or output current under a given temperature and irradiance. The maximum power attainment involves the adjustment of a load line under variations in temperature and irradiation level.

A wide variety of algorithms and methods have been proposed and implemented to attain MPP tracking [4–6], categorized namely offline methods, online methods, and hybrid methods. Offline methods are dependent on solar cell models, online methods do not specifically rely on the modeling of the solar cell behavior, and hybrid methods are a combination of the two abovementioned methods. On the other hand, the offline and online methods can also be referred to as the model-based and model-free methods, respectively.

### 3.1.1. Offline methods

In case of offline methods, it is generally required to know one or more of the solar panel values, such as the open-circuit voltage,  $V_{OC}$ , short-circuit current,  $I_{SC}$ , temperature, and irradiance.  $V_{OC}$  and  $I_{SC}$  are two values that can be calculated based on measurement of the solar irradiance and temperature or be measured by applying an open circuit or a short circuit to the PV system. While the accuracy of the calculated values is limited by the accuracy of the PV characteristic provided by the manufacturer's specifications, the latter approach does not involve the load interruption necessary for measuring the  $V_{OC}$  and  $I_{SC}$ . The two values,  $V_{OC}$  and  $I_{SC}$ , are employed to generate the control signal, which is necessary for driving the solar cell to its maximum power point (MPP). In the course of the tracking of maximum power point operation, the abovementioned control signal remains constant if ambient conditions can be regarded as fixed and there are no attempts to regulate the output power of the PV system.

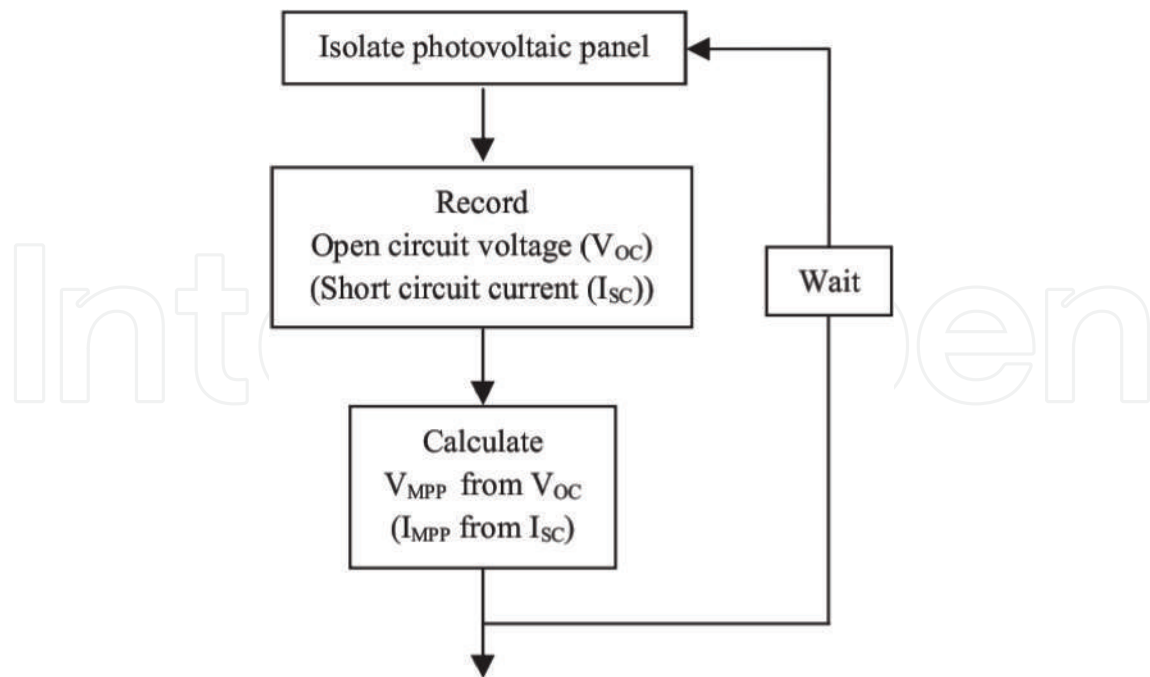


**Figure 6.** A flowchart of open-circuit voltage (short-current circuit) method [4].

The offline methods known as open-circuit voltage method (OCV), short-circuit current method (SCC), as well as the MPPT method based on artificial intelligence (AI) take variables such as temperature and irradiation as input and calculate the MPP.  $I_{SC}$  and  $V_{OC}$  can be measured or calculated based on mathematical models provided by the manufacturer or based on experimental data, which reflect the dependence on temperature or irradiance. AI models extract learning-based models using the known relationship between OCV or SCC and temperature and/or irradiance. A flowchart of these methods, which are the simplest offline methods, is depicted in **Figure 6**.

Both of OCV and SCC methods cannot deliver the maximum output power to the load because of two reasons. First, load interruption occurs during the measurement of  $I_{SC}$  or  $V_{OC}$ , and the second reason is that MPP can never be tracked quite exactly using these methods in the first place as suggested by approximately linear relationship between the open-circuit voltage  $V_{OC}$  and  $V_{MPP}$  or  $I_{SC}$  and  $I_{MPP}$ .

These two methods cannot be categorized as “true seeking” MPP methods; however, the simplicity of these algorithms and the ease with which they can be implemented make them suitable for use as part of novel hybrid methods [7, 8].

Artificial intelligence (AI) techniques, as other offline methods, are becoming popular as alternative approaches to conventional techniques or as components of integrated systems. They have been used to solve complicated practical problems in various areas. In [9], only the applications of artificial neural networks (ANNs) and fuzzy logic (FL) are discussed, while AI techniques consist of several disciplines.

The ANN-based method advantage lies with the fact that the trained neural network can provide a sufficiently accurate MPPT without requiring extensive knowledge about the PV

parameters. Most of PV arrays exhibit different output characteristics; however, it must be mentioned that an ANN has to be specifically trained for the PV array with which it will be used. The time-varying characteristics of a PV array imply that the neural network has periodically trained to be guaranteed to track MPP accurately. Implement training periodically needs collecting data, which is a time-consuming process.

Fuzzy logic controllers take full advantages of the following: the ability to work with imprecise inputs, the requirement shortage of an accurate mathematical model, the ability to handle nonlinearity, and fast convergence. However, the approximation of achieving learning ability and accuracy depends on the fuzzy level number and the membership functions form. In most fuzzy systems, there is a connection between membership function, fuzzification and defuzzification, as well as the antecedent and the consequent fuzzy rules that are determined through trial and error, which can take a long time to perform.

### 3.1.2. Online methods

In case of online methods, the control signals are usually generated by using the instantaneous values of the PV output voltage or current. The control signal is applied to the PV system along with a small methodical and premeditated perturbation in voltage or current or duty cycle (control signal), and the resulting output power is determined. By analyzing perturbation response on the output power of a PV panel, the direction in which the control signal changes (decrease or increase) is determined. Hence, in contrast to the offline methods, the control signal can no longer be regarded as constant when a perturbation is applied. Therefore, the maximum output power tracking involves some oscillations around the optimum value.

In online methods, also known as model-free methods, control signals are usually generated by the instantaneous values of the PV output voltage or current. The more known online methods are Perturbation and Observation method (P&O), Extremum Seeking Control method (ESC), and the Incremental Conductance method (IncCond).

P&O method is considered by a number of researchers due to the fact that it is one of the simplest online methods [10]. P&O can be implemented by applying perturbations to the reference voltage or the reference current signal of the solar panel. **Figure 7** depicts this method's flowchart, which is also known as the "hill climbing method," where "X" is the reference signal. In the algorithm, taking the reference signal, X, as the voltage, (i.e.,  $X = V$ ), the goal will involve pushing the reference voltage signal toward  $V_{MPP}$ , thereby causing the instantaneous voltage to track the  $V_{MPP}$ . As a consequence, the output power will approach the maximum power point. With this end in view, a small but constant perturbation is applied to the solar panel voltage.

A systematic ECS methodology supported by rigorous theories such as averaging and singular perturbation was recently presented. This real-time optimization methodology involves a nonlinear dynamic system with an adaptive feedback. This ESC method has been successfully applied in PV systems in order to track MPP [11]. With the self-optimizing extremum algorithm as the MPPT controller, the control objective is for the PV system operating point to rapidly trace the MPPs subject to uncertainties and disturbances from the PV panel and the external load.

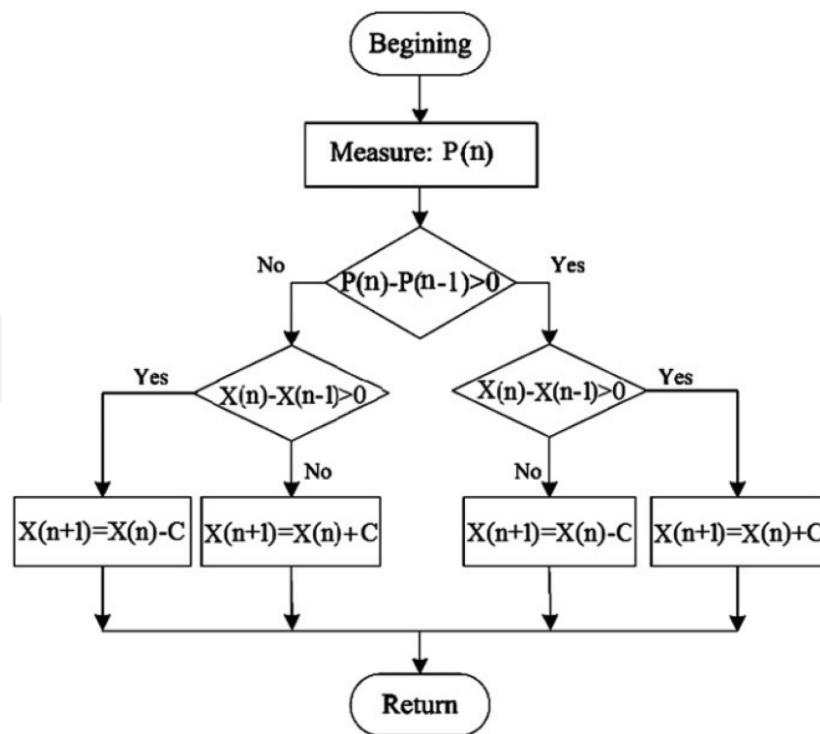


Figure 7. Perturbation and observation algorithm [4].

A small sinusoidal current represented by  $\Delta I = a \sin(\omega t)$  is supposed and added to the reference current ( $I_{ref}$ ) as a perturbation. This leads to making a ripple on the power ( $\Delta P$ ), whose phase and amplitude are dependent on the relative location of the operating point relative to the MPP. The sinusoidal current perturbation will be added to the reference current and applied to the PV system, as it is clear in **Figure 8**. If the resulting ripple in the current is in phase with the output power ripple, the output power will fall to the left of MPP, and the reference current will be less than  $I_{MPP}$ ; therefore, the controller will increase the reference current.

On the other hand, if the ripple in the current is not in the same phase with that in the output power, the output power will drop down to the right of MPP, and the reference current will exceed the  $I_{MPP}$ . As a result, the controller will reduce the reference current until reaching MPP. The ripple power ( $\Delta P$ ) can be extracted by passing the output through a high-pass filter. Then, the ripple power is demodulated through multiplication by a  $\sin(\omega t - \varphi)$  signal. The resulting signal, zeta, is either positive or negative depending on the position in the power output curve. After that, zeta is applied to an integrator in order to modify the value of  $I_{ref}$  to reach MPP. In the case of falling in the MPP operating point, the amplitude of the ripple will be negligible, and the output power ripple frequency will be twice as many as the current ripple.

There are two major advantages for ESC approach. The first is the optimization problem involving power maximization that is explicitly solved by using the dynamic adaptation-based feedback control law for a sinusoidal perturbation. Hence, attainable MPP is guaranteed when the control algorithm is convergent. The disadvantage of the ESC method lies in the complexity associated with its implementation as well as the necessity to evaluate signals of relatively low amplitude.

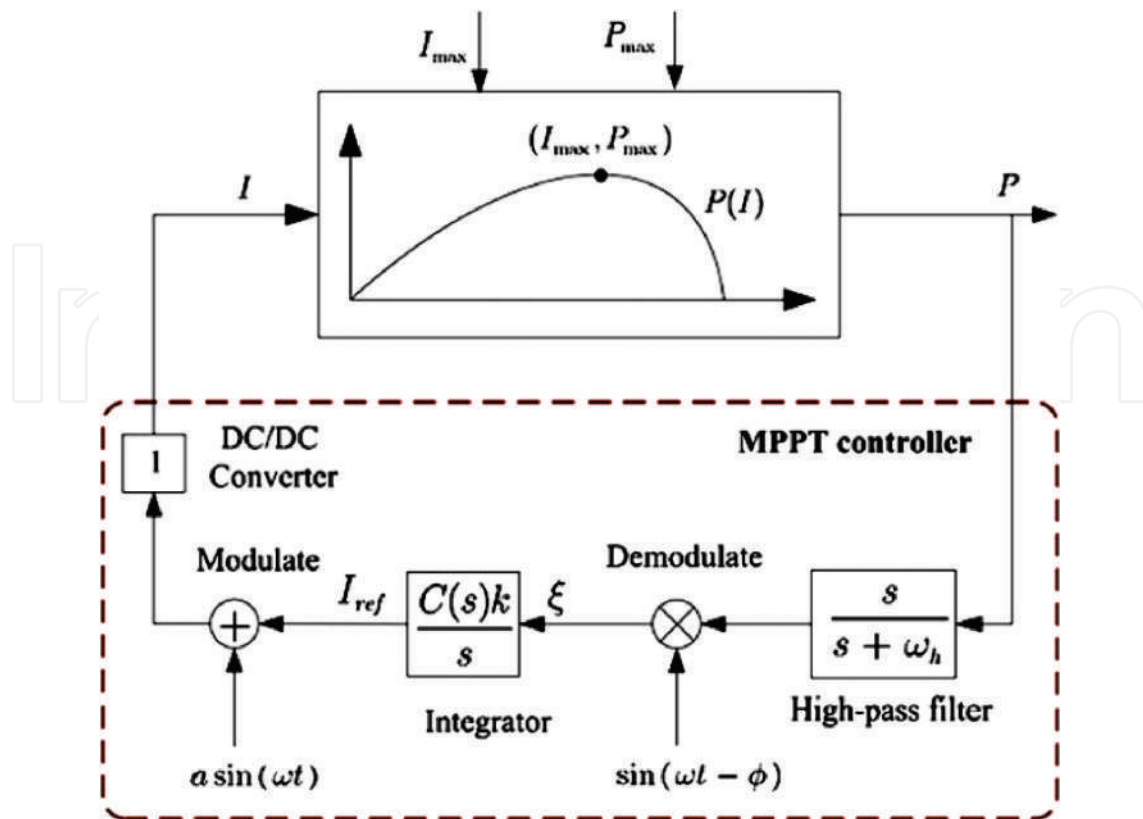


Figure 8. An MPPT controller scheme for the PV system [4].

The method employs the slope of the PV array power characteristics to track MPP that is known as incremental conductance (IncCond) method [12]. In this method, the curve slope of the PV array power is indicated. Based on this, it is zero at the MPP, positive for the output power values, which are smaller than MPP, and negative for values of the output power greater than MPP. The amount of the increment or decrement indicates the MPP tracking speed. An incremental increase may lead to fast tracking, but due to some oscillations around the MPP, the system may not exactly operate at the MPP. That is to say, the usage of IncCond method would be a sort of trade-off between convergence speed and the likelihood of causing oscillations in the MPP.

The main advantage of this algorithm is that it offers an effective solution under rapidly changing atmospheric conditions. The main drawback associated with the IncCond method is that it requires a complex control circuitry.

### 3.1.3. Hybrid methods

Hybrid MPP methods, a combination of the offline and online methods, are based on tracking of the MPP which are performed in two steps of estimation and exact regulation of MPP. The MPP estimation step relies on offline methods to place the set point close to MPP. The next step, regarded as a fine-tuning step, relying on online methods, attempts to reach the MPP actual value. As expected, the hybrid methods are more efficient to track MPP. In hybrid

methods, the associated control signal has two parts, which are generated based on a separate algorithmic loop.

The first one is determined according to one of the simplified offline methods as a constant value, which depends on the given atmospheric conditions of the PV panel and represents the fixed steady-state value. In this first part, control signal is not intended to track the MPP accurately, while it is required for a fast response to the environmental variations. This part can be generated using one of the previous offline methods or simplifications based on the relationship between output power characteristics and ambient.

The second part obtained based on an online method involving steady-state searches represents attempts to follow MPP exactly. In contrast to the previous part, this second part attempts to reduce the error in steady state and does not require a fast response to the environmental variations. The algorithm, which is provided in **Figure 9**, represents a general description of the hybrid method. As pointed earlier, the first part of the control signal is generated using an offline method through the set-point calculation loop. By employing an online method via the fine-tuning loop, the second part is obtained.

A hybrid method, which has two loops, is presented in [13]. In the first estimation loop based on the open-circuit voltage at a constant temperature, MPP is approximated. In the second precise loop, the P&O method is applied to seek the exact amount of the maximum output power. The transient and steady-state responses are improved by maintaining the small amount of amplitude and frequency of perturbation. The authors in [6] proposed a hybrid approach in which an offline method is used to bring the operating point of the PV array near to the MPP. After that, an online IncCond method is used to track the MPP with high accuracy. Through proper control of the power converter, the initial operating point is set to match a

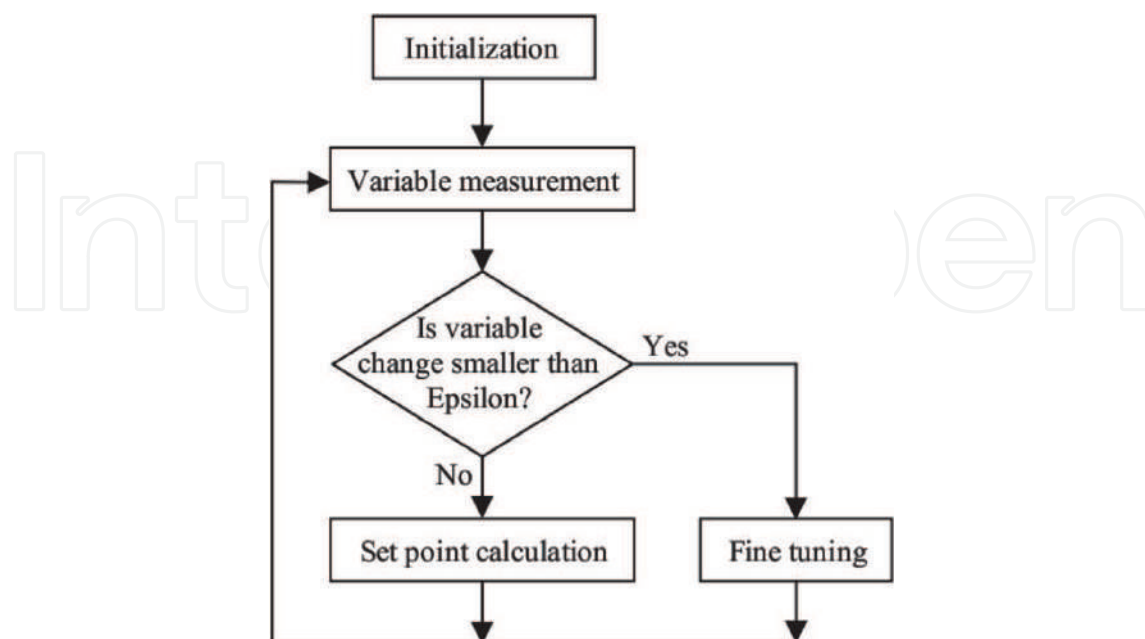


**Figure 9.** General algorithm of hybrid methods [6].

load resistance proportional to the  $V_{OC}/I_{SC}$  ratio associated with the PV array. In this hybrid method, the real MPP tracking is able to ensure that multiple local maxima are presented.

Implementing variable size perturbations by fuzzy logic is a matter of discussion in [14], in the context of achieving improved transient and steady-state responses. The converter duty cycle is adjusted to move the operating point toward the MPP region as soon as possible, thereby improving the response of transient state. A modified P&O algorithm that works based on fuzzy logic and optimized for small variations around the MPP is used simultaneously when MPP region is reached. This method decreases oscillations and increases power produced under the steady-state conditions. Every loop in these chapters applies the P&O approach using perturbations of different amplitude. Here, fuzzy logic decides which loop should be implemented. The peak current control as well as the abovementioned method can result in improving the transient response and decreasing the power loss under steady-state conditions, simultaneously [14].

### 3.2. DC-link voltage control

One significant feature of the PV-SAF is that typically a DC capacitor is connected between the voltage converter of a PV system and an SAF inverter, rather than a DC source. Because neither PV nor SAF is lossless, a special DC-link voltage controller is required to maintain the DC capacitor average voltage at a constant level. In the PV-SAF, the shunt active filter is usually responsible for this voltage regulation. In the steady state, the average DC-link voltage is maintained at a certain preset level, but during the transient, this is not the case. Such a transient can occur when a change occurred in the output power of a PV plant or a load is either connected or disconnected to/from the SAF. Since it takes a finite-time interval to calculate the new reference current, the shunt compensator cannot immediately respond to the load change. In addition to this, some settling time is required to stabilize the controlled parameter around its reference. Consequently, after a PV output power or a load changing instant, there exists some transient period during which the average voltage across the DC capacitor deviates from its reference value.

**Figure 10** shows a strategy of DC-link voltage control in an algorithm, which has two main modes. The first mode would be when the PV produces the power that is ( $P_{PV} > P_{min}$ ) delivered to the network through the SAF, while the second mode is when the threshold  $P_{min}$  is more than the power generated by the PV. It needs to be noted that in the two modes,  $V_{DC}$  must be greater than  $V_{min}$  to have a satisfactory operation of the SAF.

The PV-SAF grid power flow algorithm is illustrated in **Figure 11**. The SAF is like a load that varies when its consumed power is changed with the power generated by PV and the  $V_{DC}$ . In the first mode, a boost converter is applied to deliver the generated power of the PV to the DC link. As stated in the control strategy, when threshold voltage ( $V_{DC-min}$ ) is greater than  $V_{DC}$ , the PV power is fed to the DC link in order to maintain it in an acceptable range.

In this situation, the power delivered to the grid through SAF ( $P_{sh}$ ) is zero; in other words, the power of the PV is solely dedicated to charge the capacitor of the DC link. As  $V_{DC}$  exceeded the  $V_{DC-min}$ , in order to charge the capacitor, a portion of the  $P_{PV}$  is used, and in that case, the rest

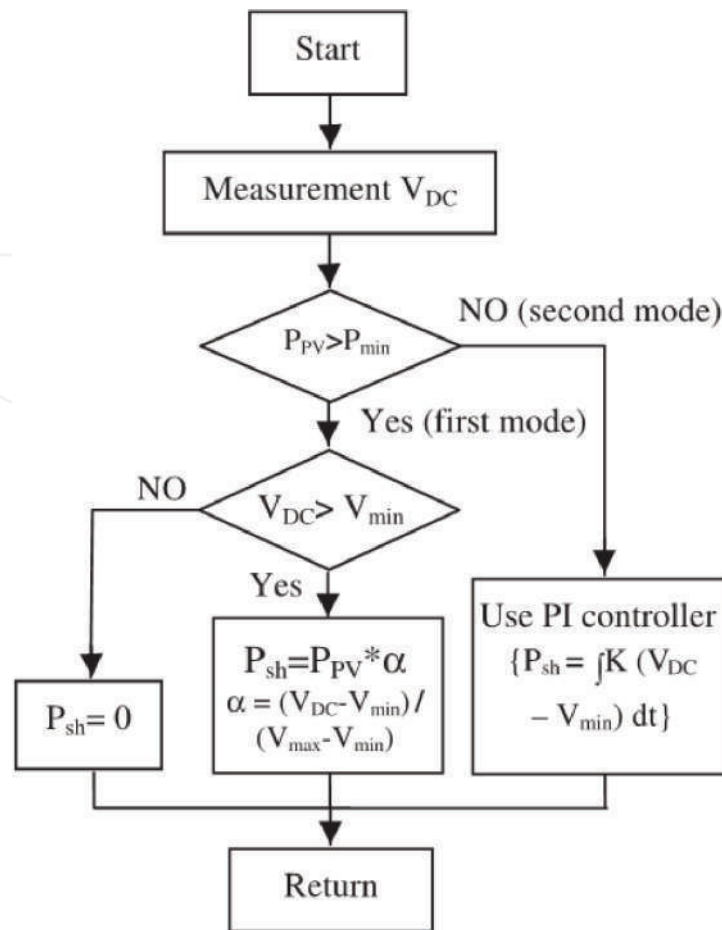


Figure 10. The overall algorithm of the DC-link voltage control [1].

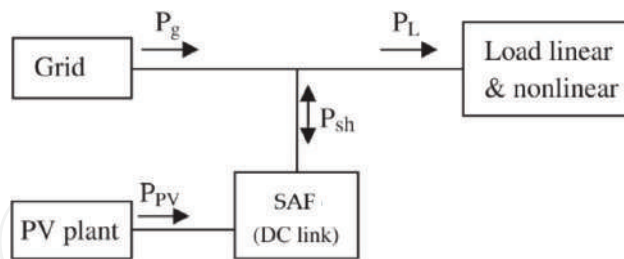


Figure 11. An algorithm of power flow of the PV-SAF [1].

will be delivered to the grid through the parallel part of the SAF. When  $V_{DC}$  reaches its maximum and allowable voltage, that is  $V_{DC-max}$ , the power of the PV is all fed to the grid.

In the situation that  $V_{DC}$  is between  $V_{DC-min}$  and  $V_{DC-max}$  there would be a linear relationship between the power used to charge the capacitor and the  $V_{DC-max} - V_{DC}$  ( $P_{sh} = \alpha P_{PV}$  and  $\alpha = (V_{DC} - V_{min}) / (V_{max} - V_{min})$ ). As a result, some of the load power has been supplied with the PV plant when  $V_{DC}$  is greater than  $V_{DC-min}$ . Following Kirchhoff's circuit laws, as seen in Eq. (8), the load current ( $I_{Load}$ ) is equal to the sum of the grid current ( $I_g$ ) and the SAF current ( $I_{sh}$ ). Also, SAF current ( $I_{sh}$ ) is equal to the sum of the PV power plant ( $I_{PVPP}$ ) and

compensated current ( $I_C$ ). Here, Eq. (7) can be rewritten to Eq. (9) in order to control the shunt active filter to deliver power of the solar power plant.

$$\begin{aligned}
 i_g(t) &= i_{Load}(t) - i_{sh}(t) \\
 i_{sh} &= i_{pvpp} + i_C \\
 \rightarrow P_g(t) &= P_{Load}(t) - P_{sh}(t) \\
 i_{PVPP}(t) &= \frac{\bar{P}_{sh}(t)}{U_1^+(t) \cdot U_1^+(t)} U_1^+(t)
 \end{aligned} \tag{8}$$

So, we have

$$\begin{aligned}
 i_g(t) &= \frac{\bar{P}_g(t)}{U_1^+(t) \cdot U_1^+(t)} U_1^+(t) \\
 i_C(t) &= i_{Load}(t) - \frac{\bar{P}_g(t) - \bar{P}_{sh}(t)}{U_1^+(t) \cdot U_1^+(t)} U_1^+(t)
 \end{aligned} \tag{9}$$

As addressed in Eq. (9), in addition to providing all negative and zero components of the nonlinear load, SAF will partially provide the positive current component of the nonlinear load, which will result in a lower source current. In the case of a voltage sag, the stored energy in the DC link is fed to the grid through the series part of the SAF. This injected energy enhances the power quality but also causes a decrease in the voltage of the DC link, which will be compensated by the energy given by the PV. In a situation where the PV does not generate power (e.g.,  $P_{pv} < P_{min}$ ), the demanded energy to charge the DC link will be provided by the grid.

#### 4. Simulation and discussion

The analysis of the three phases has been done in MATLAB/ SIMULINK environment. The system has a three-phase AC source of 230 V at 50 Hz which is represented as an ideal, balanced, delta, three-phase voltage source, feeding a three-phase nonlinear load (75KVA). The maximum generated power of the PV system is 60 KW.

PV-SAF is utilized for the improvement of power quality in which parallel-connected inverter is operated to perform line current harmonics elimination and reactive power compensation. To study the performance of the proposed algorithm, the results are presented for PV-SAF, where the solar power plant consists of several series-parallel solar panels, which are connected to a boost converter, and delivers the generated power of the solar power plant to the DC link. This power will be delivered by the active filter to a nonlinear load with TDH of more than 40% through a three-phase AC grid with a frequency of 50 Hz and a voltage of 230 V.

**Figure 12** shows the voltage and power of solar power plant for MPPT methods of [1, 6]. For both methods of MPPT, an estimation of the operation point is used to set the operation point to a fairly close point near the MPP, and then by means of a fine-tuning loop, MPP will be reached. In the method of [6], the voltage of the MPP is approximated above the actual  $V_{MPP}$

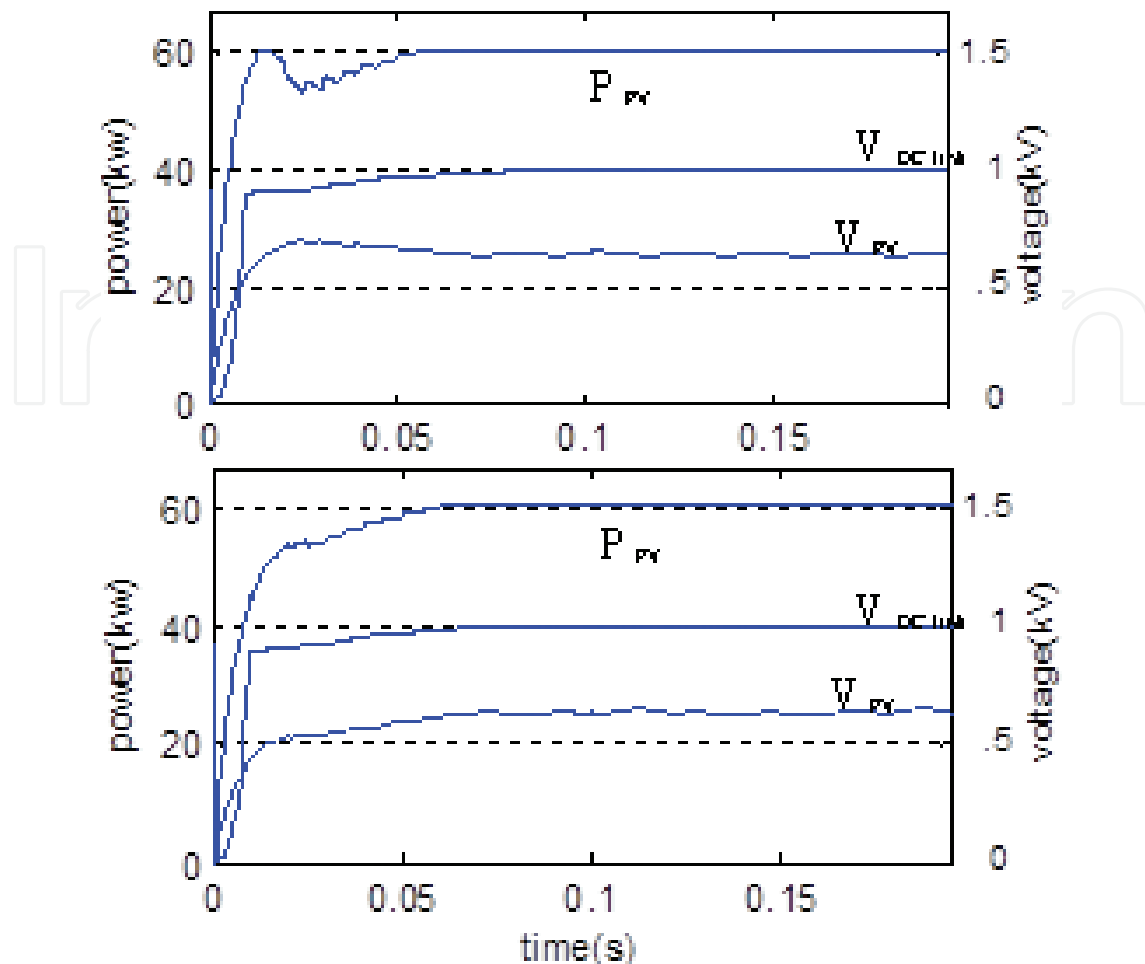


Figure 12. Voltage and power of the PV using MPPT methods of (a) [6] and (b) [1].

operation point consequently, by an increase of  $V_{DC}$  from 850 V to 1 kV; the operation point is deviated from MPP and then returns after several milliseconds. It should be noted that the slope of the P-V characteristic curve is greater for voltages more than  $V_{MPP}$  in comparison to smaller voltages, meaning that a small change in voltage leads to a great change in the power of the solar panel. It can be seen that in the method of [1], the power smoothly increases until it reaches the MPP. This is because of the independency of the control signal to  $V_{DC}$ .

**Figure 13**,  $I_{Load}$ , illustrates the simulated grid current without PV-SAF operation. It is obvious that the grid current is non-sinusoidal and consists of the 50-Hz fundamental component along with lower-order harmonics like the third harmonic (150 Hz), fifth harmonic (250 Hz), seventh harmonic (350 Hz), and so on. **Figure 13**,  $I_g$ , shows the grid current with PV-SAF operation. It is clear that the harmonic currents of nonlinear load are almost compensated with the PV-SAF operation so that the line current is nearly a sinusoidal wave. The total harmonic distortion of line current is lower than 4%. **Figure 13**,  $I_{shv}$ , shows the injected current of the shunt part of the PV-SAF to compensate the current harmonics of the load so that the grid current can be sinusoidal. Meanwhile, it delivers the power of the PV to the load.

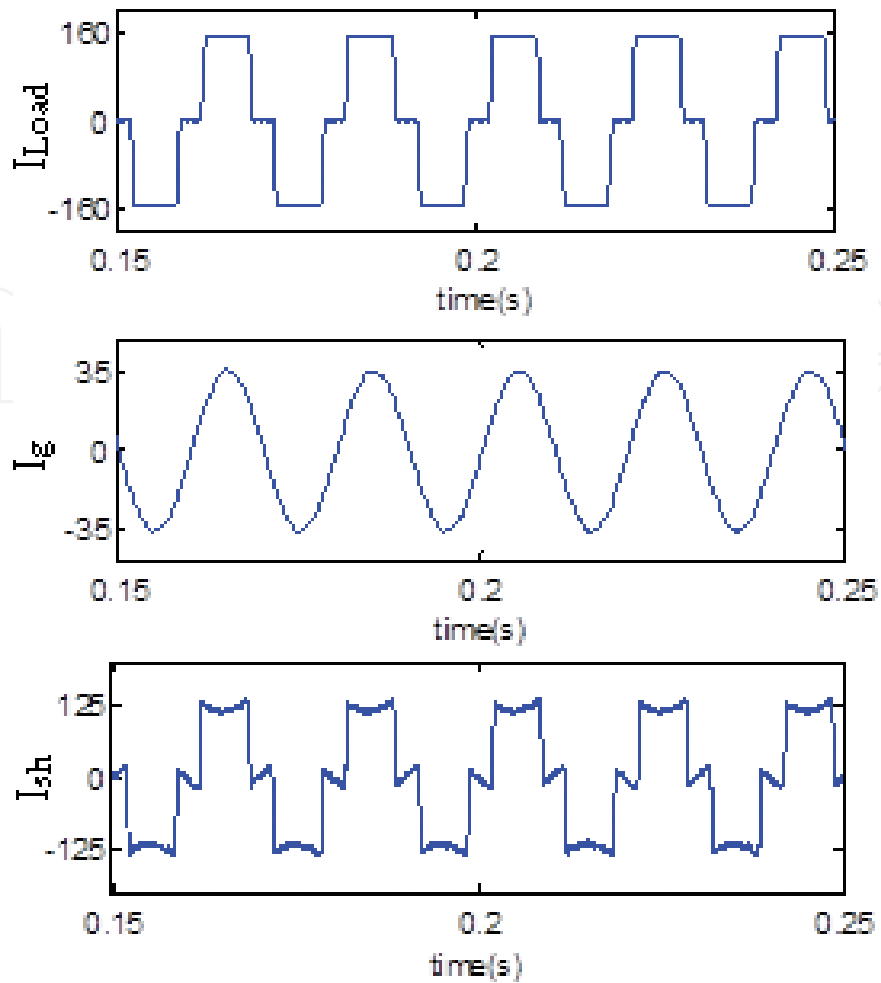


Figure 13. Grid current without PV-SAF ( $I_{Load}$ ), grid current with PV-SAF ( $I_g$ ), and the current of part shunt PV-SAF ( $I_{sh}$ ).

## 5. Conclusions

In this chapter combined with power conditioner and renewable energy, SAF-PV system has been explained for the optimal designing of PV grid connected. Meanwhile, considering the Advanced Generalized Theory of Instantaneous Power (A-GTIP) algorithm, the SAF-PV system leads to suppress grid-end current harmonics caused by the distorted unbalanced load-terminal voltages. Hence, the grid-end currents could remain purely sinusoidal. Also, PV power is injected to the grid via active filter converter and MV/HV transformer. It means that by using the SAF-PV system, there will be capital investment savings since one less converter and MV/HV transformer will be used in comparison with separated SAF and PV systems. In this chapter, different maximum power point tracking (MPPT) algorithms have also been reviewed which can serve as a guide for the selection of the appropriate MPPT method for specific PV system applications. Various simulation results verify the performance of the combined PV-SAF.

## Author details

Ali Reaz Reisi<sup>1\*</sup> and Ashkan Alidousti<sup>2</sup>

\*Address all correspondence to: reisi.alireza@gmail.com

1 Electrical Engineering Department, Technical and Vocational University, Isfahan, Iran

2 Young Researchers and Elite Club, Shahrekord Branch, Islamic Azad University, Shahrekord, Iran

## References

- [1] Reisi AR, Moradi MH, Showkati H. Combined photovoltaic and unified power quality controller to improve power quality. *Solar Energy*. 2013;**88**:154-162
- [2] Albuquerque FL, Moraes AJ, Guimara CG, et al. Photovoltaic solar system connected to the electric power grid operating as active power generator and reactive power compensator. *Solar Energy*. 2010;**84**:1310-1317
- [3] Pashajavid E, Bina MT. Zero-sequence component and harmonic compensation in four-wire systems under non-ideal waveforms. *Przegląd Elektrotechniczny*. 2009;**85**:58-64
- [4] Reisi AR, Moradi MH, Jamasb S. Classification and comparison of maximum power point tracking techniques for photovoltaic system: A review. *Renewable and Sustainable Energy Reviews*. 2013;**19**:433-443
- [5] Eshram T, Chapman PL. Comparison of photovoltaic array maximum power point tracking techniques. In: *IEEE Transactions on Energy Conversion*. 2007;**22**(2):439-449. DOI: 10.1109/TEC.2006.874230
- [6] Moradi MH, Reisi AR. A hybrid maximum power point tracking method for photovoltaic systems. *Solar Energy*. 2011;**85**:2965-2976
- [7] Zhang C, Zhao D, Wang J, et al. A novel two-mode MPPT method for photovoltaic power generation system. In: *IEEE 6th International Conference on Power Electronics and Motion Control*. 2009. Wuhan, China: IEEE; 2009. p. 2100-2102
- [8] Yang C, Hsieh C, Feng F, Chen K. Highly efficient analog maximum power point tracking (AMPPT) in a photovoltaic system. In: *IEEE Transactions on Circuits and Systems I: Regular Papers*. July 2012;**59**(7):1546-1556. DOI: 10.1109/TCSI.2011.2177008
- [9] Salah CB, Ouali M. Comparison of fuzzy logic and neural network in maximum power point tracker for PV systems. *Electric Power Systems Research*. 2011;**81**:43-50
- [10] Abdelsalam AK, Massoud AM, Ahmed S, Enjeti PN. High-performance adaptive perturb and observe MPPT technique for photovoltaic-based micro grids. In: *IEEE Transactions on Power Electronics*. 2011;**26**(4):1010-1021. DOI: 10.1109/TPEL.2011.2106221

- [11] Lei P, Li Y, Seem JE. Sequential ESC-based global MPPT control for photovoltaic array with variable shading. *IEEE Transactions on Power Electronics*. 2011;**2**(3):348-358
- [12] Mei Q, Shan M, Liu L, Guerrero JM. A novel improved variable step-size incremental-resistance MPPT method for PV systems. In: *IEEE Transactions on Industrial Electronics*. 2011;**58**(6):2427-2434. DOI: 10.1109/TIE.2010.2064275
- [13] NSD' Souza LAC, Liu LXJ. Comparative study of variable size perturbation and observation maximum power point trackers for PV systems. *Electric Power Systems Research*. 2010;**80**:296-305
- [14] Kobayashi K, Takano I, Sawada Y. A study on a two stage maximum power point tracking control of a photovoltaic system under partially shaded insolation conditions. In: *IEEE Power Engineering Society General Meeting*. Vol. 4; 2003. pp. 2612-2617



# We are IntechOpen, the world's leading publisher of Open Access books Built by scientists, for scientists

6,300

Open access books available

171,000

International authors and editors

190M

Downloads

Our authors are among the

154

Countries delivered to

TOP 1%

most cited scientists

12.2%

Contributors from top 500 universities



WEB OF SCIENCE™

Selection of our books indexed in the Book Citation Index  
in Web of Science™ Core Collection (BKCI)

Interested in publishing with us?  
Contact [book.department@intechopen.com](mailto:book.department@intechopen.com)

Numbers displayed above are based on latest data collected.  
For more information visit [www.intechopen.com](http://www.intechopen.com)



---

# Experimental Study of Current-Voltage Characteristics for Fixed and Solar Tracking Photovoltaics Systems

---

Chukwuemeka Ikedi

Additional information is available at the end of the chapter

<http://dx.doi.org/10.5772/intechopen.79710>

---

## Abstract

The efficiency of solar electric systems basically depends on the materials used in making the solar cells and regardless of the type of application: fixed or tracking photovoltaics (PV), the quality and quantity of power produced by PV systems depend on both the amount of solar radiation incident on the solar panels as well as the current and voltage characteristics of the load. This present work, which involves field installation of a fixed PV alongside an existing equivalent tracking PV, simultaneously monitored the current and voltage response of both systems to changing solar radiation and ambient temperatures. The comparative results of the study provide a framework for decision-making on the choice of either of the systems and have shown that in the UK, both systems have a relatively slow electrical response to sunrise while the performance of fixed PV systems approximates that of tracking PV systems at noon time.

**Keywords:** fixed PV, solar tracking PV, voltage-current (I-V) characteristics, maximum power, solar radiation

---

## 1. Introduction

Photovoltaics, otherwise called photoelectricity, is a compound word for photo that is light and voltaic that is electric (from Volta the inventor). It is simply the conversion or generation of electricity from light. Jacques Bequerel, a French physicist discovered in the 1890s, that certain materials produce electric current when exposed to light. This phenomenon is called photoelectric effect and forms the basis for the science and technology of photovoltaics.

Photovoltaics (PV) technology has been in existence for more than 50 years now [1] with various innovative applications. For instance, the Swiss solar aircraft, "Solar Impulse 2", achieved

the longest non-stop solo flight in history making the first solar-powered aerial circumnavigation in 2015. The wide range of fixed PV applications include—lighting (e.g. for buildings, streets, traffic signals and navigation), transportation (e.g. solar-powered vehicles, boats, ships), telecommunications, astronomy and space electrical power supplies.

Other applications include roadside emergency telephones, parking ticket machines, remote sensing and cathodic protection of oil and brewery pipe lines.

This chapter presents an overview of basic photovoltaics materials and components and most significantly, investigates and analyses the electrical characteristics of two types of installed PV systems namely: fixed and solar tracking PV simultaneously, under varying solar radiation and temperature conditions in the UK.

By deducing and comparing the maximum power for each of the systems at different points in time, interesting observations were made which led to vital conclusions regarding the relative choice of either of the systems with respect to their respective maximum power performances and cost under similar applications and conditions.

## 2. Photovoltaic materials and solar panels

In order to appreciate any solar electric or PV system and applications, whether experimental as in this present study or otherwise, a brief overview of the background becomes inevitable.

The basic component of a PV module or panel is the solar cell. Although recent research and innovations have identified some other materials, extensive literature reviews in this study has identified silicon as the key material used in making the solar cells for most PV panels and unless broken or exposed to harmful elements, they could last for a period of more than 20 years and usually protected behind transparent glass materials. Three major configurations of silicon photovoltaic materials were identified in use for solar panels, namely: monocrystalline, polycrystalline and amorphous cells.

**Monocrystalline cells:** These were found to be the first commercially developed solar cells. They are cut from single crystals of silicon and have an efficiency of about 11–16%. They are chemically stable [2]. They have negligible defects and impurities and are usually grown from a sophisticated but expensive process, known as Czochralski process.

**Polycrystalline cells:** Cut from many silicon crystals, they have a single colour tone, multiple patterns and an efficiency of about 9–13%. They are cheaper in production than monocrystalline types, but less efficient, because of their light-generated charge recombination effect [3].

**Amorphous cells:** These are silicon cells in non-crystalline form, usually used in thin film technology. They are cheaper to produce but have a lower operating efficiency of about 3–6% [2]. They decay over time and are usually used in devices like watches, calculators and toys.

Apart from silicon, other crystalline materials are found to be in use for PV solar cells. One of such materials is the compound semiconductor, gallium arsenide (GaAs). PV cells made

from GaAs are more expensive but more efficient than silicon cells. They withstand high temperatures and are therefore used in concentrating PV systems and also for applications that demand very high efficiency, irrespective of cost, like in space operations.

Organic materials are now available for use in solar cells. Most organic photovoltaic cells are made from polymers and compared to silicon solar cells, polymer solar cells are lightweight and cheap to fabricate and have safer environmental impact. The capability to be transparent has made polymer solar cells useful in applications like windows, glass walls and skylight roofing devices. One downside with organic solar cells is that they produce a relatively low level of the efficiency compared to silicon materials [4].

Presently, research is advancing towards the development of more efficient and cheaper materials for generating photo electricity. A new approach, using millimetre-sized polycrystalline silicon spheres on thin sheet aluminium foils have been developed by Texas Instruments, US for PV cells.

It is important to note that each silicon solar cell usually has a voltage output of 0.5 V, and when a collection of such cells are electrically connected for the purpose of meeting certain specified load requirements, it is referred to as a PV module or panel. Furthermore, an electrical combination of two or more PV modules or panels to achieve a specific voltage and current as required by a given load or appliance in a particular application is referred to as PV arrays. The individual modules could be either similar or dissimilar and can be connected either in series or in parallel, unlike the case of cells in the module. The systems installed and used in this experimental study consists of an array of two similar solar PV modules electrically connected in series for either of the applications: fixed and tracking. In general, arrays provide increased power output.

The other components of a PV system include the battery, the charge controller and the inverter and when all connected together becomes referred to as photovoltaics generator.

## **2.1. Fixed and tracking PV**

This experimental study simultaneously monitored a fixed and a tracking PV system. It becomes important therefore to provide a brief explanation of both systems. The Earth moves round the Sun in an elliptical orbit; in a counter clockwise direction on an imaginary line called its axis, tilted with respect to the plane of its orbit at an angle of about  $23.4^\circ$ . Due to this movement of the Earth around the Sun and the consequent effect on solar radiation, some PV systems are designed to track the Sun's movement and hence maximise solar incidence on the modules/arrays by maintaining an optimum orientation between the Sun and the solar panels. Such systems are referred to tracking PV. The complex and usually delicate operations involved in tracking PV systems has meant that most PV applications are of the fixed category resulting in benefits of simplicity, least cost and convenience of operation.

On the other hand, fixed PV systems are defined as such because the solar modules or arrays are permanently fixed at a particular angle towards the Sun, with the aim of maximising solar capture. Fixed systems can be installed either as pole mounted, ground mounted or roof mounted systems.

Pole and ground mounted PV's as in this study are usually installed remote from building envelopes, while other types of PV systems are either installed on structured framework on the roofs of buildings or integrated with the building envelope in such a way that it is referred to as building integrated photovoltaic (BIPV). These involve the integration of the PV modules into parts of the fabric of a building as roof tiles, asphalt shingles, facade materials or shading elements. Used in this way, the integrated PV modules replace conventional building envelope materials thereby benefiting from capital cost reduction and hence improved payback period and life cycle cost.

### 3. Research methodology

As a preliminary step, an extensive review of previous works was carried out prior to this present study. Most work and research carried out earlier on PV materials were found to be mainly on cell characterisation and development [5–7], etc. Shivakumar et al. carried out a test on interface adhesion strength in multilayered structures; Dauskardt et al. examined the mechanisms of debonding in photovoltaic back sheets; Budiman et al. applied Synchrotron X-ray on c-Si Solar PV cells for micro-diffraction analysis, and these are to mention a few. Few researches conducted on solar tracking PV suggest the average experimental gain of tracking PV systems over the fixed types to be about 25% [8–11].

However, when the use or application of fixed and tracking PV systems is considered at different seasons of the year putting into consideration, obtainable costs of maintenance, a controversy begins to arise which seems to question the credibility of the claimed gain of the tracking PV system over the fixed option. Comparative study on specific aspects of the systems such as power outputs gives a clearer understanding of the respective performances.

Further reviews were carried out on current voltage (I-V) characteristics of photovoltaics materials [12–14]. James et al. showed I-V characteristics with reverse bias slopes to be due to wavelengths of light below semiconductor band gap, while Schottky I-V characteristics were due to wavelengths of light above the semiconductor band gap; Zhang et al. proposed a method to predict I-V curves under different operating conditions, while Ibrahim investigated the response of crystalline silicon (Si) solar cell at different conditions of solar irradiance and showed possible performance defects.

This present study simultaneously monitors and compares the voltage–current response of fixed and solar tracking PV systems under the same varying conditions of solar radiation and ambient temperatures.

#### 3.1. Identification and selection of research case study

As a further preliminary step to achieve a good experimental method, a case study was identified for use in the comparative analyses for the two systems, fixed and tracking PV, respectively. One key requirement for the selection of a case study in this study is that the fixed

and tracking PV systems should be installed within the same location and at the closest possible vicinity to each other. This becomes necessary to ensure that the ambient temperatures around the two systems are significantly the same under the same solar insolation. Another key requirement or criteria for the selection of a case study is that the two systems must be of the same system specification and size.

The exact location used for the experimental study is the school of the built environment at the University of Nottingham, UK. The geographical and meteorological details of the location are as follows: Latitude 52.5° North, Longitude, Altitude 48 m and Azimuth 0° (true south).

For the photovoltaic systems, the fixed and the solar tracking PV consist of 2 PV modules tied together in serial connections, respectively. The PV module used for the installations is a BP 275F solar module with a nominal peak power ( $P_{max}$ ) of 75.00 W, maximum power voltage ( $V_{mp}$ ) of 17.0 V and maximum power current ( $I_{sc}$ ) of 4.45 A. The extra features on the tracking system include the solar tracking sensor, made of monocrystalline cells and a 24 inch actuator motor jack for the tracking mechanism. The tracking PV system which was originally used to power a water fountain was already existing while the tracking PV was installed right beside the tracking system for the purpose of the comparative analyses in the study.

### 3.2. Experimental method

The experimental rig for the study consists of fixed and tracking PV systems, each made up of two BP 275 PV modules with the terminals in each system applied to the electrical circuit in **Figure 1**. The two systems were installed to have the same orientation, south facing at zero azimuths with module inclination of 52°s (which approximates the latitude of the location), having a nominal standard test condition (STC) open-circuit voltage of 21.4 V, short-circuit current of 4.75 A and peak power of 75 W.

STC is an abbreviation for the “standard test condition” by which PV modules are tested and calibrated which is insolation level of 1000 W/m<sup>2</sup>, air mass of 1.5 AM and cell temperature of 25°C.

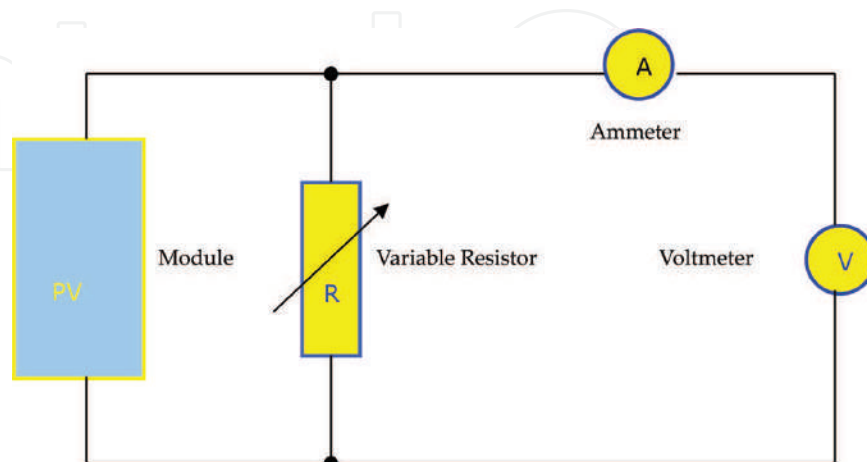


**Figure 1.** Layout of I-V electrical circuit.

While one of the systems remained fixed relative to the position of the Sun, the other (tracking) kept moving automatically with the aid of a solar tracking sensor and mechanical actuator jack to follow the changing positions of the Sun.

By using a potentiometer type of rheostat, the impedance in the circuitry (**Figure 1**) was varied, while the corresponding current and voltage at each point was monitored and recorded with the aid of the ammeter and the voltmeter.

This process was carried out every 1 h for 2 days between the solar window from 12.00 pm to 4.00 pm for the first day and 9.00–3.00 pm for the second day. One major problem encountered during the measurements was the dramatic change/drop in observed values in some cases due to sudden changes in insolation. This was because UK unlike some tropical locations has a very sloppy insolation gradient within the solar window such that each change in the insolation implies a big difference in the observed values.

#### 4. Results and discussions of experimental work

From the maximum power and the I-V curves, it can be noticed that the gap between the curves for the fixed and tracking systems at each point in time oscillates from infinity towards zero and then towards infinity with noontime as a turning point from sunrise to sunset respectively.

This is because, around and within noontime, the fixed PV system sees the Sun at approximately a perpendicular position and at such point in time also, the tracker device in principle positions the tracking PV system at the same position, hence the difference in performance between the two systems becomes apparently cancelled and so the fixed system almost, approximates to the tracking system.

From noontime towards either sunrise or sunset, the effect of the tracking device on the tracking PV system becomes pronounced as the system becomes more resolved in orientation to the Sun relative to the fixed system.

From basic PV principles [15], the current flowing in the circuit above (**Figure 1**) at each point in time, can be given as

$$I = I_L - I_D(V) \quad (1)$$

assuming a linear superimposition of the photo and dark currents where the photocurrent

$$I_L = eA_c \int_{E_c}^{\infty} S(E) [1 - \rho(E, W) - \tau(E, W)] dE \quad (2)$$

and the dark current

$$I_D(V) = I_0 \left[ \exp\left(\frac{eV}{mkT-1}\right) \right] \quad (3)$$

where  $\alpha(E, W)$  is the spectral absorbance,  $S(E)$  is the number of photons of energy  $E$  incident on the cell per unit area,  $A_c$  is the area of the illuminated cell,  $k$  is the Boltzmann's constant,  $T$  is the absolute temperature, and  $m$  is 1 at high voltages and 2 at low voltages.

From the graphs, (Figures 2 and 4), when the resistance is zero, the current in the circuit becomes the maximum (short-circuit current). At this point, the voltage  $V = 0$  and from Eq. (1), the short-circuit current becomes

$$I_{sc} = I(V = 0) = I_L \quad (4)$$

Also from the same graphs, at open circuit, the current becomes zero while the voltage becomes the maximum (open-circuit voltage)  $V_{oc}$  and expressed as:

$$V_{oc} = \frac{mkT}{q \ln \left\{ \frac{I_L}{I_0 + 1} \right\}} \quad (5)$$

For each of the cases, the area under the curve, which is the product of the voltage and the current, gives a measure of the power output.

At  $V_{oc}$  and  $I_{sc}$  the power output becomes zero and maximum at a particular point between these points. This is the point at which the systems deliver the maximum power (maximum power point).

The values of the voltage and current at such points denote the maximum power voltage and the maximum power current  $V_M$  and  $I_M$ , respectively.

The monitored and measured results for the different days are shown and described as follows:

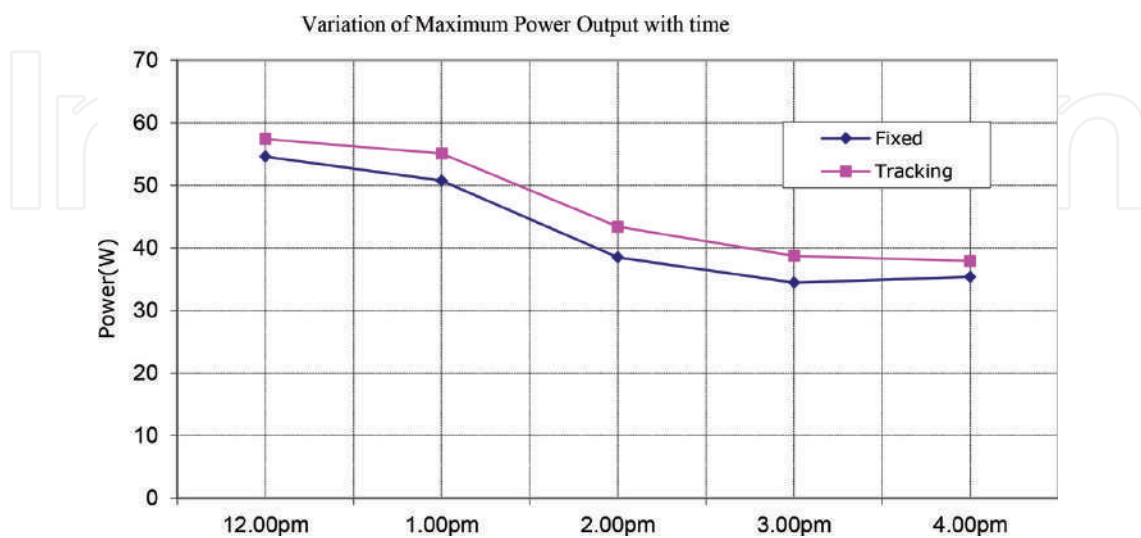
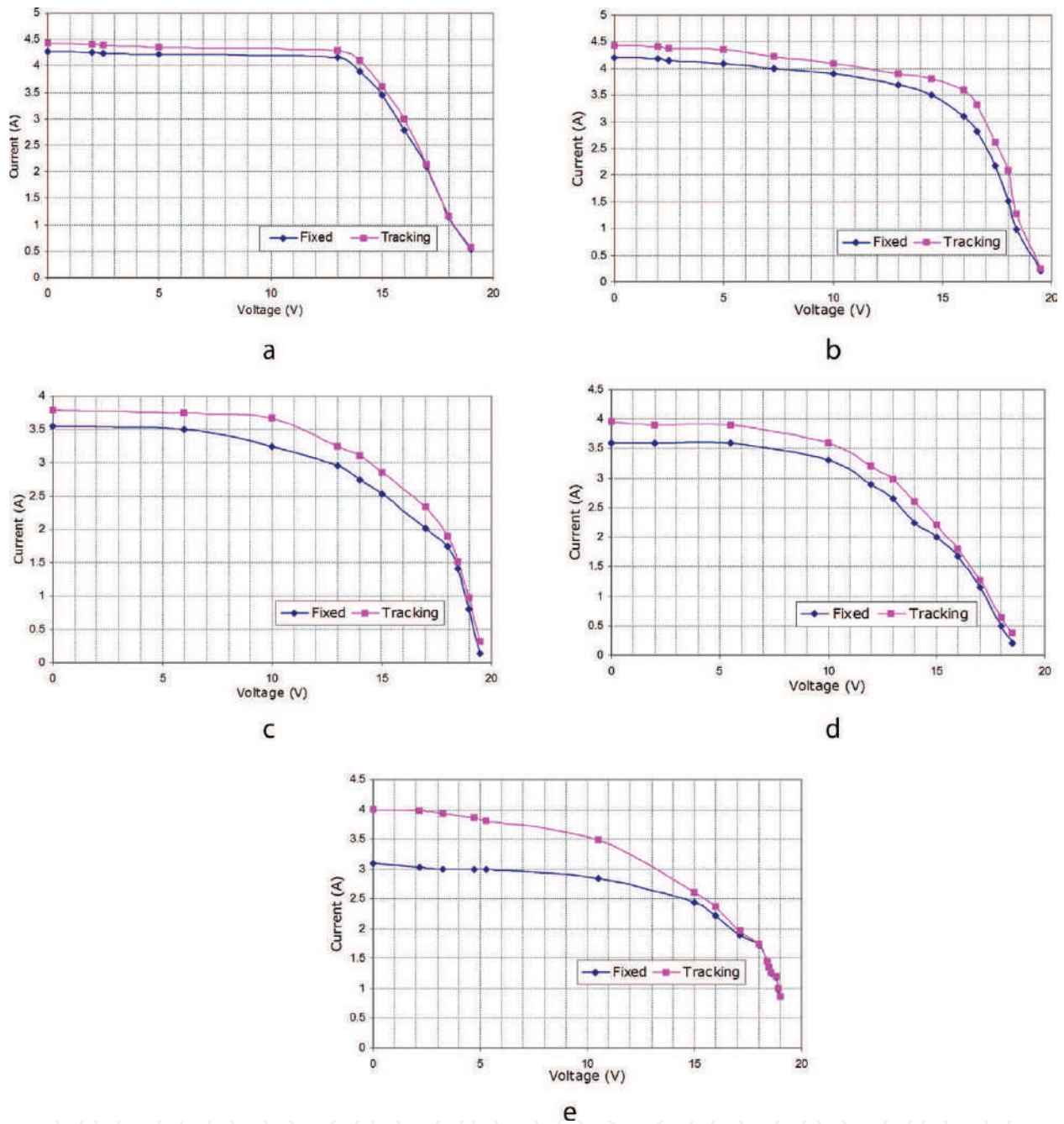


Figure 2. Timely maximum power output.



**Figure 3.** (a) I-V curves at 12.00 pm (hor rad. - 667.9 KWh/m<sup>2</sup>. Ambient temp: 22.3°C), (b) I-V curves at 1.00 pm (hor rad. - 517.8 KWh/m<sup>2</sup>. Ambient temp: 20.7°C), (c) I-V curves at 2.00 pm (hor rad. 616 KWh/m<sup>2</sup>. Ambient temp: 22.7°C), (d) I-V curves at 3.00 pm (hor rad. 517.1 KWh/m<sup>2</sup>. Ambient temp: - 21.2°C), (e) I-V curve at 4.00 pm (hor rad. 509.8 KWh/m<sup>2</sup>. Ambient temp: 20.8°C).

#### 4.1. Day 1

**Table 1** contains the values of the short-circuit current and the open-circuit voltages for each of the observations and summarises the results of the measurements and observations carried out on day 1.

Below is the diagram comparing the maximum power output for the two systems (fixed and the tracking PV) for day 1.

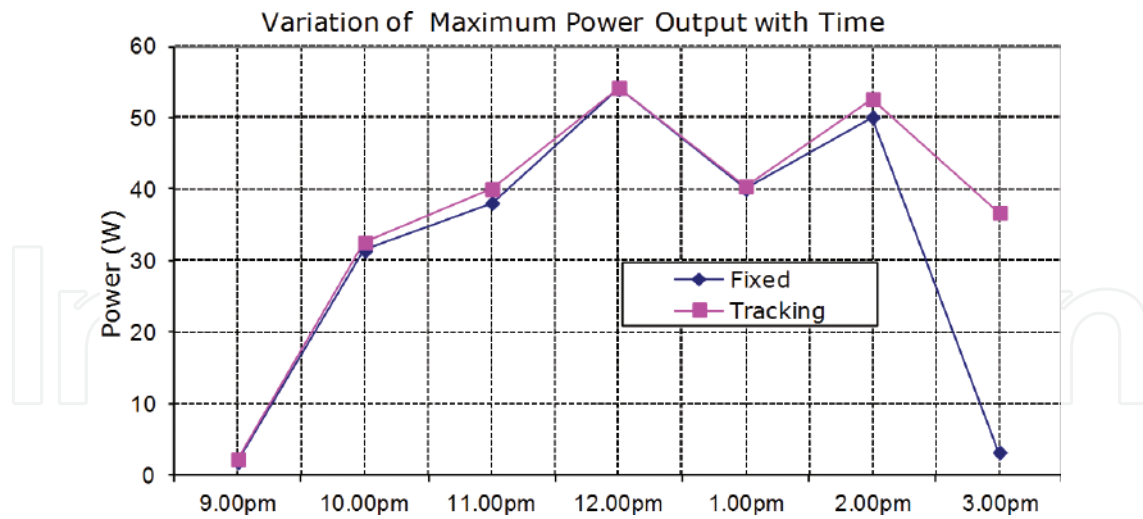


Figure 4. Timely maximum power output for day 2.

Time	Vmp (v)		Imp (A)		Pmp (W)		Voc (V)		Isc (A)	
	Fixed	Trk	Fixed	Trk	Fixed	Trk	Fixed	Trk	Fixed	Trk
12 pm	14.0	14.0	3.90	4.10	54.60	57.40	19.0	19.0	4.28	4.42
1 pm	3.50	3.80	3.70	3.80	50.75	55.10	19.5	19.5	4.20	4.43
2 pm	14.0	14.0	2.75	3.10	38.50	43.40	19.5	19.5	3.54	3.79
3 pm	13.0	13.0	2.65	2.98	34.45	38.74	18.5	18.5	3.60	3.95
4 pm	16.0	16.0	2.21	2.37	35.36	37.92	19.5	19.5	3.09	4.00
Average maximum power (W)					42.73	46.51				
Percentage power gain by tracking (%)					8.85					

Table 1. Measurements and observations for day 1.

It should be recalled from above that power variation approximately oscillates with noontime as the turning point. This is evident from the graphs above as the entire graph for the case of the respective date, represents only about one half of the daily solar window. As earlier pointed out, this was due to the poor climatic condition (Uneven radiation gradient) during the earlier part of the day before noontime.

Nevertheless, the picture of the entire cycle may be observed in the next investigation (Figure 3).

It can be concluded from the graphs that the average daily maximum power of the two systems increases from sunrise and peaks around noontime and then gradually decreases towards sunset with the tracking system maintaining a higher output at all times.

The response to sunrise and sunset generally depends on season and climatic conditions of a location [16], for instance, in temperate locations like some parts of Africa, PV panels would be readily responsive to the solar position as at 7.30 am where as in the UK during the time

of this experimental work, the graphs of the two systems (fixed and tracking) were almost parallel to the voltage axis as at 9.00 am (**Figure 4a**).

Finally, the voltage-current characteristics was plotted and investigated under varying load conditions (resistance), solar insolation and ambient temperature.

The diagrams below (**Figure 3a–e**) show the I-V curves every 1 h from 12.00 pm to 4.00 pm for day 1.

One interesting thing to note in the above graphs (**Figure 3a–e**) is the change in the power margin between the two systems. Around noontime, the power margin tends very close to zero. The reason for this is explained in the third paragraph of Section 5.

On the other hand, it tends towards infinity around sunrise and sunset. It should also be noticed that at lower load impedance (maximum voltage), the two graphs in most cases begin to overlap.

The explanation for this is that such points approximate to the open-circuit voltage position where the current tends to zero irrespective of fixed or tracking process. Hence, the two graphs overlap.

#### 4.2. Day 2

**Table 2** summarises the results of the observations and measurements carried out on day 2. Unlike the previous investigation above, the measurements started 3 h earlier from 9.00 am.

**Figure 4** shows the graphical comparison of the observed maximum power output for the fixed and the tracking systems.

It is important to emphasise that the pattern of the maximum power curves (**Figures 2 and 4**) does not take into account the behaviour of the power over the entire interval of the observations and measurements. It depicts the power under the I-V curves with maximum rectangular

Time	V <sub>mp</sub> (V)		I <sub>mp</sub> (A)		P <sub>mp</sub> (W)		V <sub>oc</sub> (V)		I <sub>sc</sub> (A)		
	Fixed	Trk	Fixed	Trk	Fixed	Trk	Fixed	Trk	Fixed	Trk	
9 pm	3.0	3.0	0.6	0.72	1.8	2.16	0.03	0.03	0.63	0.75	
10 pm	16.1	16.1	1.95	2.02	31.41	32.54	0.12	0.12	2.8	3.15	
11 pm	15.0	15.0	2.54	2.67	38.1	40.05	0.13	0.13	3.27	3.56	
12 pm	14.0	16.0	3.86	3.39	54.04	54.24	0.13	0.01	4.09	4.19	
1 pm	14.0	16.5	2.86	2.45	40.04	40.43	0.01	0.15	3.57	3.79	
2 pm	14.0	14.0	3.58	3.76	50.12	52.64	0.15	0.15	3.95	4.56	
3 pm	10.5	10.5	2.87	3.5	3.14	36.75	0.15	0.15	3.0	3.84	
Average maximum power (W)					31.24	36.97					
Percentage power gain by tracking (%)					18.34						

**Table 2.** Measurements and observations for day 2.

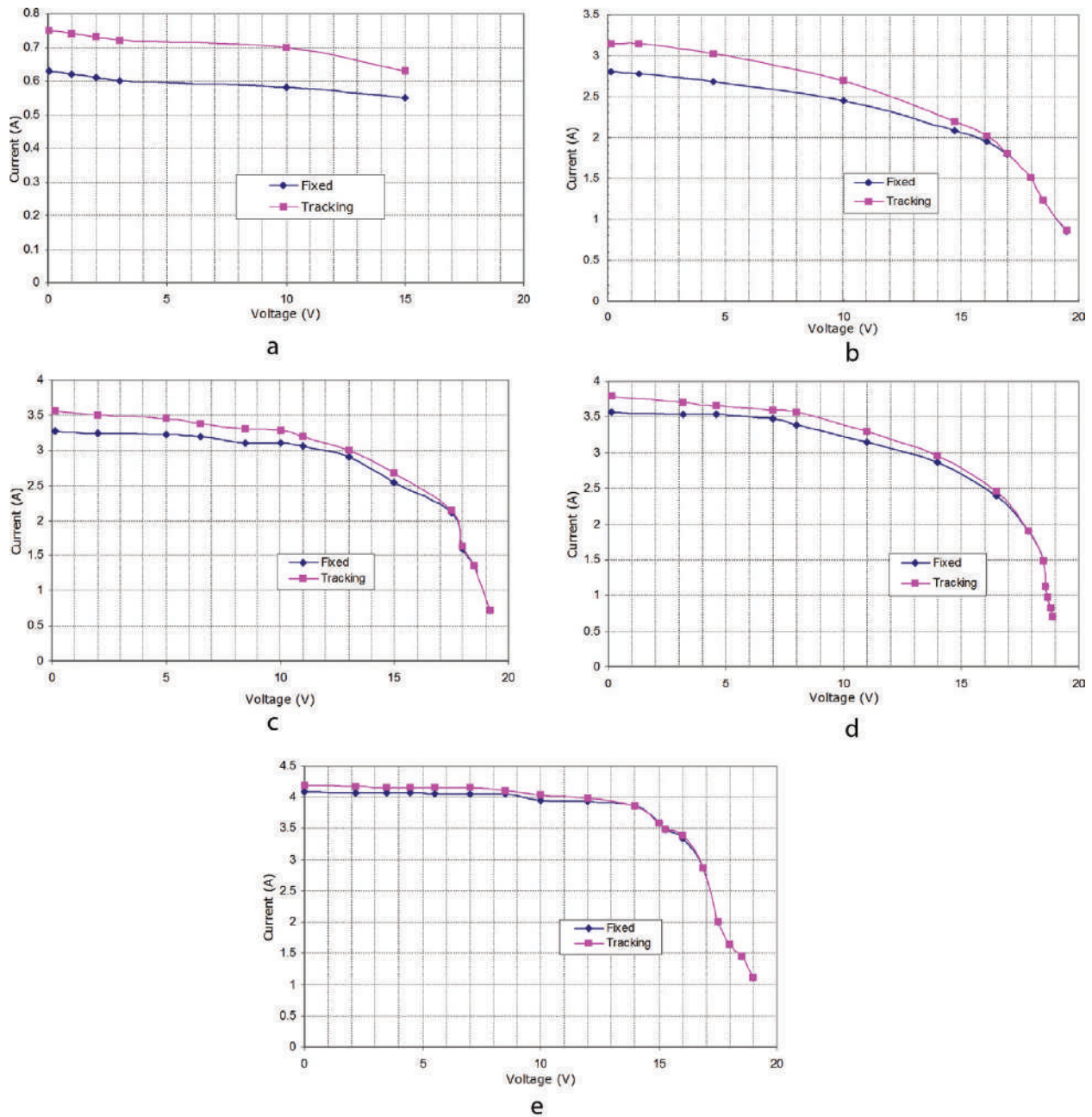


**Figure 5.** (a) I-V curves at 9.00 am (hor rad. - 223.7 KWh/m<sup>2</sup>. Ambient temp: 14.6°C), (b) I-V curves for 10.00 am (hor rad. - 340 KWh/m<sup>2</sup>. Ambient temp: 16.5°C), (c) I-V curves for 11.00 am (hor rad. - 499.9 KWh/m<sup>2</sup>. Ambient temp: 19.23°C), (d) I-V curves for 12.00 pm (hor rad. - 576.2 KWh/m<sup>2</sup>. Ambient temp: 20.48°C), (e) I-V curves for 1.00 pm (hor rad. - 606.4 KWh/m<sup>2</sup>. Ambient temp: 21.2°C), (f) I-V curves for 2.00 pm (hor rad. - 653.1 KWh/m<sup>2</sup>. Ambient temp: 21.67°C), (g) I-V curves for 3.00 pm (hor rad. - 629.5 KWh/m<sup>2</sup>. Ambient temp: 22°C).

areas. For this reason, the power margin between the fixed and the tracking system at every point along the curves may appear closer as can be seen from the diagram above (**Figure 5**).

The closeness becomes more pronounced in a day with an even high insolation distribution. Comparison of the daily solar radiation for the first and the second day confirm that from the respective diagrams.

Observe the position of the curves in **Figure 5** above at 3.00 pm. At such position, the fixed system was beginning to lose site of sufficient direct radiation as the incident solar angle.

On the other hand, the tracking system was still busy following the Sun at that point as was observed in the field.

The I-V characteristics for day 2 were also plotted and compared for the two systems, fixed and tracking PV. **Figure 5** below show the characteristic curves.

The explanation for the above diagrams is the same with that of **Figure 4(a–e)**. The only notable difference is the appearance of the curves in **Figure 5a** at 9.00 pm.

The reason for this is that at that time for that particular day, the position of the Sun was such that the incidence angle was close to maximum and because the system output has been found to be inversely proportional to the incidence angle, hence the current for both the fixed and the tracking systems at that time appeared parallel to the voltage axis. The values of the current for both systems at the time were approximately the short-circuit currents of 0.63 A and 0.75 A for the fixed and tracking systems, respectively.

Recall that at the short-circuit current, the voltage becomes zero Eq. (4).

Hence, from the relation

$$P = IV \quad (6)$$

The power output for the systems approximated to zero. However, the maximum powers for the systems at that point as can be seen from **Table 2** are 1.8 and 2.16 W, respectively.

## 5. Conclusions

Key features of the research outcomes which contribute both to the aims of the study and knowledge are outlined below:

1. **Experimental Significance:** The study is absolutely an experimental work which involved a complete PV installation process for the fixed PV alongside the existing tracking PV originally used to power a water fountain. Based on the results of the I-V characteristics for the two systems: fixed and solar tracking PV in UK climate, it can be concluded that in UK and other locations with similar climatic conditions, both the fixed and tracking PV systems have a relatively slow response to sunrise. At noon time in UK, the performance of fixed PV systems approximates that of tracking PV systems. Also in the UK, fixed PV systems compared to tracking PV usually begin to lose sight of sufficient direct radiation after 3.00 pm, while the tracking system relatively remains further active as it still follows the Sun at such points
2. **Decision-Making:** The information gathered from this study can be used to reach decisions on the choice of either of the systems based on the electrical performance of both systems under the same insolation level and ambient temperatures. A common idea prior to this experimental study is that tracking PV generally out-matches the fixed systems. This no doubt is true however, from the results of the I-V characteristics, the margin between the electrical responses of both systems under similar conditions in the UK remain negligible for a longer part of the day. This implies that when the cost and maintenance for

tracking PV systems are put into consideration at such location and other locations with similar climatic conditions, it may make more economic sense to choose the fixed option rather than the tracking PV option.

Finally, it has been shown that the materials used for solar cells in every solar PV module primarily determine the intrinsic efficiency of every solar PV module and system; Gallium arsenide was identified in the study to produce more efficient photovoltaic systems but much more expensive compared to silicon while polycrystalline or organic materials are much more cheaper but produce less efficient photovoltaic systems. It becomes inevitably necessary therefore to pay more attention to the research and development of cheaper and high efficient solar cell materials.

## Author details

Chukwuemeka Ikedi

Address all correspondence to: [ikedienergy@yahoo.com](mailto:ikedienergy@yahoo.com)

Energy Commission of Nigeria, SunLab Technologies, Nottingham, UK

## References

- [1] Spanggaard H, Krebs FC. A brief history of the development of organic and polymeric photovoltaics. *Solar Energy*. 2004;**125**:146-183
- [2] Hankins M. *Solar Electric Africa*. 2nd ed. Commonwealth Science Council; 1995
- [3] Halliday D, Resnick R. *Fundamentals of Physics*. John Wiley and Sons Inc; 2013
- [4] Luther J, Nast M, Fisch N, Christoffers D, Pfisterer F, Meissner D, Nitsch J. *Solar Technology* 2008. DOI: 10.1002/14356007.a24\_369
- [5] Shivakumar R, Tippabhotla SK, Handara VA, Illya G, Tay AO, Novoa F, Dauskardt RH, Budiman AS. Fracture mechanics and testing of interface adhesion strength in multilayered structures. *Solar Energy*. 2016;**47**:55-89
- [6] Dauskardt RH, Novoa D, Fernando C, David M. Environmental mechanisms of debonding in photovoltaic back sheets. *Solar Energy*. 2014;**87**:93-120
- [7] Budiman AS, Illya G, Handara V, Caldwell A, Bonelli C, Kunz M, Tamura N. Enabling thin silicon technologies for next generation c-Si solar PV. *Renewable Energy*. 2014;**130**:303-308
- [8] Bruno R, Bevilacqua P, Longo L, Arcuri N. Small size single-axis PV trackers: Control strategies and system layout for energy optimization. *Solar Energy*. 2015;**82**:737-743
- [9] Bazilian M, Onyeji I, Liebreich M, MacGill I, Chase J, Shah J, Gielen D, Arent D, Landfear D. Re-considering the economics of photovoltaic power. *Renewable Energy*. 2013;**53**:329-338

- [10] Huang BJ, Ding WL, Huang WC. Long-term field test of solar PV power generation using one-axis 3-position sun tracker. *Solar Energy*. 2011;**85**:1935-1944
- [11] Koussa A, Cheknane A, Hadji S, Haddadi M, Noureddine S. Measured and modelled improvement in solar energy yield from flat plate photovoltaic systems utilizing different tracking systems and under a range of environmental conditions. *Applied Energy*. 2011;**88**:1756-1771
- [12] James AR, Kauer M, Mellor AV, Paul N, Nicholas J, Ekins D. Current voltage characteristics of a metallic structure for a hot-carrier photovoltaic cell. *PVSC*. 2016. DOI: 10.1109/PVSC.2016.7749770
- [13] Zhang Y, Gao S, Gu T. Prediction of I-V characteristics for a PV panel by combining single diode model and explicit analytical model. *Solar Energy*. 2017;**144**:349-355
- [14] Ibrahim A. Analysis of electrical characteristics of photovoltaic single crystal silicon solar cells at outdoor measurements. *Smart Grid and Renewable Energy*. 2011;**2**:4965-4972
- [15] Lorenzo E. *Solar Electricity: Engineering of Photovoltaics*. John Wiley and sons; 2000
- [16] Ikedi CU. Numerical assessment of energy contribution by building integrated Photovoltaics in a commercial/office building refurbishment in UK. *International Journal for Low Carbon Technologies*. 2014;**11**:338-348